TWO QUANTUM PHOTOEMISSION AND dc PHOTOMIXING IN SODIUM

A Thesis

Presented to the Faculty of the Graduate School

of Cornell University for the Degree of

Doctor of Philosophy

by

Malvin Carl Teich

February 1966

BIOGRAPHICAL SKETCH

Malvin Carl Teich was born in New York City on May 4, 1939. He entered the Massachusetts Institute of Technology in September, 1957, and was graduated in June, 1961, with the degree of Bachelor of Science in Physics. He then entered Stanford University, from which he received the Master of Science Degree in Electrical Engineering in June, 1962.

Mr. Teich entered Cornell University in September, 1962, working in quantum electronics under the direction of Professor George J. Wolga. In connection with his Ph.D. thesis, he has co-authored the following publications: "Double-Quantum Photoelectric Emission from Sodium Metal," Phys. Rev. Letters 13, 611 (1964), and "Silicon-Controlled-Rectifier Long-Pulse Driver for Injection Lasers," Rev. Sci. Instr. 39, 973 (1965). While at Cornell University, he also co-authored an article entitled "Growth and Properties of Ruby Whiskers," to be published in J. Appl. Phys. (March, 1966).

During summer vacations, Mr. Teich has worked for the MITRE Corp. in Bedford, Massachusetts, North American Aviation Space and Information Systems Division in Downey, California, and the Motorola, Corp. in Chicago, Illinois.

He has also spent one summer at the N.V. Philips Gloeilampenfabrieken in Eindhoven, The Netherlands, under a student technical exchange program. Mr. Teich is a member of the American Physical Society, the Optical Society of America, and the Institute of Electrical and Electronics Engineers.

ACKNOWLEDGMENTS

It is a pleasure to thank my major advisor, Professor George J. Wolga, for suggesting this topic, and for his invaluable guidance and continual encouragement throughout the course of this investigation. I would like to thank Professors Donald F. Holcomb and Lester F. Eastman for acting as members of my special committee, and for reading the manuscript of this thesis and providing helpful comments. The members of the Quantum Electronics Laboratory at Cornell University, and in particular, D. A. Berkley, are to be thanked for many stimulating and informative discussions. It is a pleasure to acknowledge David M. Schuster for valuable suggestions and encouragement. Walter Hurley was very accommodating in his help with some translations from the German.

I am very grateful to A. L. McWhorter and T. M. Quist of M.I.T. Lincoln Laboratory for providing the semiconductor injection lasers which made this work possible. T. M. Quist is to be thanked for especially patient and helpful tutoring concerning their use. R. O. Carlson and T. J. Soltys of the General Electric Research Laboratory, and C. L. Tang of Cornell University (through the Raytheon Co.) also made semiconductor injection lasers available to me.

Fellowship support during the tenure of this work was kindly provided by Cornell Aeronautical Laboratory through the James Clerk Maxwell Fellowship and by the Ford Foundation through a Special Engineering Fellowship. Assistance from Professors G. C. Dalman and L. F. Eastman for the year 1962-63 through Contract No. AF30(602)-2573 (Rome Air Development Center, Griffis AFB, New York) is also acknowledged. Financial support for the project was provided by the Advanced Research Projects Agency through the Materials Science Center at Cornell University. I would like to thank Mrs. Betty Blake and Mrs. Barbara Boettcher of the Materials Science Center for their fine secretarial and drawing work, and for their cheerful cooperation.

TABLE OF CONTENTS

Chapter Page

LIST OF FIGURES

LIST OF TABLES

ABSTRACT

Two photon volume photoelectric emission from sodium has been observed. The two quantum yield for the process, $\Lambda(\lambda,T)$ was found to be

$$\Lambda\,(8450A,\ 300°K) = 8\times10^{-16} I_o \text{ amps/watt},$$

where I_o is the intensity of the incident radiation in watts/cm^2. A theoretical model for the process, in which the interaction arises from direct interband transitions, gives a double quantum yield which is in good agreement with the observed value above.

By illuminating the sodium surface with two superimposed laser beams which were obtained from the same source, two photon dc photomixing has also been observed. With the laser operating well above threshold, the dc photomixing current $i_T^{(2)}$ was found to respond to

$$i_T^{(2)} \propto (I_1+I_2)^2 ,$$

where I_1 and I_2 are the intensities of the individual beams. This result is discussed in terms of quantum mechanical coherence theory. Using results recently derived by Titulaer and Glauber, it is shown that one double-quantum detector may be used as a self-integrating Hanbury Brown-Twiss type experiment.

The two quantum current induced by a thermal source of intensity I_o is shown to be twice as large as the two quantum current induced by a single-mode laser of the same intensity. Because this effect arises from photon correlations, a similar result should also hold for other two quantum processes. Other experiments are proposed in which the double quantum photoelectric effect may be used to provide information about higher order correlation functions for the radiation field.

Finally, a simple method of work function estimation is discussed, in which only one (single quantum) photocurrent measurement is necessary. The method requires the incident photon energy to be less than the work function of the material under investigation, and relies on the rapid decrease of the density of states above the Fermi level.

I. INTRODUCTION

With the development of the laser, double quantum transitions of various types have been observed in the optical region of the electromagnetic spectrum.[1-4] Research in such higher order effects has also resulted in the observation of double quantum transitions involving a combination of coherent and incoherent,[5] and completely incoherent[6,7] radiation.

Double quantum photoelectric emission becomes important when the first order effect is "forbidden," that is, when

$$\frac{e\varphi}{2} < h\nu < e\varphi$$

where $h\nu$ is the photon energy and $e\varphi$ is the work function of the metal under consideration. A theoretical treatment of the double quantum surface photoelectric effect in a metal was first given by R. L. Smith[8] in 1962. Smith used the Sommerfeld model of a metal, and made a second order perturbation theory calculation of the photocurrent. He concluded that observation of this effect should just be possible. The theoretically predicted double quantum surface photocurrent is proportional to the square of the incident radiation power and inversely proportional to the area irradiated.

Smith's result was extended to the case of a sinusoidally modulated signal* by Bowers[9] in 1964 who, in addition, corrected some errors in Smith's development. Also in 1964, Adawi[10] obtained a more general formulation of the two quantum surface photoelectric effect by using the steady-state method of scattering theory, which is equivalent to the time-proportional transition method. In the limit of the square well potential, the photocurrent obtained by Adawi reduces to Smith's corrected result.

A theoretical treatment of the double quantum volume photoelectric effect in a metal was given by P. Bloch,[11] also in 1964. In this case, transitions occur between energy bands within the bulk of the material rather than at the surface. Just as Smith's second order treatment of surface photoemission is based on the earlier first order treatment given by Mitchell,[12] Bloch's second order treatment of volume photoemission is likewise based on the earlier first order treatment given by Fan.[13] As in the case of surface photoelectric emission, the theoretically predicted double quantum volume photocurrent is proportional to the square of the incident radiation power and inversely proportional to the area irradiated.

---

* When the modulation period is much greater than any characteristic time in the photoemission process, the adiabatic approximation yields this extension for arbitrary waveform.

For the alkali metals, Thomas and others[14-17] have given clear experimental evidence indicating that first order photoelectric emission is purely a volume effect. In the immediate vicinity of photoelectric threshold, nevertheless, there is still some question regarding the mechanism of photoemission, although there is good evidence[13-15] that the volume effect is the primary mechanism in this region as well. For photon energies well above the threshold, photoemission studies on copper and silver have shown the data to be completely consistent with a volume effect. Furthermore, nondirect optical transitions have been shown to be stronger than direct ones in both metals.[18] Thus, conservation of crystal momentum ($\vec{k}$) need not be an important selection rule in the photoelectric process.[19]

Several attempts had been made to experimentally observe the double quantum photocurrent from a metal,[9,11] in order to establish the validity of a particular theoretical model, but various experimental difficulties complicated the task. This work reports the observation of double quantum photoelectric emission[8-11] and cw photomixing from sodium metal. Two photon photoelectric current was obtained from a sodium surface of work function 2.0 eV when irradiated by photons of energy 1.48 eV from a GaAs semiconductor injection laser. Because of the

small size of the photocurrent, it was necessary to use coherent (phase-sensitive) detection[20,21] to observe it.

A quantity suitable for describing the efficiency of double quantum photoelectric emission is the "double quantum yield", $\Lambda(\lambda)$ expressed in amps/watt.* Here, λ is the wavelength of the incident radiation. Because a second order effect is under consideration, Λ will be proportional to the intensity I_o of the incident radiation. For double quantum photoelectric emission from sodium metal, Λ has been experimentally found to be

$$\Lambda_{Na}\ (8450A) = 8\times10^{-16}\ I_o\ \text{amps/watt}$$

where I_o is the intensity of the incident radiation at 8450A expressed in watts/cm^2. This value is about 1000 times larger than the theoretically expected value calculated on the basis of Smith's[7] model. It is in order of magnitude agreement with the theoretically expected yield calculated on the basis of the volume photoelectric effect, however. For this calculation, a model permitting only interband transitions was used. Considering the intermediate state to be virtual, the $\vec{A}.\vec{p}$ term

---

* This quantity is called the efficiency since it is very closely related to the number of photoelectrons emitted per incident photon: Λ(amps/watt) = $\frac{e}{h\nu}\Lambda$(electrons/photon) where $h\nu/e$ is the photon energy expressed in eV and is of order unity.

in the Hamiltonian was found to be dominant. The model used is somewhat similar to that used by P. Bloch but differs from it in several significant respects. The agreement with theory, plus the large increase in double quantum current which was observed upon coating more sodium onto the experimental surface, provide evidence that the two quantum emission observed arises from a volume effect.

Single quantum photoemission can also take place for $h\nu<e\varphi$, although with greatly reduced efficiency. This emission comes about from the high energy electrons present in the Fermi tail for a material at temperature $T>0°K$. This type of single quantum photoemission has also been observed. The photoelectric yield for this process has been found to be (experimentally)

$$Y(8450A,\ 300°K) = 1.7\times10^{-15}\ \text{amps/watt}.$$

This single quantum yield is, of course, independent of I_o. With the help of the Fowler theory of photoemission, the value of yield above has been used to provide a good estimate for the work function of the sodium surface. This method of work function estimation entails only one measurement of the photoelectric yield, with a radiation source whose photon energy is less than the work function of the material. It should be a generally applicable method.

Indirect experimental evidence indicates that this single quantum emission (from electrons in the Fermi tail) may arise from a surface effect. This is based on the observation that for experiments with a freshly coated sodium surface, "pure" double quantum photoemission has been obtained, the admixture of single quantum being <.03%.

Double quantum photoelectric emission has also been obtained in materials other than metals. H. Sonnenberg, H. Heffner, and W. Spicer[22] obtained double quantum volume photoelectric emission from Cs_3Sb, a semiconductor. The source of radiation was a Nd-doped-glass laser which emits photons with an energy of 1.17 eV. The photoelectric threshold energy for the first order effect in Cs_3Sb is about 2 eV as it is in Na metal. The observed double quantum photoelectric yield from Cs_3Sb was

$$\Lambda_{Cs_3Sb}(8450A) = 1.1 \times 10^{-11} I_o \text{ amps/watt},$$

where I_o is the incident light intensity in watts/cm^2. This result has been corrected* to λ = 8450A so that it

---

* The correction from 1.06μ radiation as used by Sonnenberg, Heffner, and Spicer[22] to .84μ radiation was small. It was obtained by simply evaluating the equation for the two photon volume photoelectric current density j_v given by Jha[22] for both 1.17 eV photons (1.06μ) and 1.48 eV photons (.84μ). The following ratio was obtained:

$$\frac{j_v \text{ (}Cs_3Sb\text{, 1.48 eV)}}{j_v \text{ (}Cs_3Sb\text{, 1.17 eV)}} = 0.55.$$

may be directly compared with the results obtained for Na metal. It may be seen that

$$\Lambda_{Na} = 7\times10^{-5}\Lambda_{Cs_3Sb}$$

showing that the double quantum yield from Na is smaller than the double quantum yield from Cs_3Sb at 8450A by a factor of $\sim10^4$. This may be compared with the ratio for the single quantum yields. Using the following numbers for the yields of the two materials at $2h\nu$: $Y_{Na}(4200A) = 3\times10^{-4}$ amps/watt[13,23] and $Y_{Cs_3Sb}(4200A) = 3\times10^{-2}$ amps/watt,[24] the following ratio obtains:

$$\frac{Y_{Na}(4200A)}{Y_{Cs_3Sb}(4200A)} \sim 10^{-2}.$$

In a unique experiment utilizing a Millikan oil-drop apparatus, Pope, Kallmann, and Giachino[7] have measured the double quantum photoelectric emission from organic single crystals of anthracene, tetracene, and perylene. These authors used a 1000 watt Hg-Xe incoherent light source, having its highest output intensity at 3650A. For anthracene, the experimentally determined value of double quantum yield was

$$\Lambda_{Anthracene} = 6\times10^{-8}\ I_o \text{ amps/watt}$$

where I_o is expressed in watts/cm^2. The authors tentatively conclude that one of the species involved in this two quantum process is either a charge-transfer exciton or a trapped electron. It may be seen that

$$\Lambda_{Na} \sim 10^{-8} \Lambda_{Antracene} ,$$

thus two quantum emission by this mechanism in anthracene is of the order of 10^8 times stronger than two quantum photoemission from sodium metal. In spite of the large two quantum yield for anthracene, the photocurrents measured in this experiment were extremely small because of the very small light power incident on each particle. With their apparatus, currents $\sim 10^{-20}$ amps have been measured.

The two quantum photoeffect is of particular interest because the two quantum process occurs in the radiation detecting device itself. The situation is unique since, in addition to providing information about the higher order physical process occurring in the detector, an opportunity is available to gain information about the properties of the incident radiation field, a topic about which there has recently been considerable discussion.[25] For a two photon detector, the counting rate is expected to be proportional to a second order correlation function,[26-28] while for the usual square-law detector,

the counting rate is proportional to a first order correlation function, and thus is proportional to the intensity of the incident beam.

The two quantum photomixing experiments described in Chapter V were initially intended to provide explicit information about the coherence time and second order coherence properties of the incident radiation. An analysis is given, in which it is shown how the two photon effect may be used as a self-integrating Hanbury Brown-Twiss type[29-32] photon correlation experiment by introducing a time delay between the two incident beams. Because of the difficulty of achieving high quantitative accuracy in the two quantum measurements, however, it was not possible to perform this experiment. Nevertheless, results of this mixing experiment were obtained with the laser operating well above theshold. It was observed that a double quantum detector in this case responds as

$$i_T^{(2)} \propto (I_1 + I_2)^2$$

where $i_T^{(2)}$ is the double quantum emitted photocurrent, and I_1 and I_2 are the intensities of the individual beams. This gives rise to a d.c. photomixing term $2I_1I_2$, corresponding to the two ways in which one photon can be absorbed from each beam. By using the second order correlation functions considered by Glauber[26,27] and by Titulaer and

Glauber,[28] this result is justified. It is also shown that the two quantum photocurrent induced by a thermal source is expected to be just twice that induced by a single mode laser source. Fourth order correlation functions of the field are discussed in connection with a proposed Hanbury Brown-Twiss type experiment using two double quantum detectors. Finally, a short discussion of two quantum excess noise and photocounting statistics is given.

The experimental apparatus used in this work is described in detail in Chapter II. In particular, the laser power supply and the sodium surface phototube were specially constructed for these experiments and a full account of them is therefore given. In Chapter III, a discussion of the theoretical aspects of two quantum processes, and of photoemission in general, is given. Chapter IV is concerned with the experimental observations relating to the double quantum photoeffect from sodium. Finally the double quantum photoemission obtained from the coincident focusing of two light beams (double quantum photomixing), and the higher order correlation functions for double quantum detectors are discussed in Chapter V.

II. THE EXPERIMENTAL APPARATUS

This chapter is divided into several sections each of which discusses one component of the overall experimental system in detail. Particular attention is given to the laser power supply (sec. B) and to the sodium surface photomultiplier tube (sec. C), since both were specially constructed for this experiment. The other sections are devoted to the laser (sec. A), and to a signal analysis of the system (sec. D).

A. The Laser

For the experiments on two quantum photoelectric emission, a GaAs semiconductor injection laser[33,34] was used as the source of radiation. The injection laser was chosen because of its relative high power, its ease of modulation and operation, and its convenient frequency. GaAs lasers were obtained from three sources: (a) M.I.T. Lincoln Laboratory (Lexington, Mass.), (b) G. E. Research Laboratory (Schenectady, N. Y.), and (c) Raytheon Co. (Bedford, Mass.).

The lasers were mounted in a copper (heat sink) block supported in a styrofoam dewar by cylindrical brass tubes which also served as exit ports for the radiation (Fig. 1). They were operated in air at 77°K; the 8450A radiation emerged through an antireflection coated glass window. A warm air blower was directed at the exit window to prevent

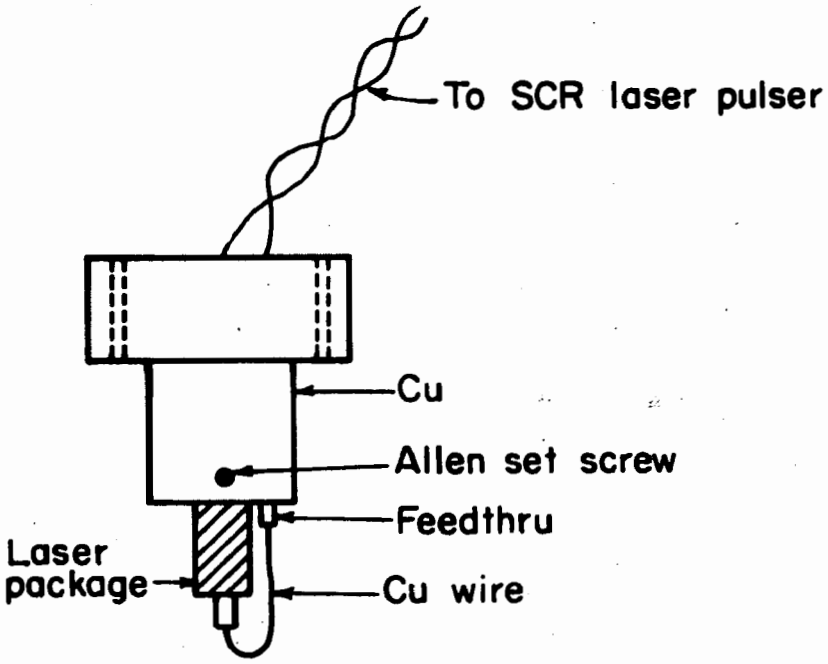

(a) Copper plug and laser (side view)

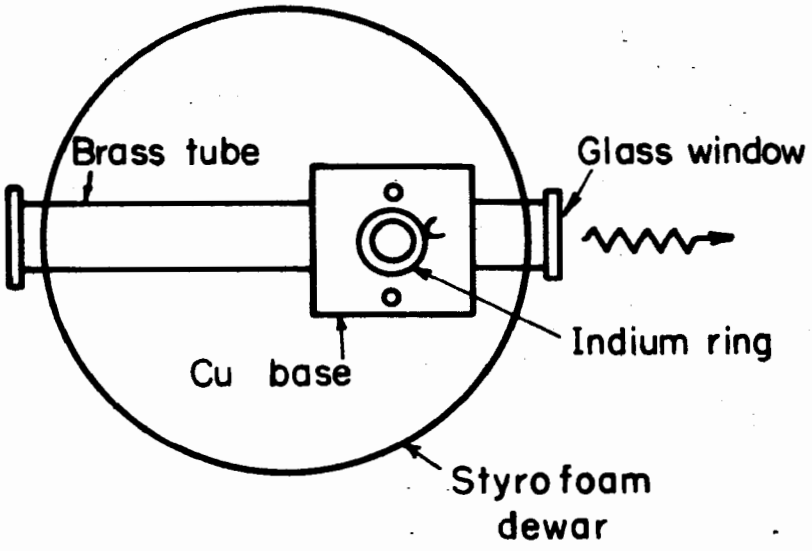

(b) Copper base mounted in styrofoam dewar (top view)

Figure 1. Laser holder. The laser is secured in the solid copper plug (a) by means of an Allen set screw, as shown. Dotted lines represent screw holes for mounting plug (and laser) in the copper base (b). The hole in the copper base which receives the plug is drilled halfway through. The plug is sealed to the base by a gasket of indium wire, which keeps liquid nitrogen from entering the region of the laser. The base is supported in a styrofoam dewar by cylindrical brass tubes which also serve as exit paths for the radiation. Figures are not to scale.

it from frosting. The peak output radiation power of several of these lasers, measured with a calibrated Dumont 6911 photomultiplier tube,* is given in Table I. The lasers were operated with the SCR pulser described in the next section, using a full pulse width of ≃35μsec, a peak curent of 21 amperes, and a pulse repetition rate of 2.2 kHz. These values were close to optimum for obtaining maximum output power from the lasers. Higher values of current, repetition rate, or pulse width tended to decrease the laser output power because of junction heating.

As can be seen from Table I, M.I.T. laser LD259 was used in all experiments performed before recoating the sodium surface photomultiplier tube (see Chapter IV). For experiments performed after recoating, however, M.I.T. laser LD256 was used. LD256 and LD259 behaved almost identically in all respects. The following discussion of the properties of the emitted laser radiation is therefore restricted to M.I.T. Lincoln Laboratory LD250 series semiconductor lasers. The M.I.T. laser configuration is shown in Figs. 2 and 3.

1. Output power related to input current

The radiation power output for a typical M.I.T. laser, as a function of both the commutation circuit voltage (see Sec. B), and the peak current supplied to the laser, is

* The Optics Technology Corp. Model 610 Optical Power Meter was found to respond nonlinearly to pulsed radiation at 8450A and thus could be used only for qualitative measurements. The power meter was used quantitatively for cw radiation at 6328A, however, in order to calibrate the 6911 photomultiplier.

TABLE I

PEAK OUTPUT RADIATION POWER (8450A) FROM

GaAs SEMICONDUCTOR INJECTION LASERS

Source of Laser	Identification Number	Peak Power mW	Remarks
M.I.T.	LD259	~400	used in initial experiments
M.I.T.	LD256	~400	used in later experiments
M.I.T.	LD257	-	casing broke; never used
M.I.T.	LD126	~ 10	not used in experiments
G.E.	L1193	~150	not used in experiments
G.E.	L1194	-	never used
Raytheon	1938	-	never used
Raytheon	1939	-	never used

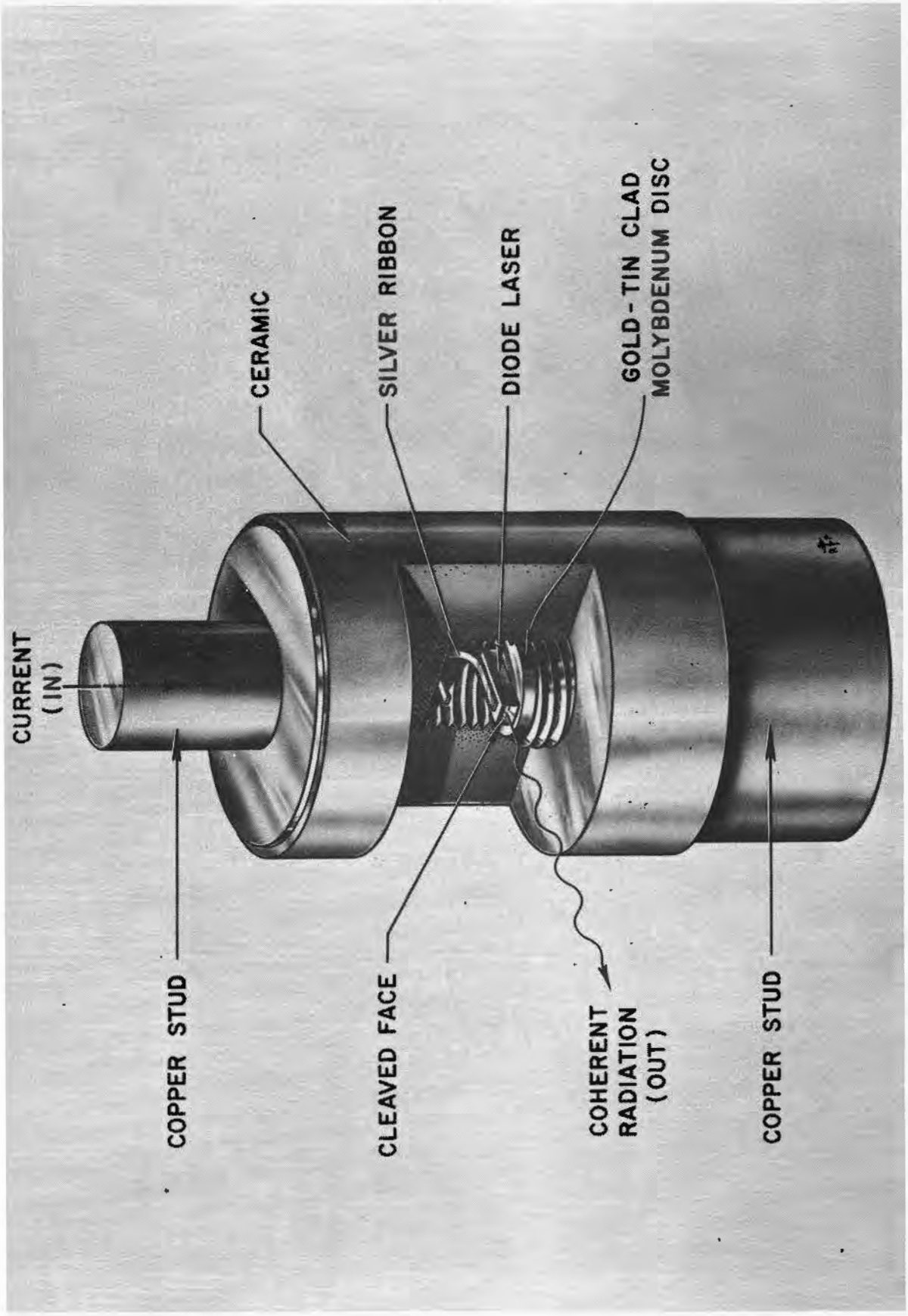

Figure 2. M.I.T. Lincoln Laboratory GaAs laser diode package (courtesy M.I.T. Lincoln Laboratory).

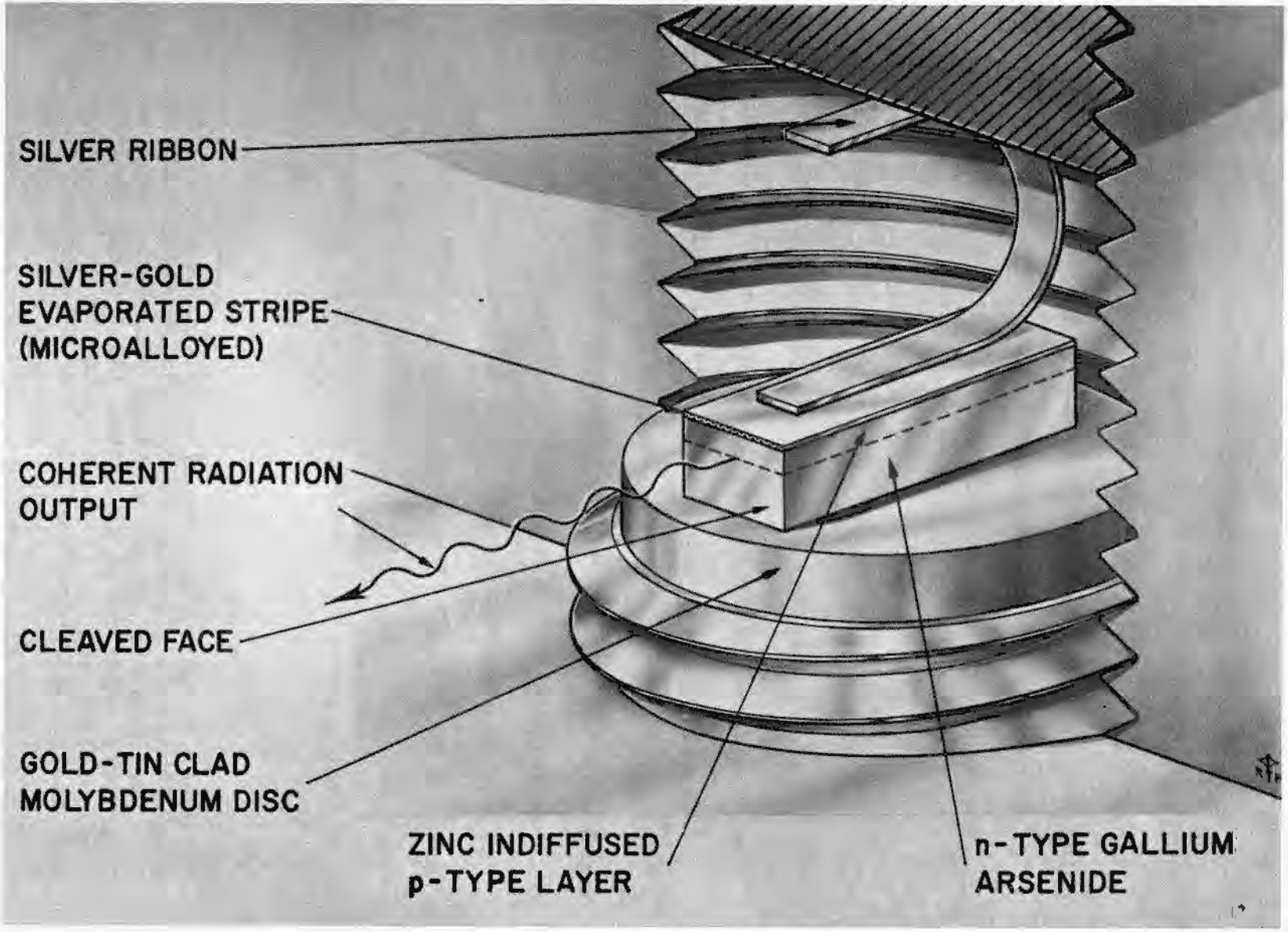

Figure 3. Magnified view of the M.I.T. semiconductor injection laser (courtesy M.I.T. Lincoln Laboratory).

given in Table II. The operating conditions are the same as those descirbed earlier. In performing experiments, the laser was generally operated at its highest power, attenuation being provided by calibrated filters. This method was used so as not to introduce extraneous variables into the experiment, such as changes in the radiation spectrum or the emitting area which occur with changing laser current.

2. Emitting area and intensity

For currents sufficiently above threshold current, the emitting junction of the laser is essentially a line which has the width of the laser diode (~200μ), and an effective height of ~10μ for GaAs.[35] Thus, the emitting area may be estimated at 2×10^{-5} cm^2. Because the dimensions of the emitting junction are larger than the diffraction limit of the lens used to focus the radiation onto the Na surface,* the junction may be imaged on the sodium surface. For the experimental configuration used, the image distance was approximately equal to the object distance, giving a magnification of unity.

* The diffraction limit of a lens is given by λf where λ is the wavelength of the radiation and f is the f-number of the lens. The lens employed in the two quantum experiments has a focal length of 57 mm and a diameter of 50 mm, and is therefore about f/1. The diffraction limit of the lens is thus ~1μ, sufficiently smaller than a dimension of the emitting junction.

TABLE II

TYPICAL OUTPUT RADIATION POWER FOR M.I.T. LASER RELATED TO PEAK LASER CURRENT AND TO COMMUTATION CIRCUIT VOLTAGE (SRC VOLTS)

Variac setting	SCR volts	Peak current (amps) (LD259)	Peak power output (mW) (LD256)
$\simeq$ 6	$\simeq$ 7		<10
7	8	$\simeq$ 7	$\simeq$30
9	10	8	
12	12.5	9.5	130
14	15		230
17.5	18		290
20	20	19	320
22	22.5		400
23.5	23.5	21.5	

At the maximum power of 400 mW (1.7×10^{18} photons/sec), the intensity of the imaged beam is then $\simeq$ 20,000 W/cm^2 (7.5×10^{22} photons/cm^2-sec). This corresponds to a maximum electric field of 2.7×10^3V/cm.

3. Pulse shape and Fourier spectrum

An oscilloscope trace of the output of M.I.T. laser LD259 observed with a Dumont type 6911 photomultiplier tube is shown in Fig. 8(b) of Chapter IV. The horizontal scale, representing time, is 10μsec/division, and the peak power output is about 400 mW. Again, the operating conditions of the SCR pulser are those described earlier. The second hump in the curve of Fig. 8(b) arises from the input current pulse, which actually attains its maximum peak current at this point.* However, the laser output has begun to decrease relative to the current input before this time because of heating. It therefore increases only a token amount at this input current spike. For lower input currents, the laser output pulse follows the current pulse much more closely.

Because of the narrow band amplifier at the input to the signal channel in the phase sensitive detector (see

---

* This spike in the current near the end of the pulse arises because of the commutation of the SCR's (see Sec. B).

Sec. D), it is only the Fourier coefficient of the signal at the frequency of phase sensitive detection which is measured.* This component of the double quantum current must therefore be estimated. A scope trace of the double quantum current waveform is shown in Fig. 8(a). This waveform may be approximated well by a cosinusoidal pulse of full width $t_o \simeq 36\mu$sec. The Fourier component at the fundamental repetition frequency $f_o = 2.2$ kHz is then found to be $\simeq (4/\pi)t_o f_o \simeq 0.1$, normalized to a unity amplitude waveform.

4. Spectroscopic observations and mode structure

Observations of the output spectrum from M.I.T. laser LD259 as a function of input current have been made by focusing the output of the laser into a Jarrell-Ash 3.4-m Ebert-type spectrograph. The laser was driven at a pulse repetition rate of 1.1 kHz and 2.2 kHz with the SCR pulser described in the next section. The pulse width was 35μsec. Measurements were made in second order, with a resolution of 2.5A/mm using a slit width of 10μ.

For SCR voltages below $\sim$ 13.5 SCR Volts (corresponding to peak currents below $\sim$ 9.5 amps), lasing occurred in

---

* The manufacturer gives harmonic rejection as 60 db for the second harmonic and 46 db for the third harmonic.

discrete modes, generally one or two of the modes dominating. Although the many lines visible on the spectrograph plate appeared to be regularly spaced, the distances between the stronger modes varied with SCR voltage, sometimes being within 2A, other times being as far apart as 10A or more. The overall breadth and appearance of the spectrum at one particular SCR voltage remained constant although different modes would dominate from experiment to experiment, depending on past history and on the pulse repetition rate. The stronger modes appeared somewhat broader than the weaker ones. The experimentally observed spacing between adjacent lines was determined to be $\simeq$ 1.2A which is in agreement with the calculated spacing $c/2n\ell$ of adjacent axial Fabry-Perot modes.[36] Here, c is the speed of light in vacuum, n is the index of refraction of the material filling the resonator, and ℓ is the length of the resonator. For GaAs, n = 3.3, and for the M.I.T. lasers, ℓ = 1 mm. Thus $\Delta\lambda_{calc.}$ = 1.1A, which corresponds to a frequency difference of 45 kMHz.

At SCR voltages $\gtrsim$ 15 SCR Volts (corresponding to $\gtrsim$ 12 amps peak current), many more lines began to appear, the spectrum broadening while its center moved to higher wavelength. These results can be understood on the basis of the temperature rise occurring in the laser during the pulse. The observations are in agreement with those of

Gooch[37] who did time-resolved spectroscopy of GaAs laser diodes driven with 10 amp, 20μsec pulses. The displacement to longer wavelength of the center of the spectrum with increasing current may be thought of as resulting from an increased average junction temperature. For a peak current of $\simeq$ 8 amp at a pulse repetition rate of 2.2 kHz, the center of the spectrum lies at about 8400A, while for a peak current of $\simeq$ 21 amp, it increases to about 8440A. As expected, for a given current, the optical spectra for a 1.1 kHz pulse repetition rate lie at shorter wavelengths than the spectra for a repetition rate of 2.2 kHz.

The increase in the width of the spectrum from about 10A at 8 amps to about 55A at 21 amps is seen to arise from the change in the temperature of the diode (and hence the emission) as a function of time, the spectrograph recording all of the modes which emitted radiation any time during the pulse duration. Thus, although at any <u>instant</u> of time a relatively narrow group of discrete modes would be expected, the spectrograph integrates over all time, producing a broad and somewhat smeared spectrum.

Some data was taken with very short pulses ($\sim$1μsec) and very low duty cycle ($<10^{-4}$) using a commercial General Electric Type C7780135 Laser Pulser.*

* The author wishes to thank J. Wenzel of the General Electric Co., Ithaca, N. Y., for the loan of this pulser.

Although good spectrographic plates were not obtained, it was observed that the center wavelength of the emitted spectrum was located at about 8330A, which is well below the values observed with long pulse length, long duty-cycle excitation as described earlier. This result is expected, since the temperature of the diodes should be far lower when fed with the short, low duty-cycle pulses.

Finally, it should be mentioned that at currents ~10X threshold, Hooge and Kalter[38] have observed that mode structure and coherence of the laser output disappear. They attribute the smooth band observed, which has a width of 15-20A, to saturation occurring in a distance smaller than the length of the diode. The experiments performed here have been well below this limit, however.

5. Polarization

The polarization properties of the radiation emitted from a GaAs semiconductor injection laser are generally a local phenomenon for each lasing filament, and vary with injection current.[39] Certain statistical trends of the polarization with injection current are evident, however, and may be categorized. In particular, the output from M.I.T. laser LD259, operated in the pulsed mode with the parameters given earlier, was found to be approximately 75% polarized with the E-vector preferentially parallel to

the plane of the junction.

B. The SCR Laser Pulser*

In order to obtain a measurable double quantum current, a laser pulser supplying relatively long pulses of high current at a high duty cycle was required. Since most of the pulsers available for driving semiconductor lasers provide rather short pulses (< 1μsec), a pulser based on a silicon-controlled-rectifier (SCR) multivibrator circuit[40] was designed to meet these requirements. The laser pulser has been used to drive both M.I.T. Lincoln Laboratory and General Electric GaAs injection lasers. The supply provides pulse lengths from about 30μsec to 1 second** with duty cycles as high as 100%. It has been previously mentioned that for the double quantum experiments described in this work, pulses of 35μsec duration at a pulse repetition rate of 2.2kHz were used to drive M.I.T. lasers LD256 and LD259.

Although similar to the standard commutation circuit pulse shape (which is asymmetrical rather than square), the precise shape of the laser current pulse depends upon the particular values assigned to circuit components L1 and C2

---

* For a published account of this work, see Rev.Sci. Instr. 36,973 (1965).

** The upper limit depends only on the maximum pulse length capability of the unit pulser used to drive the SCR pulser. The Genral Radio 1217C provides pulses of up to 1 sec in duration.

(see Fig. 4). Increasing the values of these components provides a rounder but more symmetrical pulse shape. Since these components affect only the beginning and end of the pulse, however, pulses greater than about 100μsec appear essentially square. Currents of about 21 amperes have been obtained with the pulser shown in Fig. 4, but it is an easy matter to increase this current by increasing the power capabilities of the circuit components. A protection circuit was incorporated in the pulser to prevent damage to the laser in the event of a circuit failure. A small unit pulser, such as the General Radio 1217, is required to drive the SCR pulser. In the double quantum experiments, a GR1217A pulser was used because of its ready availability. The GR1217B was found to be superior, however. Laser current pulse length and repetition rate are regulated directly by the controls on the unit pulser, while laser current amplitude is controlled by the Variac (T1). The three constituent blocks of the pulser (dc power supply, commutation circuit, and protection circuit) are indicated in Fig. 4.

The pulse length setting on the unit pulser must be above a certain minimum value in order for the SCR pulser to operate. The lower limit on pulse length is governed by the value of commutation capacitor C3 (in conjunction with R1 and R2). However, if the capacitance is below a

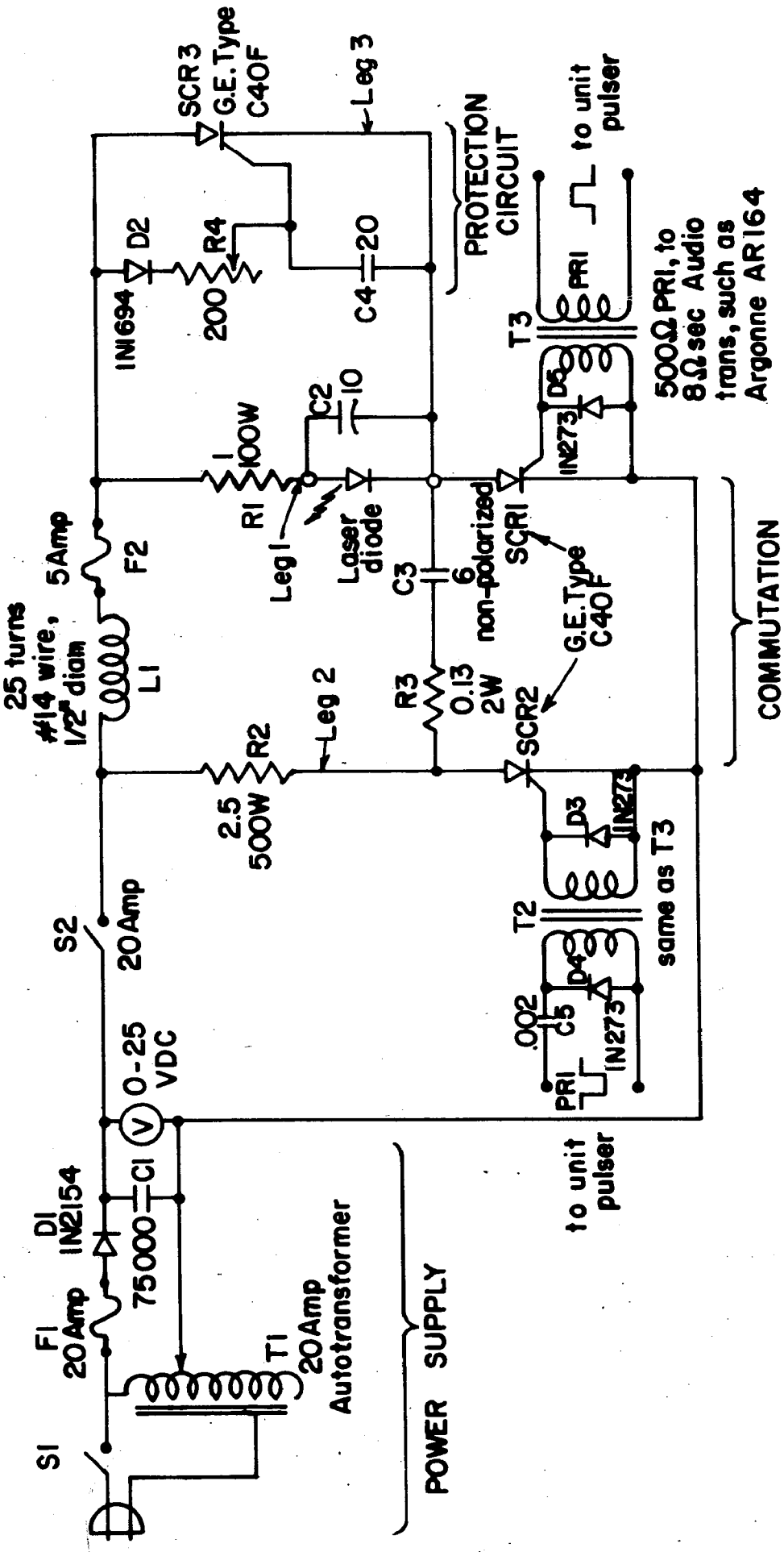

Figure 4. Schematic diagram for the SCR laser pulser. The three constituent blocks (dc power supply, commutation circuit, and protection circuit) are indicated. All resistors are wirewound, and values are given in ohms. Capacitors have a minimum working voltage of 25 V dc, and values are given in μF.

critical value (which depends on the individual circuit), the circuit will not commutate at all. A commutation capacitance of 6μF has been found to be suitable. It provides a minimum pulse length of 30μsec. For best operation, the dc resistance of legs 1 and 2 of the commutation circuit (see Fig. 4) have been made as close as possible. Circuit elements L1 and C2 were inserted to reduce the current spike which typically occurs at the end of each pulse in a multivibrator circuit. Resistance R3 was inserted to minimize transients. Small transformers were used to couple power from the unit pulser to the SCR gates. Capacitor C5 combined with the transformed secondary impedance of transformer T2 (about 2500Ω) form a pulse differentiator, which when combined with diode D4 insures that SCR is properly triggered at the end of the unit pulser input pulse. Proper heat sinking for the SCR's was provided by the use of mica insulating kits and silicone high thermal-conductivity grease.

The protection circuit operates by integrating the signal appearing across the laser. After a specified time delay (determined by the capacitance C4 and the protection potentiometer R4), SCR3 is triggered thereby shunting the laser. Because the resistance of this leg (leg 3) is low, a very heavy current is drawn, causing fuse F2 to blow quite rapidly. Thus, if for any reason, current flows

through the lasers for a time longer than that prescribed by the setting of R4, current to the laser is cut off. The value of F2 was chosen to be just above the <u>average</u> laser current. Protection resistance R4 was adjusted such that the time to trigger SCR3 be longer than the pulse length but shorter than the damage time to the laser. For operation at pulse lengths longer than several hundred microseconds, it might be necessary to increase R4, C4, or both.

The components employed in the pulser were used because of their ready availability. Therefore, although the particular values used in the supply are those specified in Fig. 4, many of these (especially the small diodes and transformers) are not critical. In fact, it is not certain that the SCR's used were C40's since they were not marked. The unit has been operated with C40's, however. The capacitors used for filtering (C1) were as large as could conveniently be obtained. Even with these large capacitors, a small amount of ripple remained giving rise to a 60 cycle modulation of a few per cent on the light output from the laser. This can be eliminated by the insertion of a very low resistance choke. A 20mH iron core inductor having a dc resistance of 1Ω in a standard π-configuration filter following the rectifier diode D1 was found to suffice. This reduced the ripple by a factor of 50, but necessitated

a higher working voltage for the input capacitor. Since the 60Hz ripple could have no effect on the two quantum experiment, however, the choke was not used during the experiments.

Capacitors of the large size used in the filter section invariably have low working voltages, and care has been taken not to exceed the stated value. In fact, the maximum current available to the laser was limited to about 21 amperes by the capacitor (C1) working voltage of 25 volts. The maximum deliverable current may be increased by increasing the ratings of the various components in the pulser. A small viewing resistor (.064ohm) was inserted in series with the laser to monitor the current, but the scope used to measure this current had to be isolated from ground. Initial adjustments and tests were made with a 1/2ohm resistor or a test diode replacing the laser. The pulser is operated by first turning on the unit pulser, and then advancing the Variac to provide more than 10V dc. Switch S2 is then closed to start laser operation. If this order is not followed, the circuit will not commutate properly and fuse F2 may blow.

A gate-turn-off device (GTO) would seem to provide an even simpler method for designing a laser pulser: A single GTO could be used, eliminating the commutation circuit and raising the efficiency of the unit to nearly

100%. Unfortunately, however, the present state of the art of these devices does not now allow them to handle currents of this magnitude.

C. The Sodium Surface Photomultiplier

A specially constructed photomultiplier containing a vapor-deposited sodium surface was used in the double quantum experiments.* A photomultiplier was used rather than a simple phototube in order to gain the advantage of "noise-free" electon multiplication. The glass envelope containing the photomultiplier structure, as well as the dynode material and the structure itself were the same as those used in the commercial Dumont type 6911 photomultiplier.

Two types of sodium photomultipliers, both manufactured by Dumont-Fairchild Laboratories (Bloomfield, New Jersey) were used. Type KM2462 had sodium deposited only on one element of the structure, that which is generally used as the first dynode in the standard 6911. The dynode is constructed of grade A nickel. Type KM2519 was a photomultiplier in which the sodium was deposited in a semi-transparent layer on the front face of the glass envelope. This is the configuration of the standard front surface photomultiplier (e.g. Dumont 6911, RCA 7102). Because the

---

* This suggestion was made by Dr. J. M. Schroeer.

first dynode was used as the cathode in KM2462, there are 11 stages of electron multiplication rather than the standard 12, as in KM2519.

Both photomultipliers contain thermal generators so that sodium could be deposited on the cathodes at any time. These generators consist of a small, cylindrical (~2mm diameter x 1.5 cm long) grade A nickel collar containing $NaCrO_4$ and Si. External leads permit the collar to be heated by means of an electric current which causes the Si to reduce the $NaCrO_4$, liberating Na vapor. The vapor deposits on the (relatively cold) cathode. Of the two sodium surface tubes, only the dynode surface tube KM2462 was used for double quantum experiments for reasons discussed below (section C7). Experiments were carried out on a portion of the cathode surface which is flat, and lies perpendicular to the incident radiation. A spot was generally chosen which lies in a region parallel to, but in from the cathode edge by about 1-2mm. The sensitivity of the Na surfaces to white light has been determined by the manufacturer to be $\simeq$ 1-2μamp/lumen, while the response time is given as $\simeq$ 25-30nsec, not including the limitation on response time placed by the load resistor and the output capacitance ($\simeq$ 4-6pF). Specific properties of the sodium surface photomultiplier tube KM2462 pertinent to the observation of double quantum photoelectric emission are discussed below.

1. Choice of sodium

Sodium metal was chosen as the material to be investigated for the following reasons: (a) Ample data is available on the photoelectric and other solid state properties of sodium. (b) It is a simple metal with a spherical Fermi surface, for which a relatively unsophisticated theory would be expected to apply. (c) The work function ($\sim$ 2eV) is ideal for the observation of two photon photoemission using incident radiation at 8450A ($\sim$1.5eV). The work function is sufficiently low so that two photons may overcome the surface potential, and yet sufficiently high so that single quantum photoemission form the Fermi tail will not swamp the double quantum photoemission.

2. Fowler plot

A Fowler plot[41,42] was used to determine the photoelectric threshold frequency (work function) of the Na surface in KM2462.[43] A Cary model C-14 spectrophotometer was used as the source of radiation for the measurements. The light output of the spectrophotometer was kept constant by internal controls. The output of the photomultiplier was measured across a 100kΩ load resistor by a Bausch and Lomb model VOM-6 chart recorder. Measurements were made for various incident wavelengths ranging from 7900A to 3500A.

For photons below 2.3eV, the Fowler plot yielded a work function of 1.9 ± 0.1eV while at photon energies corresponding th $2h\nu$ = 2.96eV, the work function was found to be 2.3 ± 0.1eV. This latter value is therefore more appropriate for calculating the two quantum current. The difference in work function at different incident photon energies may be understood in terms of the presence of a small number of crystallites with a low work function orientation. Above the photon energy 2.3eV, the contribution to the photoelectric emission from these crystallites may be neglected; it is important only when photoemission from the more numerous higher work function crystallites is forbidden. The work function of metallic sodium is given variously as 1.9 to 2.46 eV.[44]

3. Work function estimation by absolute yield measurement

In this section, a simple method is proposed for estimating the work function of a material. It requires only one measurement of the single quantum photoelectric yield, which must be made with incident photon energies below the photoelectic threshold. As an introduction to the method, a brief discussion of the mechanism of single quantum photoemission in the vicinity of the photoelectric threshold is given.

(a) Photoemission near threshold: Photoemission of

electrons from metals is observed with incident photon energies which are near or even below the photoelectric threshold energy. To understand how this interaction occurs, a schematic diagram of the one dimensional dispersion curves for the conduction and next higher energy bands are shown in Fig. 5 for a typical alkali metal. On this diagram, the interband threshold energy for direct transitions, $h\nu'$ (this is the minimum incident photon energy for which $\vec{k}$- conserving interband transitions may occur at 0°K) is shown to lie below the photoelectric threshold energy $e\varphi$ (work function). This relation,

$$h\nu' < e\varphi \qquad (2.1)$$

is generally satisfied for pure elements, e.g. elements which do not have monolayers of other elements deposited on them.*

From the diagram, it is seen that electrons located near or above the Fermi level cannot escape from the metal by means of direct transitions. These electrons do escape, however, as evidenced by the experimentally observed temperature dependence of photoemission. Therefore, these electrons either escape by means of indirect (phonon-assisted) transitions[17] (as shown by the oblique line in Fig. 5), or by means of the surface photoelectric effect, which cannot be represented on this diagram. In the case

* For example, for Na: $h\nu' = 2.06eV \lesssim e\varphi = 2.25eV$; for K: $h\nu' = 1.24eV < e\varphi = 2.25eV$; for Ag: $h\nu' = 3.9eV < e\varphi = 4.4eV$. For the sodium surface in KM2462, however, $h\nu \simeq e\varphi$.

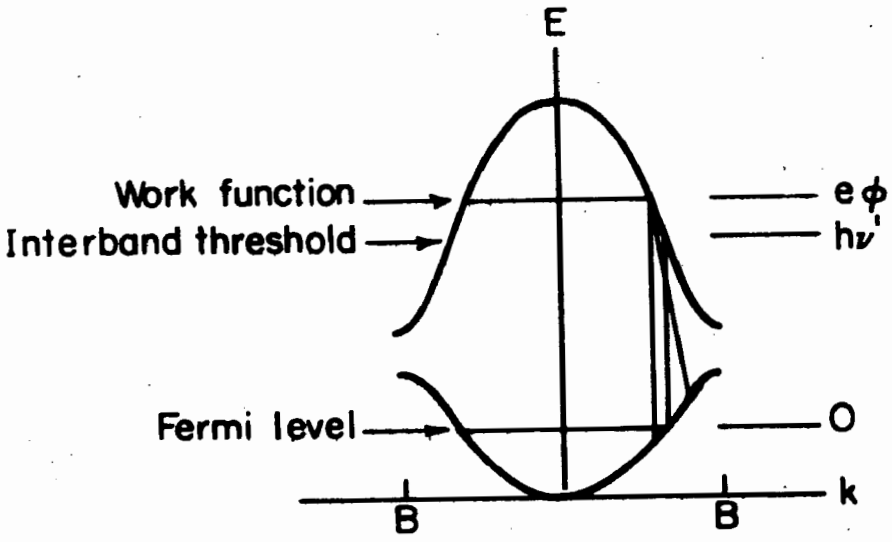

Figure 5. Schematic diagram of (one dimensional) lowest energy bands for alkali metal in reduced zone scheme (not to scale). B represents the Brillouin zone boundary. Oblique line represents the only escape path via volume photoemission of an electron in the Fermi tail.

of the surface photoeffect, of course, the surface itself provides for momentum conservation. Which of these mechanisms is more important in the immediate vicinity of threshold is a question which has not yet been completely resolved.[14,15,42,45,46] In Chapter IV, section C2, experimental evidence is presented which could be interpreted as indicating that the single quantum emission arising from electrons in the Fermi tail is a surface effect.

In the discussion to follow, however, it will be shown that the particular mechanism giving rise to the photoemission (be it surface or volume) is not significant.[15,17]

(b) Application of Fowler theory: In the immediate vicinity of threshold, the validity of the Fowler theory[41] relies upon the stationarity of all variables in comparison with the rapidly varying Fermi function (with incident frequency and temperature). Because this condition is satisfied for both a volume and a surface model of photoemission, the Fowler theory cannot be used to distinguish between the two;[15] it is an approximation to both models in the region near threshold.[15,17] The proportionality constant α, in the expression for the yield (see next paragraph) is determined experimentally in the Fowler theory. If it were desired to <u>theoretically</u> calculate the proportionality constant α, then a detailed knowledge of

the stimulating mechanism would be necessary since this constant contains the matrix element for the transition and the probability of electron escape over the surface barrier. For a volume effect, it also contains the attenuation factor of the incident radiation, and the escape depth of the photoelectrons.

It is clear that the Fowler theory for photoemission is valid in the vicinity of (both <u>below</u> and <u>above</u>) the photoelectric threshold. The specific applicability of the theory to a simple work function determination for photon energies <u>below</u> the work function lies in the very rapid decay of the Fermi tail in this region. Again variations in the parameters in α may be neglected in comparison with variations in the Fermi tail.*

The expression for the yield in the Fowler theory is given by[41,42]

$$Y = \alpha A T^2 \varphi(x) \qquad (2.2)$$

where α is the experimentally determined constant of proportionality, $A = 4\pi mk^2/h^3$, T is the absolute temperature.

---

* If the volume effect is responsible for the transitions, however, then for films below a certain critical thickness d_{crit}, α depends on the thickness of the film.[14] That is, below d_{crit} (which is the depth of photoemission), α will increase linearly with film thickness, reflecting the amount of sample present.

For photon energies <u>below</u> the photoelectric threshold, the expression $\varphi(x)$ is given by

$$\varphi(x) = [e^{x} - \frac{e^{2x}}{2^2} + \frac{e^{3x}}{3^2} - \ldots] \qquad x \leq 0. \qquad (2.3)$$

Here, $x = (h\nu - e\varphi)/kT$ so that for $h\nu < e\varphi$, only the first term in the above series need be considered, provided $|h\nu - e\varphi| \gtrsim kT$. Thus, to good approximation,

$$Y \simeq \alpha A T^2 \exp[(h\nu - e\varphi)/kT]. \qquad (2.4)$$

The expression for the work function may therefore be written

$$e\varphi = h\nu + kT \ln[\alpha A T^2/Y]. \qquad h\nu < e\varphi \qquad (2.5)$$

With a single yield (Y) measurement, all of the parameters in this equation, except $e\varphi$, are known; in particular, the frequency of the incident radiation is generally known with high accuracy.

A determination of the work function of a material by this method has the advantage that it entails only <u>one measurement</u> of the absolute photocurrent. Because of the rapid decay of the Fermi tail for electron energies above the Fermi level, relatively precise measurements are expected. For polycrystalline materials, the work function obtained by such a measurement will be that of the lowest work function crystallites, since these contribute most heavily to the photocurrent. For single crystals, of course, the work function obtained will correspond to the particular

crystal face investigated. Since the incident photon energy is below the work function energy of the material, the measured photocurrent will be small. It may be measured with an electrometer, of if sufficiently small, with the help of phase sensitive detection.

The method described above has been experimentally used to determine the work function of the vapor deposited Na surface in photomultiplier KM2462 with two radiation sources: a GaAs laser emitting radiation at 8450A(1.48eV), and a He-Ne gas laser emitting radiation at 6328A (1.96eV). The measurements were carried out at room temperature ($T = 300°K$). The constant A has the value 7.5×10^{20} electrons/sec-deg^2-cm^2 in cgs units, and a typical value[23] for α is $\simeq 4\times10^{-32}$ cm^2-sec/quantum. For the experimental conditions used, then $\alpha AT^2 \simeq 2.7\times10^{-6}$. The two cases are considered separately below.

(a) Radiation at 8450A: Using the measured value for the single quantum yield as given in Chapter IV, Y(300°K, 8450A) = 1.7×10^{-15} amps/watt, the expression for the work function becomes

$$e\phi \simeq 1.48\text{eV} + 0.025\text{eV}[\ln(2.7\times10^{-6}/1.7\times10^{-15})]$$

or

$$e\phi(8450\text{A}) \simeq 2.01 \pm .03\text{eV}.$$

(b) Radiation at 6328A: Using a He-Ne gas laser emitting approximately 0.7mW, a current of 1.3×10^{-9} amp was observed from the cathode* of KM2462. Thus, Y(300°K, 6328A) = 1.9×10^{-6} amps/watt, and

$$e\varphi \simeq 1.96\text{eV} + 0.025\text{eV}[\ln(2.7\times10^{-6}/1.9\times10^{-6})]$$

or

$$e\varphi(6328\text{A}) \simeq 1.97 \pm .03\text{eV}.$$

For radiation at 6328A, however, the validity of the requirement $|h\nu - e\varphi| \gtrsim kT$ is questionable. Nevertheless, both of these work function determinations are seen to be in agreement with each other, and with the value 1.9 ± 0.1eV obtained from the Fowler plot.** These results were obtained with the unrecoated surface (Sec. C5), as was the Fowler plot.

Only a rough value of the yield is necessary to estimate the work function quite accurately. Thus, if the surface under investigation is within a photomultiplier as is the case with the experiments performed here, the gain of the photomultiplier need not be known with high accuracy.

---

* In fact, the single quantum contribution to the photocurrent from the Fermi tail was so large for the incident radiation at 6328A, that it precluded the observation of a double quantum current. In this case, the cathode current was measured directly.

** This Fowler plot determination was rather coarse. Usually an accuracy of .01eV can be attained.

Similarly, the calculated value of the work function is rather insensitive to the value of α used. Thus, to first approximation in the work function determination of any metal, a general value for α may be used. This is especially true since the values of α do not differ too much from metal to metal.*,[42] Furthermore, this result justifies neglecting the frequency dependence of α and using the value obtained at threshold. The relative insensitivity of the work function on the parameters α and Y is seen to arise from the presence of these parameters in the argument of the logarithm, which is a slowly varying function.

4. Gain of the photomultiplier

In measuring the gain of photomultiplier KM2462, a small pilot bulb was used as the light source, and a Kiethley model 200B electrometer was used to measure the cathode current directly. High voltage was supplied to the photomultiplier by a Kepco type ABC2500M power supply. The gain[43] was found to be $\simeq$ 50,000 when operated with a high voltage of 2000 V. This was the standard operating voltage

* For example,[23] α(Na) $\simeq$ 4×10^{-32} cm^2-sec/quantum while α (Ba) $\simeq$ 2×10^{-32} cm^2-sec/quantum.

used for measurements. For comparison, the manufacturer quoted an expected gain of 90,000.

It was found that the initial gain of the photomultipler sometimes changed with time, generally decreasing with a time constant of the order of several minutes, and then leveling off. In fact, during early operation of the tube, just such a decay was seen in the double quantum current. This decay may now be understood in terms of the change in photomultiplier gain. These variations diminished after regular use of the tube, however. The overall fluctuation was $\lesssim$10%, so that the use of a mean value for the gain (chosen as 50,000) was adequate. When a variation in time was observed at the beginning of an experiment, the gain would be permitted to reach a plateau before measurements were made.

A load resistor was placed across the output of the Na photomultiplier, which directly fed the low noise tuned preamplifier by means of a length of RG-58A/U coaxial cable. The cable capacitance is 28.5 pF/foot. The input capacitance to the preamplifier is given by the manufacturer as $\simeq$ 10pF, and the output capacitance from KM2462 is $\simeq$ 5pF as mentioned previously. The resistor-cable combination therefore provided no filtering (unity transmission) for the 2.2kHz fundamental frequency component being measured.

Photomultiplier KM2462 was used in two different bases

or sockets, denoted as Base I and Base II. Base I uses 150 kΩresistors in the photomultiplier chain, with the exception of the first stage which uses a 300 kΩresistor. Base II was originally constructed for use with KM2519, and as such has an extra resistor in the chain. In order that Base II be used for KM2462, however, the second stage, as well as the first stage, was provided with a larger resistor (560kΩ) than the other stages (300kΩ). KM2462 was operated with a high voltage of 2000Vdc when used in Base I. When Base II was used with KM2462, however, the photomultiplier voltage used was 2215Vdc so that again 2000Vdc would appear across the photomultiplier. The remaining 215V was dropped across the extra resistor contained in Base II.

5. Recoating the sodium tube and sodium film thickness

The method used for recoating both the front surface and dynode surface cathodes was that prescribed by the manufacturer. It consisted of slowly increasing the voltage (provided by a Variac) across the internal thermal generator until sodium was observed to evaporate. The voltage was then slowly decreased. For later experiments with KM2462, more sodium was recoated onto the cathode. The procedure followed in recoating KM2462 was indentical to that used in recoating KM2519. The time during which

sodium was being evaporated was $\simeq$ 1.5 minutes.

It is therfore reasonable to expect that the thickness of both films will be of the same order of magnitude. It can safely be assumed that any previous Na on both cathodes was small in comparison with the recoated amount. This follows from two observations: (a) When the front surface tube (KM2519) arrived at Ithaca, there was very little sodium visible on the front surface, and only in one particular position. After recoating, on the other hand, it was quite "foggy". (b) As will be shown in Chapter IV, the double quantum photoelectric current increased by more thn two orders of magnitude after recoating the dynode tube (KM2462). The most reasonable explanation for this is that considerably more sodium was present on the dynode after recoating. It should be mentioned that when the front surface tube left the manufacturer, some two weeks before arrival here, the front surface was foggy indicating that some sodium was on the surface.[47] It is therefore clear that the low vapor pressure of sodium within the tube envelope causes the sodium to evaporate in time.

The thickness of the front surface film can be quite readily estimated by comparing the fractional amount of light transmitted by the front surface of phototube KM2519 with that passing through various neutral density filters. It was determined that the Na film, at its thinnest point

was equivalent to a 0.8ND Kodak Wratten filter and, at its thickest point, to a 1.1ND Kodak Wratten filter. A fluorescent lamp was used as the source. Thus, the transmission T of the front surface Na film lies between 8% and 16%. Taking a mean value of about 12%$\sim 1/e^2$, it is clear that the film has an approximate thickness 2δ, where δ is the skin depth for the intensity. The skin depth δ, for which the intensity of the incident wave drops to 1/e of its initial value, is given by[48,49] $\delta = \lambda/4\pi k$, where λ is the wavelength of the incident radiation and k is the extinction coefficient. For sodium[49] at optical frequencies*, $k \simeq 2.4$ and therefore $\delta \simeq 2.8 \times 10^{-6}$ cm. Thus, as a rough estimate, the expected thickness of the sodium film, for both the front surface and the dynode coated tubes, is about 500A. Although the optical constants of thin films vary as a function of both wavelength and thickness,[50,51] the value of k above is a reasonable approximation.[52] As a check, the experimentally observed transmission of silver films $\sim$ 400A thick, for which data is available, is in good agreement with the value observed above.[53]

After recoating the front surface tube, the film

---

* The convention used here is $\tilde{n} = n+ik$ when $\tilde{n}$ is the complex index of refraction and k is the extinction coefficient. Born and Wolf[49] use the convention $\tilde{n} = n(1+i\kappa)$ so that the value given above for k is that given by Born and Wolf for $n\kappa$.

appeared bluish-green in color at the edge where the film was thinnest. Similarly, the sodium coating on the dynode tube (KM2462) appeared bluish-green. This might be a further indication that the films of both tubes were approximately of the same thickness, since the colors arise from rapid variations in the absorption peak of the thin film sample as a function of wavelength and therefore change with thickness. They can be explained with the help of the Maxwell Garnett[50,51,54] theory for thin film optical properties, as discussed in Chapter III.

6. Relation of radiation incident on photomultiplier face to radiation incident on sodium surface

After recoating the dynode surface tube (KM2462), it was observed that a thin film of sodium remained on the glass face of the photomultiplier tube. This film had a transmission to fluorescent light approximately equivalent to a 0.4 ND Kodak Wratten filter, and therefore passed approximately* 40% of the incident radiation in the visible.** The amount of light transmitted should be approximately the

* This course estimate may be considered to include reflection losses at the face of the photomultiplier.

** Actually, the face of the photomultiplier was heated with the yellow flame of a bunsen burner which removed some of the sodium from the front surface; the above amount remained, however.

same at 8450A.[53] The maximum effective light power at the sodium surface was therefore ~160mW for the experiments performed after recoating the tube (for a power incident on the face of the photomultiplier of ~400mW). The double quantum yield is thus increased by a factor of 6.2 from the value calculated on the basis of the measured radiation power. This factor is included in the estimate of the double quantum yield given in Chapter I. These considerations in no way affect the single quantum yield, however, which was estimated before the tube was recoated.

7. Experiments using translucent photocathodes

Attempts to observe double quantum current were made with several translucent front surface cathode phototubes:

(a) Dumont-Fairchild KM2519 photomultiplier (Na metal),

(b) RCA 1P42 phototube (S-9 response; Cs_3Sb semiconductor surface), and

(c) EMI 9552S photomultiplier (S-13 response; Cs_3Sb semiconductor surface).

All of these tubes have considerably shorter threshold wavelengths than the incident radiation at 8450A. The 1P42 (S-9) in particular, has a very steeply declining output; at 6500A, its response is down by a factor of 100 from the maximum, and its rate of decrease appears to be the fastest of any surface. It was therefore thought to be most

suitable for double quantum experiments in the sense that the single quantum current would be extremely low.

However, as was the case with the other translucent cathode tubes, the 1P42 gave a very large cathode current which appeared to be a single quantum current, i.e. it was proportional to the incident intensity. The currents were measured using M.I.T. laser LD259 as the radiation source (~400mW peak power) and a 1kΩ photomultiplier load resistor. The maximum cathode current observed for the EMI 9552S was $\sim 10^{-8}$amp while for the 1P42, it was $\sim 5 \times 10^{-8}$amp, the same order of magnitude. These values are very much larger than the single quantum currents of $\sim 10^{-15}$amp observed for the dynode sodium surface photomultiplier, KM2462.

The output currents observed from <u>all</u> of the front surface tubes attained maximum values when the laser junction was focused onto the cathode. For ordinary single quantum photoelectric emission, the yield should not depend upon focusing.[55] In light of the above observation, a possible explanation of the effect is that the observed current was due to thermionic emission. It would be expected that heating would be more important for a translucent cathode, since there is no substrate to carry the heat away. Furthermore, thermionic emission might well give a current proportional to the incident light intensity.[9]

D. Signal Analysis of the System

In this section, the signal detection method and the overall gain of the system are considered. Attention is also directed to the noise generated by the various electronic components in the detection circuitry, and finally to a calculation of the signal-to-noise ratio (SNR) through the power spectral density of the electronic process.

1. Phase sensitive detection

The use of phase sensitive detection for the recovery of small coherent signals in noise is well known.[20] Because of the small magnitude of the double quantum current, this method of signal detection was applied to the experiments described in this work.

Phase sensitive detection, which is an optimum detection technique for periodically modulated signals, permits very narrow band filtering of the detected signal, resulting in a low detected noise power. In the time domain, this is equivalent to cross correlation with a local signal. For random information signals, rather than periodic signals, only autocorrelation precedures would be possible. However, that job is better handled by an optimum linear filter which cuts out the noise-noise component of the signal, f_{nxn}, at the same time.[56] For known nonperiodic signals, a matched filter maximizes the SNR. From a

generalized viewpoint, matched filtering may be considered to be a form of cross-correlation.

The commercial phase sensitive detector used for the experiments described in Chapter IV was preceeded by a commercial tuned preamplifier (Princeton Applied Research Corp. model CR-4 or CR-4A) since more gain was necessary than could be supplied by the phase sensitive detector amplifier alone. The preamplifier was operated in the "Hi-Z" mode, which has an input impedance of ~50MΩ shunted by about 10pF. The unit was operated single ended, with a gain of 10, 10^2, or 10^3. The filter rolloffs were generally set at 300 Hz and 10 kHz, for operation at the fundamental repetition frequency of 2.2 kHz.

The output from the preamplifier was fed directly into a PAR model JB5 (or JB4) phase sensitive detector.* The reference signal for the phase sensitive detector was obtained from the "synchronization pulse" output of the small GR1217A unit pulser used to drive the SCR laser pulser. A small GR type 1232A tuned amplifier, operating at the fundamental laser pulse repetition frequency of 2.2kHz, was inserted in the reference leg to provide a sufficiently

---

* According to the manufacturer, the JB5 (JB4) should be able to recover 2-5x10^{-10}V down by 40db from the noise. (E. Fisher, American Dynamics Corp., sales representative).

large reference signal at this frequency. Time constants (for integration of the output from the mixer stage in the phase sensitive detector) from 0.1sec to 10sec were used, depending on the strength of the signal and the amount of noise present.*

The balanced output from the phase sensitive detector fed directly into a Bausch and Lomb model VOM-6 recorder, which was operated in the voltage mode. The recorder was isolated from ground, and was used on the 0.25 and 2.5 volt scales. In early experiments, the recorder was operated with a 1500Ω resistor shunting the input. This reduced the observed voltage by the ratio f=1500/(1500+5000) =0.23 since the output of the phase sensitive detector has a series 5000Ω resistor.

2. Overall gain of the system

The gain of the phase sensitive detector was constant to within < 10% over the measured frequency range from 2.2kHz to 19.8 kHz. Its value (rms input to dc output) was determined to be 16,000 on one occasion and 10,500 on another occasion. Its precise value depends quite heavily on the state of adjustment (alignment) of the unit through

* The output filter characteristic was set to decrease at 12db/octave.

the "Q" of the signal amplifier. The manufacturer quotes a value for the gain of >9000. Its value is taken to be 10,000. The gain may be attenuated by a known factor by means of a calibrated "signal level" control on the phase sensitive detector.

The observed cathode current, $i^{peak}_{fundamental}$, from phototube KM2462 may be related to the observed output voltage from the recorder V_o as follows:

$$i^{peak}_{fund.} = \sqrt{2}V_o[G(KM2462):G(CR\text{-}4):G(JB5):f\cdot R]^{-1} = \gamma V_o \quad (2.6)$$

where G( ) is read "the gain of". G(JB5) is the actual gain of the phase sensitive detector, including the attenuation factor due to the "signal level" control setting. R is the value of the load resistor on the output of the photomultiplier. As mentioned previously, the photomultiplier output cable and load resistor combination have a gain of close to unity at 2.2kHz. The rolloffs on the preamplifier are sufficiently far away from 2.2 kHz so as not to affect the gain setting on the CR-4. Two calculations for the gain are made below, corresponding to the two sets of experimental conditions described in Chapter IV. The values used in these calculations are given in Table III.

TABLE III

PARAMETER VALUES USED IN CALCULATION OF THE OVERALL SYSTEM GAIN

Parameter	Value for Case B (before recoating)	Value for Case A (after recoating)
G(KM2462)	5×10^{4}	5×10^{4}
G(CR-4)	10	10
G(JB5)	10^{3}	200
Attenuation factor (JB5)	0.1	.02
R	$10^{6}\Omega$	$10^{5}\Omega$
f	0.23 (1500Ω across input to VOM-6)	1 (no resistor across input to VOM-6)
γ	$1.3\times10^{-14}\simeq10^{-14}$ mho	7×10^{-14}-1.4×10^{-13} mho
V_o	0.1V	1.4V
$i_{fundamental}^{peak}$	$\sim10^{-15}$ amp	$1.4\times10^{-13}\simeq10^{-13}$ amp

3. Sources of noise

Noise in the system arising from the electron multiplier, the load resistor, and the preamplifier are considered below.

(a) Photocathode and electron multiplier noise: The power-spectral-density (PSD) for the noise-in-signal contribution of a rectangularly pulsed, stationary Poisson process, $S_{\sigma n}(f)$, is given by

$$S_{\sigma n} = \frac{\tau_1}{T} \bar{n}' e^2 \qquad (2.7)$$

as shown in the next section (Sec D4). The applicability of this model to the problem at hand is also discussed in the next section. In the above formula, τ_1 represents the full width of the rectangular pulse, T represents the period of the modulation function, and $\bar{n}'$ represents the average number of electrons emitted per unit time during the "on" time of the modulating pulse. Because there is unavoidable noise due to ambient light leakage at the photomultiplier cathode, an additional term must be added. Thus,

$$S_{\sigma n} = \frac{\tau_1}{T} (\bar{n}' + \bar{r}') e^2 \qquad (2.8)$$

where $\bar{r}'$ represents a quantity of the order of the mean number of stray (photoelectron producing) photons which strike the surface per unit time. In practice, it would, however, be difficult to estimate the value of $\bar{r}'$. That

stray light leakage can be considerable is manifested by the sharp increase in noise registered by the recorder when the black cloth shielding the photomultiplier from ambient light is removed in the darkened laboratory.

The process of electron multiplication involves secondary emission which itself is a random process and therefore introduces additional noise into the signal. The increase in noise resulting from the electron multiplier may be expressed as a multiplicative factor, κ, which may be estimated to be about 1.3 for the sodium surface photomultiplier used.[57] The problem may be considered from a theoretical point of view, and the additional noise is then seen to arise from the variance in the probability distribution for the production of secondary electrons.[58] Including secondary emission noise, then, the noise PSD is given by

$$S_{\sigma n}(f) = \kappa \frac{\tau}{T} (\bar{n}' + \bar{r}') \qquad (2.9)$$

Other factors contributing to noise in the photomultiplier through the dark current[59] may be lumped in $\bar{r}'$.

(b) Johnson noise and preamplifier noise: After passing through the electron multiplier, the signal is fed into a load resistor and processed by a low noise preamplifier. It is of interest first to consider the noise contributed by the preamplifier and then to consider the Johnson noise resulting from the load resistor.

Based on the specifications of the manufacturer, the "noise figure" to be expected for the source impedances employed (1MΩ or 100kΩ) is about 3db.[60] It is clear from the procedure described for the noise figure measurement[61] that it is actually the "standard noise figure",[62] F, which is quoted by the manufacturer. The standard noise figure, F, is referred to Johnson noise at the standard temperature of 290°K.

The relation between the operating noise figure (which is the quantity of interest), F_o, and the standard noise figure is given by[63]

$$F_o = 1 + \frac{T_o}{T_{es}} (F-1) \qquad (2.10)$$

where T_o is the standard noise temperature (290°K) and T_{es} is the effective source noise temperature. T_{es} may be expressed as follows,

$$T_{es} = \frac{N_{as}}{k\Delta f} \qquad (2.11)$$

where N_{as} represents the incremental available noise power from a source, k is Boltzmann's constant, and Δf is a small frequency band about the center frequency. It is clear that

$$\frac{T_{es}}{T_o} = \frac{N_{as}}{J} \qquad (2.12)$$

where J represents the Johnson noise generated by a standard temperature resistor in the same band width.

In performing the two quantum experiment at higher currents ($>5\times10^{-17}$ ampere), it was experimentally observed that fluctuations about the average value on the recorder trace were very much greater when the photomultiplier voltage was on then when it was not. Since the load resistor is always in place, providing a noise source at standard temperature, it must be concluded from this observation that the source noise temperature, T_{es}, is considerably greater than the standard noise temperature, T_o. Evaluating the operating noise figure by inserting a standard noise figure of 2 (corresponding to 3 db) into the expression relating F and F_o, the following approximation obtains:

$$F_o = 1 + \frac{T_o}{T_{es}} \simeq 1 . \qquad (2.13)$$

At high currents, therefore, the contribution to noise arising from both the preamplifier and the load resistor may be neglected.

In line with experimental observations, which show a decrease of noise with decreasing signal, it may be expected that the Johnson and preamplifier contributions may become important at lower currents. The decrease of source noise with decreasing signal may be viewed as a decrease of the source noise temperature. This implies that as lower

values of current are measured, the noise figure will rise. Although negligible at higher currents, the presence of the load resistor and preamplifier introduce a constant level of noise which is not necessarily negligible at low currents. These components therefore provide a lower bound for the total system noise. Low level noise fluctuations when the photomultiplier is either blocked from laser light with an opaque screen or its voltage is turned off (both give about the same noise) are attributed to this Johnson contribution. It is clear that only values of noise obtained at higher currents with rectangular pulsing may be justly compared with the previously derived noise spectrum.

4. The signal-to-noise ratio (SNR)

A calculation of the SNR for a stochastic process requires a knowledge of the PSD, which in turn may be obtained from the statistics of the random process. The standard semiclassical treatment* of the two photon photoelectric emission (as with the single photon process) under a "constant" light intensity results in a constant photoelectric emission current density, $\vec{j}$. No information about the statistics of the emission process is obtained from this treatment.

* See Chapter III.

Elementary considerations of the problem usually consider additional conditions to be satisfied, such that the resulting photoelectric emission is Poisson distributed.[64] In analogy with the single quantum case,[65] however, the correct statistical distribution in time for double quantum photoemission may undoubtedly be obtained in terms of the density matrix for the incident radiation field.

Since the GaAs laser used in the experiments described was operating quietly,[66] however, the emission of photoelectrons may be assumed to obey a Poisson distribution,[65] in which case the shot-noise spectrum represents the process.* Because the frequency of operation is much smaller than the reciprocal of the transit time in photomultiplier KM2462, the PSD for the pure Poisson process [denoted by $S_s(f)$] may be approximated by its low frequency form:[67]

$$S_s(f) = (e\bar{n}')^2\delta(f) + \bar{n}'e^2 = \bar{I}'^2\delta(f) + \bar{n}'e^2 \qquad (2.14)$$

where f is the frequency in Hz, e is the electronic charge, $\bar{n}'$ is the average number of electrons emitted per second, and $\bar{I}'$ is the average total current.

---

* Poisson distributed emission may be assumed for the case of two quantum photoemission as well, provided that the radiation source is a quietly operating laser (see Chapter V).

The considerations of the last paragraph apply to a photoelectric emitter upon which a constant radiation intensity is incident. Because the laser is periodically pulsed, however, the process of interest consists of stochastically distributed electron emission during the times the laser is on and no current during the times the laser is off. Furthermore, signal processing of the photoelectric signal (and the PSD) generally occurs because of the transmission of the signal through the electron multiplier and the load resistor/photomultiplier cable combination. The effect of the electron multiplier on the SNR is small and has been discussed in the last section. The load resistor/photomultiplier cable combination is a linear, causal system and will therefore affect the power spectral density of the signal and the noise equally, thus leaving the SNR unchanged.

Taking the pulsing of the laser into account, the output of the photomultiplier $\sigma(t)$ may be mathematically considered as a product of two independent functions, under certain special conditions to be considered below:

$$\sigma(t) = s(t) \cdot p(t) . \qquad (2.15)$$

Here, $s(t)$ represents the photoemission process, and $p(t)$ represents the periodic modulation function resulting from the pulsing of the laser. Since the output current for

double quantum photoelectric emission is proportional to the square of the incident radiation intensity, p(t) represents the square of the laser output intensity function $\ell(t)$:

$$p(t) = [\ell(t)]^2 \ . \qquad (2.16)$$

For the case of rectangular laser pulsing, the assumption that $\sigma(t)$ may be represented as the product of two independent functions s(t) and p(t) rests on the hypothesis that there is nothing unique about the photoemission process at the starting time or at any other time during the laser pulse. That is, the assumption is made that the emission is Poisson distributed during times when a constant light intensity impinges on the photoemitter (laser "on" times) and that there is no emission in the absence of light intensity (laser "off" times). Extremely short measured times for the onset of photoelectric emission ($<10^{-9}$ sec.) make this assumption possible.

For non-rectangular pulsing, the situation is considerably different. Here, the changing incident radiation intensity itself induces a deviation from Poisson statistics: photoelectrons being emitted more profusely at higher intensities. In general, therefore, the mathematical assumption of scalar multiplication of s(t) by the modulating function p(t) is unjustified.

It is not the amplitude of the pulses which the modulation affects but rather the time distribution. Such a model may be treated analytically with the theory of periodic random processes,[68] provided that the condition of wide-sense stationarity* is fulfilled. Because of the complexity of the general case, however, the analytical treatment to follow is based upon the idealized model of a rectangularly modulated Poisson process.

To calculate the PSD on the basis of this model,[69] the autocorrelation function for the process "σ" is first considered:

$$R_\sigma(t,t-\tau) = R_\sigma(\tau) \cdot \qquad (2.17)$$

In writing $R_\sigma(\tau)$, the assumption has been made that $\sigma(t)$ is a stationary random process, at least in the wide sense. Since the mathematical model has been defined so that $s(t)$ and $p(t)$ are independent, the autocorrelation function splits into the product

$$R_\sigma(\tau) = R_s(\tau) \cdot R_p(\tau) \qquad (2.18)$$

From the Wiener-Khinchin Theorem, the PSD of the process $S_\sigma(f)$ is simply the Fourier transform of the autocorrelation

---

* A random process whose autocorrelation function depends only on the time difference $\tau = t_1 - t_2$, but whose probability distribution may not be invariant under a shift of the time origin, is defined as wide-sense stationary (see Ref. 68, p. 60).

function. Therefore,

$$S_\sigma(f) = S_s(f) * S_p(f) \qquad (2.19)$$

where the symbol * denotes the convolution integral.

The simple shot-noise PSD is well known, and for the frequency range of interest, is given by

$$S_s(f) = \bar{I}'^2\delta(f) + \bar{n}'e^2 \qquad (2.20)$$

as indicated earlier. The PSD for the rectangularly pulsed modulation waveform $S_p(f)$ is given by the square of the Fourier transform. Thus,[70]

$$S_p(f) = \left(\frac{\tau_1}{T}\right)^2 (\text{sinc}^2 n\pi f_o\tau_1)\delta(f - \tfrac{n}{T}) \quad n=1,2,3... \qquad (2.21)$$

where τ_1 represents the pulse width, $T = f_o^{-1}$ represents the period of the modulation waveform, and sinc x is an abbreviation for the function (sin x)/x. The total PSD for the process σ is therefore

$$S_\sigma(f) = \bar{I}'^2\left(\frac{\tau_1}{T}\right)^2 (\text{sinc}^2 n\pi f_o\tau_1) + [\bar{I}'e * S_p(f)] \qquad (2.22)$$

The first term above is proportional to $\bar{I}'^2$ and has the Fourier spectrum associated with p(t). The power is concentrated at discrete frequencies which are multiples of the fundamental frequency of 2.2kHz. This term represents the contribution to power which arises from the dc or constant component of the random photoelectric emission. Because of this, it represents the signal component, and is denoted by $S_{\sigma s}(f)$. The second term is denoted by

$S_{\sigma n}(f)$, and may be specifically evaluated as follows:

$$\begin{aligned} S_{\sigma n}(f) &= \bar{I}'e * S_p(f) \\ &= \bar{I}'e \int_{-\infty}^{\infty} S_p(f)df \end{aligned} \tag{2.23}$$

since $\bar{I}'e$ is a constant. By Parseval's theorem,[71] however,

$$\int_{-\infty}^{\infty} S_p(f)df = \frac{1}{T} \int_{o}^{T} |p^2(t)|dt = \frac{\tau_1}{T} \tag{2.24}$$

and therefore,

$$S_{\sigma n}(f) = \bar{I}'e \left(\frac{\tau_1}{T}\right) = \left(\frac{\tau_1}{T}\right)\bar{n}'e^2. \tag{2.25}$$

This term is independent of frequency (this is strictly true only in the low frequency limit) for the stationary Poisson process and arises from the randomness of electron emission. In the time domain, this corresponds to fluctuations about the dc value (which may be reduced by narrow-banding the signal), i.e. noise. In the experiments at hand, $S_{\sigma s}(f)$ is associated with the "signal."

Including the sources of noise considered in the last section, the total power spectral density $S_{\sigma s}(f)$ for the rectangularly pulsed Poisson process may therefore be written

$$S_{\sigma}(f) = \bar{I}'^2\left(\frac{\tau_1}{T}\right)^2(\mathrm{sinc}^2 n\pi\tau_1 f_o)\delta(f - \frac{n}{T}) + \kappa\left(\frac{\tau_1}{T}\right)(\bar{n}'+\bar{r}')e^2 \tag{2.26}$$

where the first term above corresponds to the signal contribution and the second term corresponds to the noise.

Because synchronous detection (phase sensitive detection) augments the signal to noise ratio by a factor of two[21] (in addition to the much greater gain in signal-to-noise ratio by virtue of the small bandwidth Δf which it permits), the expected SNR for the signal is given by

$$\text{SNR } (f = nf_o) = \frac{2\bar{I}'^2 (\frac{\tau_1}{T})^2 \text{sinc}^2 n\pi\tau_1 f_o}{\kappa (\frac{\tau_1}{T})(\bar{n}'+\bar{r}')e^2\Delta f} . \qquad (2.27)$$

Here Δf represents the full bandwidth of the final filter in the phase-sensitive detector and f_o is the fundamental frequency of 2.2 kHz. Denoting the <u>measured</u> component of current (at the nth multiple of the fundamental frequency) by $\bar{I}(nf_o)$ the following relation ensues:

$$\bar{I}(nf_o) = \bar{I}'(\frac{\tau_1}{T})\text{sinc } n\pi\tau_1 f_o . \qquad (2.28)$$

The effective bandwidth for a double RC filter with a decrement of -12 db/octave is shown to be[72] $\Delta f = \frac{1}{4\tau_o}$ where $\tau_o = RC$ represents the time constant of each of the final filters in seconds. Finally, assuming sufficiently good light shielding to neglect the stray light contribution $\bar{r}'$, the expression becomes

$$\text{SNR}(nf_o) = \frac{2\bar{I}'(\frac{\tau_1}{T})\text{sinc}^2 n\pi\tau_1 f_o}{\kappa e : \frac{1}{4\tau_o}} = \frac{8\tau_o \bar{I} \text{sinc } n\pi\tau_1 f_o}{\kappa e} . \qquad (2.29)$$

The voltage signal-to-noise ratio, VSNR, which is the value measured at the output of the recorder, is then given by

$$\text{VSNR } (f=nf_o) = \left[\frac{8\tau_o \bar{I} |\text{sinc } n\pi\tau_1 f_o|}{\kappa e}\right]^{\frac{1}{2}} \qquad (2.30)$$

With $\kappa = 1.3$, it is found that

$$\text{VSNR } (f=nf_o) = 2.5\sqrt{\frac{\bar{I}\tau_o}{e}}(|\text{sinc } n\pi\tau_1 f_o|)^{\frac{1}{2}} . \qquad (2.31)$$

It may be seen from this expression that the optimum frequency for operation is that frequency where sinc $n\pi\tau_1 f_o$ is maximum since this frequency gives the highest SNR. This, of course, occurs at the lowest frequency possible (aside from dc) which is the fundamental frequency of 2.2 kHz. At this frequency, sinc $n\pi\tau_1 f_o \simeq 1$ and neglecting the stray light contribution, the VSNR for the rectangularly pulsed Poisson process may be written

$$\text{VSNR}(f=f_o) \simeq 2.5\sqrt{\frac{\bar{I}\tau_o}{e}} . \qquad (2.32)$$

Values for the theoretically predicted rectangular wave VSNR based only on the noise-in-signal contribution, along with observed values, are given in Table IV (for the fundamental frequency component).

TABLE IV

COMPARISON OF CALCULATED AND OBSERVED VSNR*

Observed current $\bar{I}$ (amps)	Time constant τ_o (sec)	Calculated VSNR (rectangular pulsing)	Observed VSNR
9×10^{-16}	3	320	~100-200
4×10^{-16}	3	220	~ 50-100
3×10^{-17}	3	60	~20
2×10^{-18}	10	30	~10

* For experiments performed with as-received Na surface.

The following general observations about the observed and calculated signal-to-noise ratios are pertinent:

(a) At the fundamental frequency, the calculated VSNR's were larger than the observed values by a factor of 2 - 3. The agreement is therefore moderately good.

(b) Noise fluctuations about the zero level were sometimes greater when the photomultiplier high voltage stayed on and the laser beam was blocked than when the photomultiplier HV was turned off. This leads to the conclusion that stray light leakage (or dark current) was in part responsible for additional noise. This contribution should be negligible at higher currents, however, since there the magnitude of the noise fluctuations is much greater when light impinges on the photocathode than when it is blocked.

(c) Noise fluctuations are evident at very low incident light levels (high equipment sensitivity) whether the HV is on and the beam blocked, or the HV is off. This may be attributed to low-level Johnson noise or stray pickup, and may also be neglected at high currents.

(d) From the derived expression, it would be expected that the VSNR should vary with frequency as $[\text{sinc } n\pi\tau_1 f_o]^{\frac{1}{2}}$. At the highest measured frequency of 19.8 kHz, therefore, the VSNR should be down from the maximum value at the fundamental frequency by about 60% (since $[\text{sinc } n\pi\tau_1 f_o]^{\frac{1}{2}} =$

0.4 for n = 9). This result would be expected in the case of a pure Poisson process with truly rectangular pulsing. The measured SNR seemed to be fairly constant over all multiples of the repetition frequency at which measurements were made. Measurements of the SNR were accurate only to ~100% because of the high value of SNR, however, so that the theoretical prediction could not be directly compared with experiment.

In conclusion, the analysis contained in this section has shown that

(a) Phase senstive detection is well suited to the experiment at hand, and in general to problems in which there may be only few electrons per detection cycle, on the average. This has been experimentally verified by the results of Chapter IV.

(b) Under proper experimental conditions, sources of noise from various parts of the system do not materially alter the large contribution due to noise-in-signal.

(c) The observed SNR is in reasonable agreement with the calculated value for the model used.

III. THEORETICAL TREATMENT OF TWO QUANTUM PHOTOEMISSION FROM A METAL

The entire energy of two photons (from a beam of electromagnetic radiation incident on a metal) may be absorbed by a single electron within the metal. If this absorption results in the ejection of the electron from the irradiated material, the process is defined as two photon photoelectric emission. The effect is of second order, and is therefore most easily observed in the absence of ordinary first order, or single quantum, photoemission. Because energy and momentum cannot be simultaneously conserved for a single free electron absorbing one or two photons, a third body, or external force, must take part in the interaction.[42] When this force is provided by the potential gradient at the surface of the metal, the process is called surface photoemission; if potential gradients in the bulk of the material take part in the interaction, the emission is referred to as volume or bulk photoemission.

The Einstein relation for the maximum kinetic energy E_{max} for an electron emitted by single quantum photoemission[73] from a material of work function φ is given by

$$E_{max} = h\nu - e\varphi \qquad (3.1)$$

where $h\nu$ is the energy of the incident light quantum. For the second order effect, this equation must be modified[8] to take into account the absorption of two quanta:

$$E_{max} = 2h\nu - e\varphi \quad . \tag{3.2}$$

However, the experiments described here are not concerned with the kinetic energy of the emitted electrons. Rather, it is the magnitude of the emitted electron current which is of interest.

A. The Hamiltonian

Because photoemission is intrinsically a quantum phenomenon, the theoretical treatment proceeds from the Hamiltonian for the system. The Hamiltonian for a charged particle in the presence of a vector potential $\vec{A}$ (representing an electromagnetic, electric, or magnetic field) may be obtained from the Hamiltonian of the particle for $\vec{A} = 0$ by simply making the replacements[74] $(\vec{p} - \frac{e}{c}\vec{A}) \rightarrow \vec{p}$ and $V + e\varphi \rightarrow V$. Here, $\vec{p}$ represents the momentum of the particle, φ is the scalar potential, e is the electronic charge and c is the velocity of light in vacuum. The arrows above are to be read "replaces". For an electromagnetic wave in the absence of currents and charges, φ may be taken to be zero without loss of generality.[75] Thus, the Hamiltonian $\mathcal{H}$ is given by

$$\mathcal{H} = \frac{1}{2m}(\vec{p} - \frac{e}{c}\vec{A}(\vec{r},t))^2 + V(\vec{r}). \qquad (3.3)$$

Expanding, this becomes

$$\mathcal{H} = \mathcal{H}_o + \mathcal{H}' = \frac{p^2}{2m} - \frac{e}{mc}\vec{A}\cdot\vec{p} + \frac{e^2}{2mc^2}A^2 + V(\vec{r}). \qquad (3.4)$$

It is generally agreed that the use of perturbation theory, applied to the Schrödinger equation, is appropriate to the solution of the photoeffect since the portion of the Hamiltonian taken as the interaction or perturbation Hamiltonian $\mathcal{H}'$,

$$\mathcal{H}' = -\frac{e}{mc}\vec{A}\cdot\vec{p} + \frac{e^2}{2mc^2}A^2 \qquad (3.5)$$

is small in comparison with the unperturbed Hamiltonian $\mathcal{H}_o$,

$$\mathcal{H}_o = \frac{p^2}{2m} + V(\vec{r}), \qquad (3.6)$$

and the initial state may be taken to be stationary. It is the choice of the potential $V(\vec{r})$ in the unperturbed Hamiltonian which distinguishes between the solutions for a surface and a volume effect.

Quite a few papers have recently appeared discussing the Hamiltonian to be used in the calculation of the transition probabilities in double quantum processes.[76] Considering the perturbation Hamiltonian above, double quantum transitions may take place either in second order through

the $\vec{A}\cdot\vec{p}$ term, or in first order through the A^2 term.[77] In particular, for two quantum absorption in anthracene and other polycyclic benzene ring compounds (with and without molecular inversion symmetry), it has been both experimentally[78,79] and theoretically[80] established that the transition arises from the $\vec{A}\cdot\vec{p}$ term in the electric dipole approximation. The transition probability due to this term has been estimated in general to be about 10^4 times larger than either the magnetic dipole-electric quadrupole contribution from $\vec{A}\cdot\vec{p}$ or from the A^2 terms.[78*] However, the observation of two photon absorption due to the A^2 term has also been considered,[81,82] and this mechanism seems to correctly account for the greater part of the double quantum photodetachment of the atomic iodine ion (I^-).[82,83] Here, however, the initial and final states considered are not orthogonal.

The photoelectric current (or rather, current density) may be directly computed by the quantum mechanical formula[+]

---

* There are no matrix elements between orthogonal states due to the A^2 term in the electric dipole approximation.

\+ This formula is obtained simply from the conservation of probability equation. It has the classical analogy $\vec{J} = \rho\vec{v}$, which is familiar from electrodynamics and hydrodynamics, and arises from the conservation of charge and particles, respectively.

$$\vec{J}(\vec{r},t) = \frac{\hbar}{2mi}(\psi^*\nabla\psi - \psi\nabla\psi^* - \frac{2ie}{\hbar c}\vec{A}\psi\psi^*) \qquad (3.7)$$

at a given surface. Or, it may be obtained by calculating the number of electrons inside the metal which have sufficient energy to escape from the material, and then by integrating over directions in the material which permit escape.

With this background, it is of interest to consider approximations to the Schrödinger equation in second order perturbation theory, first for the surface photoeffect, and then for the volume photoeffect.

B. Surface Photoelectric Emission

The theory of single quantum surface photoelectric emission was initially developed by Mitchell[12] who made use of the Sommerfeld model[42] for a metal, and neglected the effects of reflection and refraction at the boundary of the metal. Mitchell used both first order time-independent and time-dependent perturbation theory, and arrived at the same photocurrent from the surface of a metal with both models. The Sommerfeld model automatically excludes the volume photoelectric effect since the free Sommerfeld electron cannot absorb a photon and simultaneously conserve energy and momentum.

In other work, Mitchell[84] has used the image field barrier,[85] which is a better approximation than the Sommerfeld model. Mitchell's model was subsequently made more realistic by Mackinson,[86] Buckingham,[87] and Huntington and Apker,[88] who included the effects of reflection and refraction, the dependence of the surface barrier on the momentum of the impinging electron, and the effect of the band structure on the surface production of photoelectrons, respectively. These modifications affected the theoretical results little, however. Theory always failed to agree with experiment in many respects, sometimes yielding a photoelectric yield several hundred times too high,[8,42] particularly in the region away from the immediate vicinity of threshold.

This disagreement was frequently ascribed to the difficulty in obtaining clean surfaces for the alkali metals. Furthermore, for the surface effect, only the component of electric field perpendicular to the local surface is effective in the production of photoelectrons.[12,15] Thus, surface photoemission theoretically cannot be stimulated by an electric field parallel to a flat metallic surface. Additional elements must therefore be brought into the model, since photoemission is experimentally observed for this case.

Smith[8] treated the case of double quantum surface photoelectric emission from a metal, assuming that the incident radiation has a frequency which is less than the work function of the metal, but greater than one-half the work function. Smith assumed monochromatic radiation to be incident on a metal having a constant potential both inside and outside of the surface, but exhibiting a step discontinuity at the surface. He then used second order time independent perturbation theory to calculate the probability flux in the outward normal direction from the metal. The Hamiltonian used by Smith does not contain the A^2 term, since this term does not correspond to absorption for the surface photoelectric effect.[8,10] Bowers[9] has explicitly shown that this term vanishes from the second order surface photoelectric current. The probability flux for a single electron is then integrated over the total number of electrons which can be excited to the free state to yield the double quantum current.

The model used by Smith is the same as that used by Mitchell, the justification being that calculations may be carried out with relative ease. Furthermore, various refinements of Mitchell's model in first order were of little help in improving the comparison of the theoretical and experimental results. Smith therefore hoped to calculate a lower bound for the two quantum surface photocurrent.

The current calculated on the basis of Smith's model turns out to be proportional to the square of the incident radiation power P, and to an integral L over those Fermi electrons which have enough energy to be excited to a state outside the metal, and inversely proportional to the area irradiated, A. The integral may be evaluated for any particular metal and radiation wavelength by inserting the proper values for the Fermi level and work function of the material, as well as the frequency of the radiation field. For Na metal* and the radiation field from a GaAs laser,+ the value of the integral‡ L obtained is $\simeq 0.02$.

The result obtained from Smith's analysis with these values is then

$$i_{surface} = 9.7 \times 10^{-23} \frac{P^2}{A} \text{ amperes} \qquad (3.8)$$

where P and A are expressed in MKS units.

---

* For Na metal, the Fermi energy $E_f = 3.12$ eV and the work function $e\varphi = 2.28$ eV.[23,89]

\+ The GaAs laser radiates at 8450A, emitting photons with energy $h\nu = 1.48$ eV.

‡ For the corrected version of L in Smith's[8] Eq. (60), see Bower's[9] Eq. (2.74). The author wishes to thank H. Bowers for supplying the values for several integrals.

C. Volume Photoelectric Emission

1. General discussion

In an early treatment of the first order photoelectric effect, Tamm and Schubin[90] distinguished between the surface and the volume effects, indicating that the volume effect became important at thresholds significantly higher than for the surface effect, and therefore could be neglected in photoemission studies near threshold. This calculation assumed that the lowest threshold would be obtained when the emitting plane was the (100) plane. However, lower thresholds are obtained from higher index planes.[13,15] Fan[13] later restudied the problem of volume photoemission from the alkali metals.

Fan's model makes use of the Bloch scheme within the metal, allowing interband $\vec{k}$-conserving transitions to occur. The energy levels of the electrons are taken as those for free electrons. This approximation in sodium should be quite good away from energy discontinuities, since the Fermi surface of sodium is spherical to 1 part in 1000.[91] The effect of surface reflection is taken into account by considering the classical theory of optical constants for the material. This method is justified since Schiff and Thomas[92] have shown that the quantum mechanical treatment of reflection for the normal field components differs from the classical theory only within approximately a lattice constant

of the surface. The tangential component of the transmitted field is the same as that derived classically. These effects would be important for the surface photoeffect, but may be neglected for the volume effect. Considering only lattice planes of low index [such as the (110)], Fan concluded that the threshold for the volume effect was only very slightly higher than that for the surface effect. The yield calculated on the basis of this model is comparable with experimentally observed values. Fan calculated the threshold wavelength for the occurrence of interband transitions in sodium to be about 6100A. However, electrons excited by photons of this energy cannot quite overcome the work function of the material to escape.

More recently, photoemission from vapor deposited potassium films has been experimentally investigated by Thomas,[14] Mayer and Thomas,[15] and Methfessel.[93] Thomas has found that the photocurrent observed from a potassium film increases with film thickness, leading to the interpretation that the observed photoemission is a volume effect. For incident light wavelengths near the photoelectric threshold ($\lambda \simeq 5500$A), the photoemission was found to rise linearly with the thickness of the film for thicknesses up to about 800A. The photoemission appears to be a volume effect over the entire spectral range investigated, from 2890A to 5780A.

It is expected that sodium would behave similarly.* Mayer and Thomas further point out that a metal will exhibit the normal threshold wavelength (the work function usually associated with the surface photoelectric effect) if the emitting surface contains crystallites corresponding to high index lattice planes, or if the excited electron experiences a change in direction before escape. Thus, the problem of a "second photoelectric threshold" above the normal threshold does not arise as it does in the treatments of Tamm and Schubin, and Fan. In fact, the above model for the metallic surface might well be a good approximation for evaporated films.[15]

The model used by Mayer and Thomas is similar to that used by Fan, with the following exceptions:

(a) Mayer and Thomas permit higher index lattice planes to appear at the emitting surface, as mentioned above;

(b) The matrix elements used by Mayer and Thomas are calculated using "nearly free electron" wave functions,[94] whereas those used by Fan are estimated from Bloch functions;[13,95]

(c) Mayer and Thomas consider an escape depth which is a strong function of the electron energy, in accordance with their experimental observations.[14]

---

* Results similar to those of potassium have been obtained with cesium, the only other material investigated which Thomas, et al. have investigated.[16]

Furthermore, Mayer and Thomas have specifically calculated the number of electrons per absorbed photon q_a in the limit of very thin films* so that they could compare the results of their model with experiment. Very good agreement was obtained. In the treatment of the second order photoelectric effect, these considerations will be taken into account.

2. The excitation mechanism: direct transitions

In order that a single electron be able to absorb the entire energy of a photon, it is necessary that a "third body" be present to conserve momentum. In the surface photoeffect, it is the potential gradient of the surface barrier which acts as the third body. In the volume effect, on the other hand, the third body may be any one of the following effects:[15]

(a) the ideal periodic lattice

(b) thermal vibrations (phonons) or lattice defects

(c) collective effects of the conduction electrons.

These mechanisms will be discussed in order below.

The ideal periodic lattice, within the Bloch formalism, may give rise to photoemission through interband transitions. Light absorption due to this mechanism in the alkali metals has been investigated by Butcher,[94] who uses the approxi-

---

* They have used this case because it permits comparison of theory and experiment with a minimum of assumptions.

mation of "nearly free" electrons* to obtain the unperturbed wave functions in the metal. With this model, Butcher predicts the absorption edge for interband transitions in sodium to be about 6000A,+ which is in good agreement with the observed value.[94] Over-all agreement of the results of Butcher's treatment with experiment is moderate; it is good for sodium, and poor for cesium. For incident light frequencies above the interband threshold, it is the interband contribution which is generally held to account for light absorption[13,48,94,96] and photoemission.[13,15]

The second process above (b), thermal vibrations or phonon interactions, has been theoretically shown to be small in comparison with absorption by interband transitions in the region in which both are effective.[15,94] Absorption occurring below the interband threshold, however, is attributed to this mechanism which is referred to as "free electron" or "free-carrier" absorption.‡[48,96] For Ag, the

---

* Butcher finds that the matrix elements vanish when taken between the Wigner-Seitz approximate wave function for the conduction band and free electron wave functions for higher bands. He therefore uses the nearly free electron approximation, for all bands. Matrix elements between Bloch states have been calculated[95] however, and are used by Fan. The general theory of direct optical transition in the Bloch formalism is discussed by Smith.[97]

+ The cutoff wavelength for interband transitions in a b.c.c. metal is proportional to the square of the lattice constant, and depends essentially only on it.[15,94] Thus, for potassium, its value is $\simeq$ 9250A.[13,15]

‡ This corresponds to phonon assisted transitions within one band.

interband threshold lies in the ultraviolet at $\sim\lambda$ = 3200A (3.9 eV).[96] Photoelectric emission from silver obtained for photon energies below 3.9 eV is therefore considered to arise from this mechanism, and the energy distribution of the emitted photoelectrons has the characteristic free electron shape.*[18] Likewise, for sodium, with incident light at 1.48 eV, free electron (phonon-assisted) absorption dominates interband transition absorption, but in contrast with the case of Ag, this absorption cannot lead to the escape of electrons because the energy of the excited electron is below the work function of the material.+ It should be noted that free electron absorption becomes the dominant absorption mechanism only when interband transitions are forbidden.[96]

Collective plasma oscillations (c) occur for incident photons with frequency equal to plasma frequency (in the absence of interband transitions),[96] and therefore need not be considered as a possible absorption mechanism in the near infrared region. In short, then, the only mechanism which can give rise to absorption at $h\nu$ = 1.48 eV in sodium is free electron absorption.‡ Because of the 2.3 eV work

---

* In these experiments, a monolayer of Cs has been coated onto the Ag so that the work function is reduced to 1.65 eV.

\+ With the exception of the electrons from the Fermi tail which for $T > 0°K$, may be emitted (see Chapter II, Section C3).

‡ Neglecting two photon transitions and interband transitions arising from the Fermi tail.

function of sodium, as mentioned earlier, it cannot give rise to an external photoelectric effect however.

3. Nondirect transitions

For photon energies near the photoelectric threshold, the possibility of nondirect transitions has already been discussed (see Chapter II, Section C3). This section is concerned with transitions in the region somewhat above (>1 eV) the photoelectric threshold. Photoemission studies on Cu and Ag, primarily in the region well above threshold, have recently been made by Berglund and Spicer.[18] They have shown that nondirect optical transitions, i.e., transitions in which the direct conservation of k-vector is not important, are stronger than direct ones in both metals. Similar statements have been made for the alkali metals by Meessen.[17] However, Berglund and Spicer have also observed rather weak direct transitions from p- and s-like states close to the Fermi level to states above the vacuum level.

They have examined the energy distributions of the electrons emitted from evaporated sodium surfaces, as observed by Dickey,[98] and conclude from the data that the transitions giving rise to photoemission from sodium for $h\nu > 3.96$ eV are nondirect. Careful consideration of Dickey's data shows, however, that the most energetic peak in the photoelectron energy distribution moves to higher energy at a slower rate than the incident photon energy.

This would indicate that direct transitions take part in the photoemission process, since the peak in the energy distribution for nondirect transitions either increases at the same rate as the increase in photon energy (corresponding to a peak in the initial density of states), or remains fixed in energy (corresponding to a peak in the final density of states).[18] A numerical tabulation of the energy increase in the peak of the energy distribution function in sodium is compared with the increase in photon energy in Table IV. Similar conclusions could be drawn from the data of Methfessel[94] and Dickey for potassium.

TABLE IV

Increase in Peak of Energy Distribution of Electrons Emitted from Sodium, Compared with Increase in Photon Energy

Incident Photon Energy, $h\nu$	$\Delta h\nu$	Electron Energy at Peak	Δ Peak
3.96 eV		1.4 eV	
	.93 eV		.85 eV
4.89		2.25	
	.91		.75
5.80		3.0	
	.91		.55
6.71		3.55	

Because of a lack of accuracy in the determinability of the above numerical values from Dickey's plots, however, the presence of direct transitions cannot be confidently affirmed. However, in the theoretical analysis for double quantum photoemission to be given later, only direct transitions will be considered.

D. Two Photon Volume Photoelectric Emission

1. Introduction

If radiation with a frequency below the interband threshold is incident upon an alkali metal, direct interband transitions are forbidden in first order. These transitions may occur in second order however, provided that the two absorbed photons impart enough energy to the absorbing electron to overcome the potential barrier at the surface of the metal. Thus, two relations must be satisfied in order that a photoelectron be ejected through an interband transition in second order:

$$\frac{h\nu'}{2} < h\nu < h\nu' \qquad (3.9)$$

and

$$\frac{e\varphi}{2} < h\nu < e\varphi \qquad (3.10)$$

Here, ν is the frequency of the incident radiation, ν' is the threshold frequency for interband transitions from the con-

duction band, and $e\varphi$ is the work function of the material. For radiation at 8450A incident on sodium metal, both of these relationships are satisfied.

A calculation of the expected two quantum current will be made using a model for the interband mechanism, considering only $\vec{k}$-conserving transitions. As mentioned previously nondirect transitions will not be considered. A preliminary model* for this interaction was first set up by Peter Bloch,[11] who made second order calculations on a simplified version of the model used by Fan.[13] This model is, however, inadequate in some respects and an attempt is made here to make Bloch's model more realistic. Consideration is therefore given to several modifications, which are discussed in the following three sections: Section 2 provides a better estimate for the depth of photoemission, making use of Thomas'[14] experimental results; Section 3 discusses the absorptivity of thin films and bulk metals and permits the very important effects of light reflection at the surface of the metal to be taken into account, and Section 4 discusses the matrix elements for the double quantum transition. Finally, in Section 5, the theoretical value for the two quantum volume photoelectric current is estimated.

---

* P. Bloch permits the reciprocal lattice vector $\vec{g}$ to take on continuous values, in contrast to Fan, so that the photoelectric threshold frequency for two quantum transitions has its normal value. Thus, Bloch disposes of the second photoelectric threshold satisfactorily.

2. Range of the photoelectrons

The depth from which photoelectrons may be emitted, i.e. the range of photoelectrons in the metal,* has been experimentally determined to be a strong function of the electron energy. Thomas[14] has made measurements on thin potassium films, and has found that the escape depth is about 200 atomlayers for light of wavelength λ = 5000A, while it is only about 2 atomlayers for light of wavelength λ = 3000A.

The short electron mean-free-path observed for higher frequencies has been attributed by Thomas to the high probability of plasmon emission at these frequencies. Berglund and Spicer[18] have shown that the effect of plasmon emission may be very easily observed in the energy distribution of photoemitted electrons. They have also considered another mechanism for inelastic scattering, electron-electron scattering, which also alters the energy distribution function, but in an altogether different way. Which scattering mechanism is of more importance can therefore be directly determined by examination of the energy distribution of photoelectrons. Berglund and Spicer have ascertained that in both Ag and Cu, the strongest scattering mechanism is

---

* The photoelectron lifetime is determined by scattering with a large energy loss, so that the electron cannot escape. This is different from the lifetime of a conduction electron, which depends on electron-phonon and electron-defect interactions.[16]

electron-electron scattering, for electrons with energies from 1.5 to 11.5 eV above the Fermi level. No evidence of scattering due to plasmon creation was found. They have also pointed out that the energy distribution of photoelectrons from Na measured by Dickey[98] contains secondary peaks which are typical of electron-electron scattering. It thus appears that this mechanism is dominant in sodium as well. A theoretical discussion of the relative effects of plasmon creation and electron-electron scattering in the determination of the mean free path of excited electrons has been given by Quinn,[99] and is in agreement with the observed results.

Because the range of photoelectrons varies in an inverse way with the energy of the photoelectron, in the two quantum process it is expected that the photoelectron range will be limited by the energy of the electron after the absorption of two photons. It is immaterial whether or not there is an intermediate state. For the double quantum process then, the absorption of two photons of energy 1.48 eV by the electron imparts to it an energy equivalent to that which would be obtained by the absorption of one photon of energy 2.96 eV. Thus, the mean-free-path for the two photon process in sodium should, to good approximation,* be determined by the experimental curves of Thomas[14]

---

* (Footnote on following page)

at 4200A. This value is approximately 90 atomic layers corresponding to a range of ~400A.

In Chapter II, it has been estimated that the sodium film used in the experiments described in this work was ~500A. This indicates that the film thickness should not limit the production of photoelectrons. Furthermore, if the film is thicker than this value, it is of no consequence with regard to the electron range, although it can affect the absorptivity of the film as discussed in the next section.

A proper evaluation of the double quantum current would entail an integration over the absorption, as a function of depth into the sample, and over the escape probability, which is also a function of depth.+ As an approximation to this case, the emission is assumed to be proportional to the average absorption, multiplied by the average escape depth. It would be very difficult to perform a more precise calculation, especially without detailed information about the structure of the metallic film. The light absorptivity of the sample is discussed in the next section.

---

* Results for the mean free path in Cs have been similar to those in K.[16] It is expected that all of the alkali metals would behave similarly.

+ For a potential such as the image potential,[85] the probability of the electron's transmission through the surface may be taken to be unity, provided that the energy of the velocity component perpendicular to the surface is greater than the height of the potential barrier.[15] This unity probability is generally assumed.[13,15,11,18]

3. The effective vector potential

In the case of the volume photoeffect, it is the vector potential inside the metal which stimulates transitions. P. Bloch's treatment of the two quantum photoeffect neglects the effect of reflection at the surface. For incident radiation with a photon energy below the interband threshold ($\simeq$ 2 eV in sodium), the dominant mechanism of absorption in the metal is the "free carrier" absorption. At these long wavelengths, the oscillations of the free electrons are out of phase with the exciting field,[49] and lead to a large reflection coefficient R for the incident radiation. Thus, only a small net field is effective inside the metal. An adequate way of determining what average percentage of the incident intensity appears inside the metal is therefore to estimate 1 - R. For a non-transmitting material, or a sufficiently thick film, this is equal to the absorption A.

Because the sodium surface considered was a thin film ~500A thick, as indicated previously, the absorption properties of films will be considered. The results for this case will then be compared with the results for solid sodium. A general approach is necessary because of the lack of experimental data for the optical properties of sodium films.

The optical properties of thin films have been investigated by many authors;[51,50,100,48,54,101,102] these prop-

erties are considerably different from those of the bulk material. The Maxwell Garnett[103] model for a thin film treats the film as consisting of a large number of spherical metal particles, each small compared with the wavelength of light and the film dimensions. Each spherical particle has the optical constants of the bulk material. The model is quite realistic, as may be seen from electron photomicrographs of thin films, and qualitatively accounts for the observed optical behavior.[54] The theory is not sufficiently sophisticated, however, to provide accurate quantitative data.*

Absorption occurs in a metal because of both bound and free electrons, free electron absorption being more important for the longer wavelengths,[97] as discussed earlier. For 8450A, below the threshold frequency for interband transitions, the absorption in sodium is due to the free electrons.+ From the Maxwell Garnett theory, free-carrier absorption in films is expected to be considerably greater than the free-carrier absorption in bulk materials.[104] Therefore, considering that the extent of aggregation of the metallic particles on the substrate is very much a function both of the thickness of the film and the rate of evaporation

---

* This is one reason why Mayer and Thomas[15] theoretically considered only the absolute quantum yield, q_a, which is the number of emitted electrons per absorbed photon (see also reference 17).

+ The absorption due to double quantum transitions and electrons in the Fermi tail is assumed to be negligible.

in forming the film, it is expected that the absorption at longer wavelengths will depend markedly on these two variables. Unfortunately, particular data for sodium films does not seem to be available,[105] but as expected for the long wavelength region, the absorption properties of films of the various metals are observed to be similar when the films have a similar aggregation state.[55,101] Because the free electron properties of Ag, Cu, and Na are in many respects similar,[106] the values observed by Sennett and Scott[55] for the free electron absorption in thin films of silver will be assumed to approximate the results for sodium films. For a film ~400A thick, and an evaporation time ~1.5 minutes, the absorptivity is ~5% at 6500A. For this range of film thickness, the absorption varies rather slowly with wavelength so that this result should be similar for 8450A.

Most of the thin film studies discussed in the literature were for films deposited on glass or quartz substrates. In the case of interest here, the sodium film was deposited on a nickel substrate, but considering the Maxwell Garnett theory, this effect should not be significant. A theoretical treatment for metallic thin films deposited on metals has been given by Vašíček,[107] but this treatment is based upon a model using Maxwell's equations for a bulk homogeneous slab of material.

The foregoing discussion was applicable for the case of a thin film. It is now of interest to compare the thin film absorption with that of a solid metal. For this purpose, it is useful to consider the Drude-Zener theory. In this model, the absorption is due to the free carriers. An expression for the reflectivity in the Drude-Zener theory is given by Bennett, et al.[48]

$$R = 1-\left(\frac{2\omega}{\pi\sigma_o}\right)^{1/2} [(1+\omega^2\tau^2)^{1/2}-\omega\tau]^{1/2} \qquad (3.11)$$

Here, R is the (intensity) reflectivity from the metal, ω is the incident circular light frequency, σ_o is the dc conductivity in esu, and τ is the lifetime of the free electron. At very long wavelengths, for $\omega\tau << 1$, this relation reduces to the familiar Hagen-Rubens relation.

The portion of the above equation in square brackets may be rewritten as follows:

$$[\omega\tau(1 + \frac{1}{\omega^2\tau^2})^{1/2}-\omega\tau]^{1/2} . \qquad (3.12)$$

For $\omega\tau$ sufficiently greater than unity, a Taylor expansion may be made on the term $(1 + \frac{1}{\omega^2\tau^2})^{1/2}$ above, yielding the following simplified form for the reflectivity:

$$R = 1-(\frac{2\omega}{\pi\sigma_o})^{1/2} [\frac{1}{2\omega\tau}]^{1/2} . \qquad (3.13)$$

This approximation should give an adequate order of magnitude estimate for the reflectivity.

Using a wavelength of 8450A, and the following values for parameters in sodium,[89]

$$\omega = 2.25\text{x}10^{15}\ \text{sec}^{-1}$$

$$\sigma_o = 2.09\text{x}10^{17}\ \text{(esu)}$$

$$\tau = 3\text{x}10^{-14}\ \text{sec},$$

it is verified that $\omega\tau \sim 100$ is sufficiently greater than unity for the validity of the Taylor expansion. Inserting these values into the equation for the reflectivity, it is seen that

$$1\text{-}R = 7\text{x}10^{-3} \sim 10^{-2}. \qquad (3.14)$$

Thus, in this region approximately 1% of the incident radiation enters the metal, the remainder being reflected. It is encouraging that the value obtained with this model is quite close to the experimental value for Ag at this wavelength; the absorptivity of silver is expected to be close to that of sodium as discussed earlier. The absorptivity of the bulk metal is seen to be less than that estimated for the rapidly evaporated thin film, in agreement with the Maxwell Garnett theory. The absorptivity for both models is of the same order of magnitude, however, so that the precise film

thickness is not a critical quantity in estimating the double quantum volume photocurrent.

4. The matrix elements

In this section, the second order matrix element for direct interband transitions involving the absorption of two photons is considered. The calculation will provide an estimate for the matrix element as well as information about the relative importance of the various terms in the interaction Hamiltonian.

For a two photon process, where transitions in first order are forbidden,[108] the transition amplitude $a_n^{(2)}(t)$ is given by[11,109,108]

$$a_n^{(2)}(t) = \hbar^{-2}\left[\sum_{n'} \frac{\langle n|\mathcal{H}^{(1)}|n'\rangle\langle n'|\mathcal{H}^{(1)}|o\rangle}{E_o - E_{n'} + h\nu} + \langle n|\mathcal{H}^{(2)}|o\rangle\right] \times \frac{e^{i(E_n - E_o - 2h\nu)t/\hbar} - 1}{E_o + 2h\nu - E_n} \quad . \tag{3.15}$$

The symbols in the above expression are to be interpreted as follows:

$\mathcal{H}^{(1)}$: $\vec{A}\cdot\vec{p}$ term in the interaction Hamiltonian

$\mathcal{H}^{(2)}$: A^2 term in the interaction Hamiltonian

o : initial state (conduction band)

n' : intermediate state

n : final state

E_o : energy of initial state

$E_{n'}$: energy of intermediate state

E_n : energy of final state

ν : frequency of incident radiation

In evaluating this transition amplitude, it is assumed that electrons make only k-conserving (vertical) transitions between Bloch states. That is, volume absorption resulting from direct transitions is the only process considered.

The term arising from second order perturbation theory $(\mathcal{H}^{(1)})$

$$\sum_{n'} \frac{\langle n|\mathcal{H}^{(1)}|n'\rangle\langle n'|\mathcal{H}^{(1)}|o\rangle}{E_o - E_{n'} + h\nu} \tag{3.16}$$

is treated first. The summation is understood to extend over all intermediate states n'. It is seen that the intermediate states are virtual since the interband threshold in sodium lies at about 2.06 eV, which is well above the energy of an incident photon (1.48 eV). The final state lies in the first band above the conduction band since the threshold for transitions to the second band above the conduction band lies in the ultraviolet.[15]

It should be noted that transitions to intermediate states are vertical, even though the states are virtual, since crystal momentum is conserved in the Bloch scheme.* Therefore, the intermediate states lie on a vertical line at a particular value of k. However, transitions from the conduction band to the next higher band are expected to dominate transitions from the conduction band to other bands for the following reasons: (a) the energy denominator $(E_o - E_{n'} + h\nu)$ is larger for higher energy bands, and (b) matrix elements of the form $\langle n|\mathcal{H}^{(1)}|n'\rangle$ are generally smaller than matrix elements of the form $\langle n|\mathcal{H}^{(1)}|n\rangle$, as will be seen later. To good approximation, then, the final state may be considered to be the only intermediate state, and the transition amplitude for this term may be written:

$$\sum_{n'} \frac{\langle n|\mathcal{H}^{(1)}|n'\rangle\langle n'|\mathcal{H}^{(1)}|o\rangle}{E_o - E_{n'} + h\nu} \simeq \frac{\langle n|\mathcal{H}^{(1)}|n\rangle\langle n|\mathcal{H}^{(1)}|o\rangle}{E_o - E_n + h\nu} . \tag{3.17}$$

The two matrix elements above, $\langle n|\mathcal{H}^{(1)}|n\rangle$ and $\langle n|\mathcal{H}^{(1)}|o\rangle$, as well as the matrix element arising from $H^{(2)}$, will be estimated in parts (a) through (d) to follow.

(a) Evaluation of $\langle n|\mathcal{H}^{(1)}|o\rangle$: The matrix element $\langle n|\mathcal{H}^{(1)}|o\rangle$ has been explicitly evaluated by R. A. Smith.[110] Using Bloch wave functions of the form $\psi_n = u_n(\vec{r},\vec{k}')e^{i\vec{k}'\cdot\vec{r}}$, and considering the vector potential $\vec{A} = A\vec{a}_o e^{i\vec{K}\cdot\vec{r}}$, where $\vec{a}_o$ is in

* The energy need not be conserved for a virtual state, however.

the x-direction, the matrix element is seen to be (see Eq. (58) in reference 110)

$$\langle n|\mathcal{H}^{(1)}|o\rangle = \frac{ie\hbar A}{2mc}\int_c u_n^*(\vec{r},\vec{k}')[\vec{a}_o\cdot\nabla u_o(\vec{r},\vec{k}')+i(\vec{a}_o\cdot\vec{k}')u_o(\vec{r},\vec{k}')]d^3\vec{x}. \tag{3.18}$$

Here, the integral is performed over a unit cell c of the crystal. The wave number of the light $\vec{K}$ has also been neglected in comparison with the electron wave number $\vec{k}'$, so that $\vec{k}'' = \vec{k}'+\vec{k}\sim\vec{k}'$. The volume element is denoted by $d^3\vec{x}$.

As Smith points out, the first term above is generally much greater than the second because of the orthogonality of the Bloch wave functions for different bands. If $\vec{k}'$ were precisely equal to $\vec{k}''$, the second integral would vanish exactly. However, the finite value of $\vec{K}$ for the light wave prevents the matrix element from being exactly zero, although the small size of $\vec{K}$ in comparison with $\vec{k}'$ and $\vec{k}''$ make the second term negligible in comparison with the first (provided that the first is not forbidden, of course). Therefore, one may write

$$\langle n|\mathcal{H}^{(1)}|o\rangle \propto \int_c u_n^*(\vec{r},\vec{k}')\nabla_x u_o(\vec{r},\vec{k}')d^3\vec{x}. \tag{3.19}$$

Before numerically estimating this quantity [this is done in part (d)], it is useful to consider the interaction term arising from $H^{(2)}$.

(b) Evaluation of $\langle n|\mathcal{H}^{(2)}|o\rangle$: Using Bloch wave functions for bands 0 and n, the matrix element for the A^2 term in the Hamiltonian becomes

$$\langle n|\mathcal{H}^{(2)}|o\rangle = \frac{e^2A^2}{2mc^2N}\int u_n^*(\vec{r},\vec{k}'')e^{-i\vec{k}''\cdot\vec{r}}e^{2i\vec{K}\cdot\vec{r}}u_o(\vec{r},\vec{k}')e^{i\vec{k}'\cdot\vec{r}}d^3\vec{x}. \tag{3.20}$$

Because of the periodicity of u_n and u_o, this integral is expressed as a sum over the unit cells of the crystal which is of the form

$$\langle n|\mathcal{H}^{(2)}|o\rangle = \frac{e^2A^2}{2mc^2N}\int_c u_n^*(\vec{r},\vec{k}'')\,u_o(\vec{r},\vec{k}')d^3\vec{x}\sum_j e^{i(\vec{k}'+2\vec{K}-\vec{k}'')\cdot\vec{R}_j} \tag{3.21}$$

where $\vec{R}_j$ is the lattice vector which determines the j^{th} cell, and N represents the number of unit cells in the crystal. This procedure is identical to that used by Smith in his calculation of the matrix element for the $\vec{A}\cdot\vec{p}$ term. The sum in the above expression is zero unless

$$\vec{k}'+2\vec{K}-\vec{k}'' = 0, \tag{3.22}$$

in which case it is equal to N, yielding the conservation of crystal momentum. Once again taking $\vec{k}' = \vec{k}''$, the matrix element becomes

$$\langle n|\mathcal{H}^{(2)}|o\rangle = \frac{e^2A^2}{2mc^2}\int_c u_n^*(\vec{r},\vec{k}')u_o(\vec{r},\vec{k}')d^3\vec{x}. \tag{3.23}$$

The integral above may now be seen to be identical to the second integral of Eq. (3.18). Therefore, by the same arguments given following Eq. (3.18), the above matrix element in Eq. (3.23) may be neglected, provided that the photon energy is of the same order of magnitude as the electron energy. This last condition takes account of the constant of proportionality in the matrix elements. Thus,

$$\langle n|\mathcal{H}^{(2)}|o\rangle \longrightarrow 0. \tag{3.24}$$

Peter Bloch,[11] in his analysis of the two quantum photoeffect, incorrectly assumed that the oscillator strength arising from the above transition was of the order of unity, and therefore (tacitly) attributed the double quantum volume photoemission to the A^2 term in the Hamiltonian.

(c) Evaluation of $\langle n|\mathcal{H}^{(1)}|n\rangle$: In the same manner, this matrix element may be written as

$$\langle n|\mathcal{H}^{(1)}|n\rangle = \frac{ie\hbar A}{2mc}\left[\int_c u_n^*(\vec{r},\vec{k}')\nabla_x u_n(\vec{r},\vec{k}')d^3\vec{x} + ik_x' \int_c u_n^*(\vec{r},\vec{k}')u_n(\vec{r},\vec{k}')d^3\vec{x}\right]. \tag{3.25}$$

In order to conserve crystal momentum in this case, the transition is actually between two very close, but distinct points in the band n. However, since $\vec{K} \ll \vec{k}'$, the usual approximation of $\vec{k}' = \vec{k}''$ may be made.

In the Wigner-Seitz approximation, u_n is a spherically symmetric function,[111] so that the first integral above vanishes (strictly forbidden).[112,113] The second integral, on the other hand, is equal to unity by the orthonormality of the Bloch wavefunctions.[110] The matrix element may therefore be written

$$\langle n|\mathcal{H}^{(1)}|n\rangle \simeq \frac{-e\hbar A k_x'}{2mc} \tag{3.26}$$

or

$$\langle n|\hat{p}_x|n\rangle \simeq \hbar k_x \ . \tag{3.27}$$

(d) Numerical estimate for $\langle n|\mathcal{H}^{(1)}|o\rangle$: Numerical values for all of the matrix elements except $\langle n|\mathcal{H}^{(1)}|o\rangle$ have thus far been obtained. The numerical value of this matrix element may be calculated with the help of the f-sum rule.[114] This rule may be written

$$\sum_{n'} f^x_{n'o} = 1 - \frac{m}{\hbar^2}\frac{\partial^2 E}{\partial k_x^2} \tag{3.28}$$

where $f^x_{n'o}$ represents the oscillator strength for the transition $|o\rangle \longrightarrow |n'\rangle$, and $\frac{1}{\hbar^2}\frac{\partial^2 E}{\partial k_x^2}$ is a familiar expression for the reciprocal effective mass.[115] For the alkali metals, this is explicitly given by[+ 116]

[+] This expression may also be derived from the Wigner-Seitz approximation for a cubic crystal.[113] This derivation is less general, however.

$$\frac{2}{m} \sum_{n'} \frac{\langle o|\hat{p}_x|n'\rangle\langle n'|\hat{p}_x|o\rangle}{E_o - E_{n'}} = 1 - \frac{m}{m^*} \qquad (3.29)$$

where m* represents the effective mass of a conduction electron, o represents the conduction band of the metal, and n' represents a band other than the conduction band.

It is the value of the matrix element $\langle n|\hat{p}_x|o\rangle$ where n is the next band above the conduction band, which is of interest. However, since this matrix element appears as only one term inside the summation sign, one cannot solve exactly for $\langle n|\hat{p}_x|o\rangle$ in terms of m/m*. Rather, an attempt must be made to isolate this term. This is only possible if matrix elements to all other bands $\langle n'|\hat{p}_x|o\rangle$ with $n' \neq n$ are small in comparison with $\langle n|\hat{p}_x|o\rangle$. For sodium, this is <u>not</u> the case since there is strong coupling between the conduction band and the bands just below and just above it. In fact, these couplings tend to be equal and opposite, just cancelling.[117] †

For lithium, however, there is no p-like band below the conduction s-like band, so that only matrix elements from states above the conduction band contribute to the summation. Furthermore, the next higher band (n) above the conduction band (o) should be coupled to it more closely than any other

† This is why $m^* \cong m$ for sodium.[117]

band by virtue of: (a) the smaller energy denominator in Eq. (3.29), and (b) the likeness of the higher energy wavefunctions to plane waves.[118] Therefore, insofar as the energy bands in lithium are similar to those in sodium, which is a reasonable assumption,[95] Eq. (3.29) may be approximated as

$$\frac{2}{m\hbar\omega_1} |\langle n|\hat{p}_x|o\rangle|^2 = f_{no}^x \simeq 1 - \frac{m}{m^*(Li)} \qquad (3.30)$$

where $E_o - E_n$ has been set equal to $-\hbar\omega_1$. The term $E_o - E_n$ represents the energy difference between the bands o and n and therefore, $-\hbar\omega_1 \simeq -2h\nu$. With[117]

$$m/m^*(Li) \simeq 0.70, \qquad (3.31)$$

the oscillator strength f_{no}^x for the transition under consideration in sodium is found to be $f_{no}^x \sim 0.3$.

Using the fact that $\langle n|\mathcal{H}^{(2)}|o\rangle = 0$, as derived in part (b), the spatial part of the transition probability from Eq. (3.15) is proportional to the following factor, defined as ρ:

$$\rho = \left[\left|\frac{2\langle n|\hat{p}_x|n\rangle\langle n|\hat{p}_x|o\rangle}{mh\nu}\right|^2\right] \qquad (3.32)$$

This expression for ρ has been placed in square brackets to indicate that it is to replace the (incorrect) expression

in square brackets in the paper by P. Bloch (reference 11, Eq. (7)). Explicitly evaluating ρ, it becomes

$$\rho = \frac{2}{mh\nu}|\langle n|\hat{p}_x|o\rangle|^2 \cdot \frac{2}{mh\nu}|\langle n|\hat{p}_x|n\rangle|^2 \qquad (3.33)$$

$$= 2f_{no}^x \cdot \frac{4}{h\nu}\left(\frac{\hbar^2 k_x^2}{2m}\right) \qquad (3.34)$$

since $\frac{2}{mh\omega_1}|\langle n|\hat{p}_x|o\rangle|^2 = f_{no}^x$ as shown in part (d), and $|\langle n|\hat{p}_x|n\rangle|^2 = \hbar^2 k_x^2$ as shown in part (c). Since $\hbar^2 k_x^2/2m$ represents the kinetic energy of the excited electron in its final state, it may be estimated at $\sim$ 2 eV above the Fermi level, or at about 5 eV. The term $h\nu$ represents the photon energy and is equal to 1.48 eV. The oscillator strength f_{no}^x has been calculated in part (d) to be about 0.3.

Finally, then

$$\rho \sim 2(0.3) \cdot \frac{4}{1.5}(5) = 8 \ . \qquad (3.35)$$

This value of ρ will be used to estimate the theoretical double quantum volume photoelectric current in the next section.

Thus, using a model which allows only direct interband transitions, it is clear that the $\vec{A}\cdot\vec{p}$ term in the Hamiltonian is dominant, and that the two photon absorption process occurs without the benefit of a real intermediate state.

5. Estimate of the two photon current

The two quantum current arising from the mechanism described in the last section will now be estimated. P. Bloch's[11] equation for the two quantum photocurrent, including corrections derived earlier for the matrix element, the photoelectron escape depth, and the reflection at the metallic surface, becomes*

$$i^{(2)} = \pi e\left\{\frac{2N-1}{N}\right\}\left[\frac{\rho dr_o{}^2 mc^2 (\beta P)^2}{(2\pi)^2 2(h\nu)^3 \nu A}\right]\left[\frac{4\pi}{3}\left(\frac{E_F}{2h\nu}\right)k_F\left(1 + \frac{e\varphi}{E_F} - \frac{2h\nu}{E_F}\right)^{3/2}\right]. \tag{3.36}$$

The symbols have the following meanings (values given are for Na):

$i^{(2)}$	:	two quantum photocurrent
r_o	:	classical electron radius = e^2/mc^2
P	:	incident radiation power
A	:	area of spot illuminated
$e\varphi$	:	work function of material = 2.28 eV
E_F	:	Fermi energy of material = 3.12 eV
k_F	:	wave number of electron at Fermi surface = 0.9×10^8 cm^{-1}

---

* Only the contribution from Eq. (17a) in Bloch's paper is considered; the contribution from Eq. (17b) is several orders of magnitude smaller. In addition, Bloch's matrix elements were too large by a factor of $(2\pi)^{1/2}$; this has been corrected here.

N : number of modes in which laser is oscillating

ν : frequency of incident radiation = 3.58×10^{14} sec^{-1} (1.48 eV)

d : escape depth or photoelectron range = 400A

β : absorption coefficient for incident radiation = 0.05

ρ : two quantum "oscillator strength" = 8.

The first factor in curly brackets, $\left\{\frac{2N-1}{N}\right\}$, has been included to take the multimode operation of the laser into account. This factor arises from random phase contributions from different mode pairs, which cause the double quantum current to be a random function, and thus enhance it. Bloembergen has discussed this factor in connection with second harmonic generation and other non-linear processes.[119] This factor may also be responsible for deviations from the quadratic dependence of the photocurrent on the intensity, as will be discussed later (see Chapter IV), in connection with the oscilloscope photographs of the double quantum current (Fig. 8). The derivation is applicable for N modes of equal amplitude; the factor has been used by others[83,120] as well as by Bloembergen.

A large number of modes were simultaneously oscillating in the laser used for the double quantum experiments, as discussed in Chapter II, section A4. Since it may be assumed

that several of these modes were oscillating at comparable amplitudes the theoretical result must therefore be increased by a factor of $\frac{2N-1}{N} \simeq 2$ (for $n > 3$).

The values for d, β, and ρ above are those estimated earlier in this chapter. Inserting the above values into Eq. (3.36) the double quantum volume photoelectric current becomes

$$i^{(2)} \sim 3.6 \times 10^{-20} \frac{P^2}{A} \text{ amperes} \qquad (3.37)$$

where P and A are expressed in MKS units. As in the case of the second order surface effect, the current is proportional to the square of the incident radiation power, and inversely proportional to the area of the illuminated spot. The above value should provide only an order of magnitude estimate to the current.

By comparison with Eq. (3.8), it is seen that the calculated two photon volume photoelectric effect is several hundred times greater than the calculated two photon surface photoelectric effect. As will be seen in Chapter IV, the estimated value for the two photon volume photoelectric effect is in reasonable agreement with the observed value.

IV. EXPERIMENTAL MEASUREMENT OF THE TWO QUANTUM PHOTOELECTRIC CURRENT FROM SODIUM METAL

While the preceeding chapter was concerned with a theroetical model for the two photon photoelectric effect, this chapter is concerned with the experimental observation of the effect from sodium metal. Experiments were conducted under two sets of conditions, as described previously in Chapter II: (a) with a freshly recoated sodium surface in photomultiplier KM2462, and (b) with the as-received sodium surface in KM2462, which was approximately 6 months old at the time the experiments were performed.

To begin with, a discussion of the experimental method is given; this was the same in both cases. Results of experiments under the two sets of conditions above are then reported. A discussion of the Fourier coefficients of the modulated photocurrent follows. Finally, other effects which may yield electron emission are discussed.

A. Experimental Method

The apparatus used for the experimental measurement of the double quantum photoelectric effect is shown in the block diagram of Fig. 6. The radiation source was a pulsed GaAs semiconductor injection laser operated at 77°K and emitting a peak radiation power of 400mW at 8450 A.

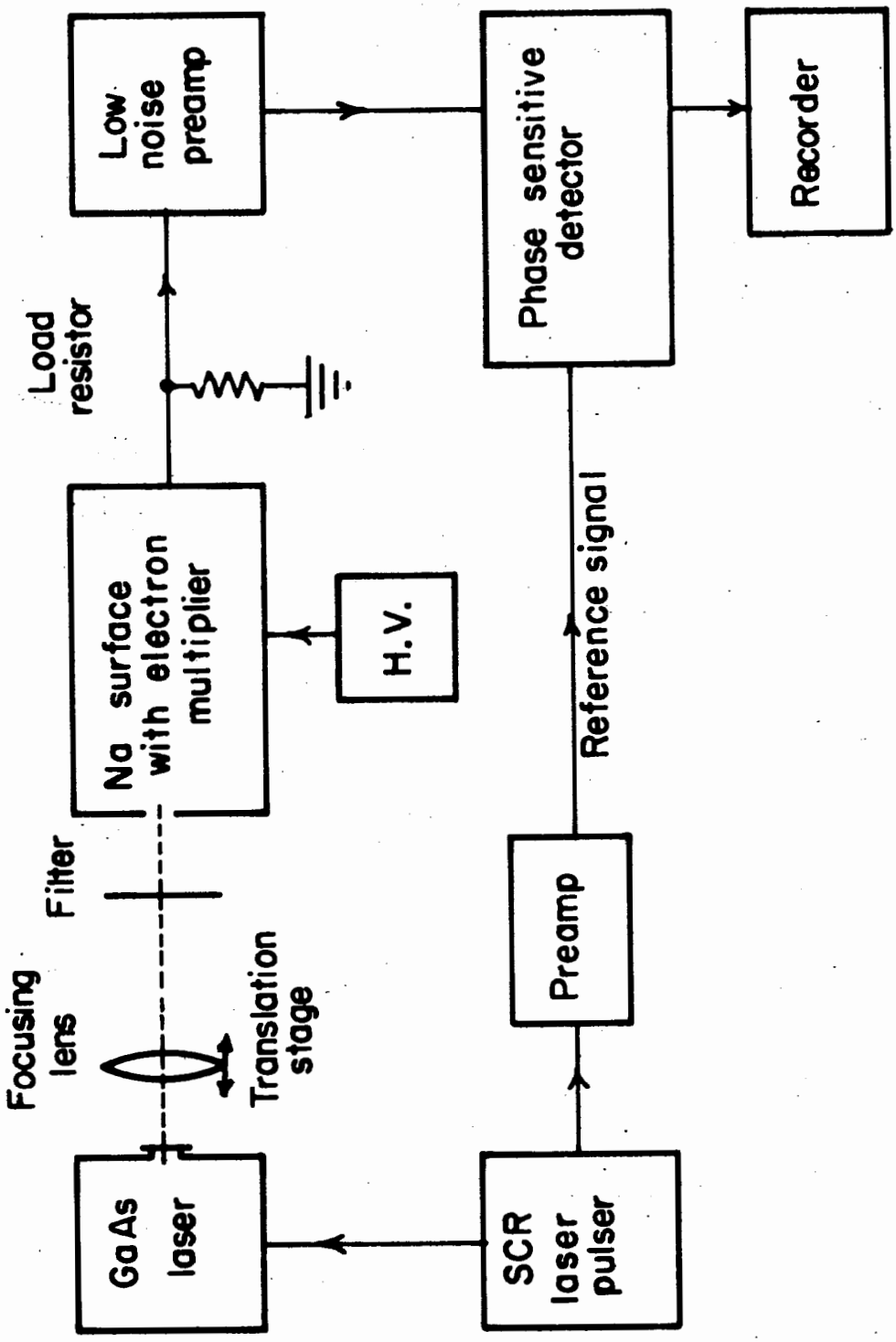

Figure 6. Block diagram of apparatus.

A translation stage supporting a lens permitted the laser radiation to be focused onto a vapor-deposited sodium surface from which double quantum photoemission was to be observed. This surface acted as a cathode in a specially constructed photomultiplier with a gain of 50,000. The amplified current was passed through a load resistor followed by a low-noise preamplifier and a lock-in amplifier. Phase sensitive detection was performed at 2.2 kHz, which is the fundamental frequency of the pulse modulated laser. The reference signal was obtained directly from the pulsed power supply driving the laser. A detailed discussion of the individual components has been given in Chapter II.

In performing an experiment, filters calibrated at 8450 A on a Cary spectrophotometer were inserted into the beam to provide known decrements of light power. Output voltage measurements were then recorded for each power level. Using the known gain of the system (see Table III), the fundamental frequency component of the cathode photocurrent was obtained. It was found that ordinary glass filters could not be used to provide the decrements of light intensity, because refraction in the glass caused the imaged spot size and position to change. Thin gelatin (Kodak wratten) filters were found to be quite suitable, however.

Before discussing the results of these experiments, it should be mentioned that two other experimental arrangements were used in an attempt to observe the double quantum photoeffect: (a) using a He-Ne gas laser as the radiation source, about 20mW of radiation at 1.15μ (1.08eV) was permitted to impinge on the sodium surface in KM2462 (before recoating), and (b) the radiation from an M.I.T. GaAs laser (8450 A) operating with a peak power of 400mW was permitted to impinge on an RCA 1P28 photomultiplier (S-5 surface; Cs_3Sb semiconductor photosurface)*. Both of these experiments were unsuccessful. In the first experiment, no photoelectric current was observed. This presumably resulted from insufficient incident radiation power, or possibly from too low a photon energy to provide a sufficiently large number of double quantum transitions. Results of the second experiment were erratic. The dependence of the photocurrent on the incident radiation power was seldom quadratic; sometimes the dependence was faster, sometimes slower. This behavior might have resulted from local overloading or saturation of the photocathode, although improved performance was not obtained with lower incident

---

* This was the phototube used by Sonnenberg, Heffner, and Spicer[22] in their observation of the two photon photoeffect from a semiconductor. They used a Nd-doped glass laser radiating at 1.06μ(1.17eV) as the radiation source, however.

light intensities.

B. Experimental Results for Freshly Deposited Sodium Surface

1. Presentation of data

The simplest way of presenting the data from experiments such as those described in the last section is graphically. A log-log plot may be used with the measured light power plotted on the abscissa, and the measured photocurrent plotted on the ordinate. In this way, a linear dependence of photocurrent on radiation power appears as a straight line of unity slope, while a quadratic dependence appears as a straight line of slope two.

The results of a typical experimental run (using the procedure described in section A) for a freshly deposited sodium surface are shown in Fig. 7, where the measured photoelectric current has been plotted against the peak radiation power incident on the face of the sodium surface photomultiplier tube. From Fig. 7, it is seen that the experimental points fall on a line of slope 2. This quadratic dependence of the photoelectric current on the incident radiation power, signifying two quantum photoelectric emission, extends for over four orders of magnitude of the photocurrent.

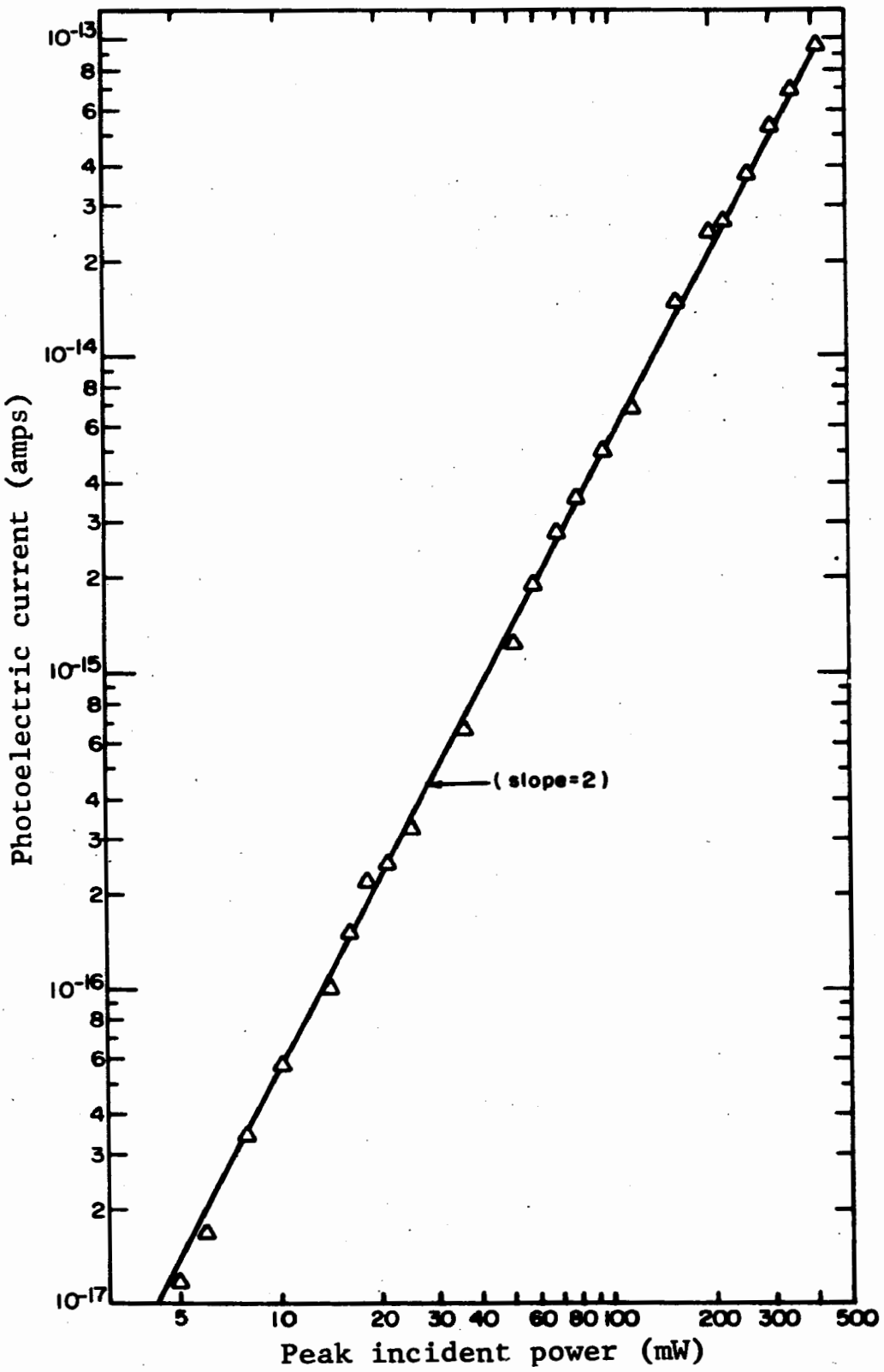

Figure 7. Fundamental frequency component of photoelectric current vs peak radiation power incident on face of sodium surface photomultiplier. Because of absorption at the face of the photomultiplier, the radiation power incident on the sodium surface is less than the value shown above (see text).

In order to compare the magnitude of this effect with other effects, a general parameter relative to cw incident radiation is useful.* As discussed in Chapter I, for the two photon photoelectric effect, the double quantum yield Λ is satisfactory for this purpose. To calculate Λ, the observed photocurrent must be divided by the first Fourier coefficient of the square of the incident laser radiation waveform, p(t). This has been estimated to be 0.1 (see Chapter II, section A3).

To obtain the peak radiation power incident on the sodium surface, which is also necessary to calculate Λ, a correction must be made for the absorption and reflection at the face of the sodium photomultiplier KM2462. In these experiments, only about 40% of the measured radiation power has been estimated to impinge on the sodium photocathode (see Chapter II, section C6).

The overall gain γ of the system for the particular experimental parameters used in this measurement was $\simeq 10^{-13}$mho, as shown in Table III. Parameter values are also given in this table. The maximum observed photocurrent is 10^{-13}amp (corresponding to 10^{-12} amp referenced to cw laser radiation) occurring at a maximum peak radiation power of 400mW incident

* The cross-section is an example of such a parameter.

on the photomultiplier face (corresponding to 160mW incident on the sodium surface). This corresponds to a double quantum yield $\Lambda_{Na}(8450A) \simeq 8 \times 10^{-16} I_o$ amps/watt. Results such as those shown above were obtained for various polarization states of the incident radiation.

2. Oscilloscope photographs

In experiments performed with the freshly coated sodium photocathode, the double quantum photocurrent was sufficiently large to be directly observed on an oscilloscope.* Figure 8(a) shows a trace of the double quantum photocurrent, $p(t)$, directly above a trace of the incident radiation waveform, $\ell(t)$, which is shown in Fig. 8(b). A Dumont 6911 photomultiplier was used to display $\ell(t)$. (Scattered light was detected.) The double quantum current was observed with a 10kΩ load resistor on the output of the photomultiplier and a (maximum) oscilloscope sensitivity of 5mV/div. The photomultiplier was operated at 2450V, above the value of 2215V generally used.

The profile of $p(t)$ is as expected: i.e. $p(t)$, which is theoretically equal to $\ell^2(t)$, is more sharply peaked than $\ell(t)$. In fact, if $\ell(t)$ were precisely hemispherical, which

* Tektronix model 555 dual-beam oscilloscope.

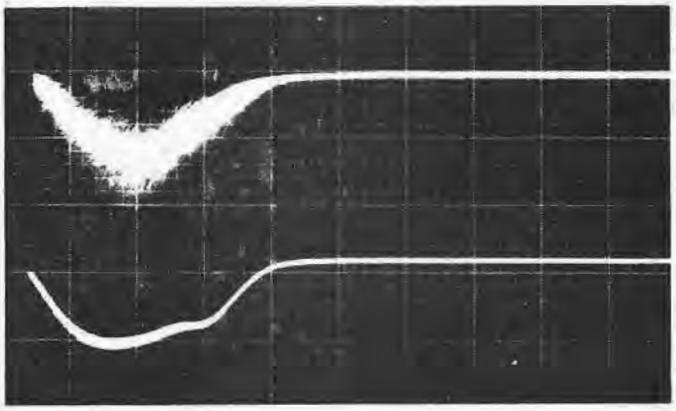

(a)
vert: 5 mV/div
horiz: 10 μsec/div

(b)
horiz: 10 μsec/div

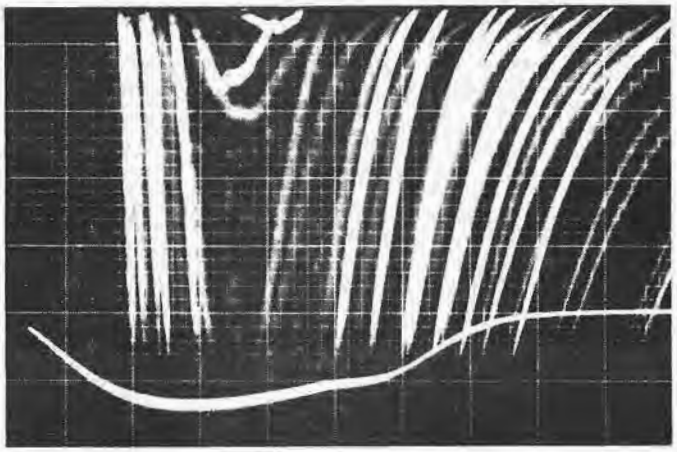

(c)
vert: 20 mV/div
horiz: 5 μsec/div

(d)
horiz: 5 μsec/div

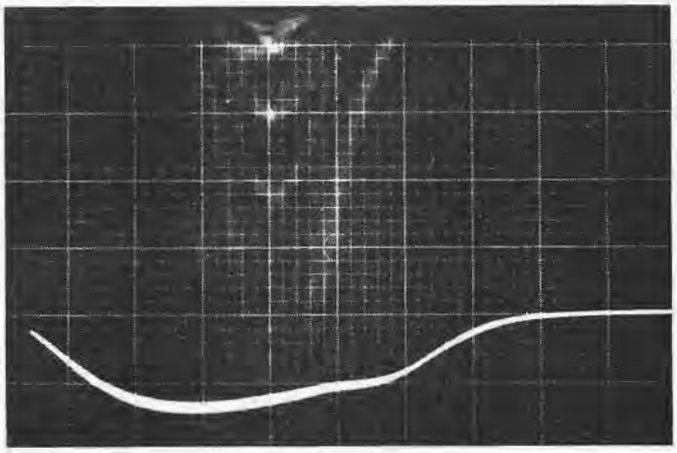

(e)
same as (c)

(f)
same as (d)

Figure 8. (a), (c), and (e): Oscilloscope trace of double quantum photocurrent waveform, p(t). (b), (d), and (f): Trace of incident laser radiation waveform, $\ell(t)$. In (c) and (e), the vertical scale is expanded and the zero line displaced upward from that of (a), to show randomly occurring large spikes of double quantum current.

is a reasonable approximation to the observed waveform in Fig. 8(b), then p(t) would theoretically be parabolic. This, in fact, is not too different from the observed shape for p(t) seen in Fig. 8(a). However, it is seen that the double quantum waveform is not simply the square of the single quantum waveform. This may be understood to arise from variations in the spatial intensity distribution of the focused laser beam as a function of time. Since the quadratic intensity dependence of the double quantum current weighs higher intensity regions more heavily than lower intensity regions, an inhomogeneous intensity distribution in space and time will enhance the non-linear effect. Thus the changing mode structure of the laser output* during the (non-square) current pulse is seen to be responsible for this effect. Similar observations have been reported by others.[119]

In Fig. 8(c) and (e), the vertical scale has been expanded, and the zero line displaced upward from that in Fig. 8(a), in order to show some typical large spikes of double quantum emission. Spikes of this magnitude were found to occur with an average repetition rate of 2/sec. For this photograph, the intensity of the upper beam

---

* See Chapter II, section A3.

of the oscilloscope was increased sharply in order to display some of these large pulses. These pictures emphasize both the randomness and the bunching (near the peak of $\ell(t)$) of the double quantum current spikes.

3. Comparison with theory

The experimentally observed two quantum photoelectric current may be compared with the theoretical estimate for the current given earlier (see Chapter III, section D5). It is recalled here that only direct interband transitions were considered. Using this theoretical model, it was found that only the $\vec{A}\cdot\vec{p}$ term in the Hamiltonian was of importance. The predicted double quantum photoelectric current (from Eq. 3.37) was found to be

$$i^{(2)} \simeq 3.6\times10^{-20}P^2/A \text{ amp}$$

where $i^{(2)}$ represents the double quantum photoelectric current, P represents the cw radiation power incident on the sodium surface, and A is the area of the focused laser beam, all in MKS units.

Qualitative verification for the inverse area dependence has been experimentally obtained: a large, but gradual rise in output current is observed when the lens is adjusted to image the laser emitting region on the sodium surface. The quadratic dependence of $i^{(2)}$ on P has been amply demonstrated experimentally in Fig. 7.

Numerically, the focused laser spot on the sodium surface has been estimated to have an area of $2\times10^{-9}m^2$, and a maximum incident radiation power of 160mW (corresponding to 400mW incident on the face of the sodium surface photomultiplier) has been assumed. Inserting these values into Eq. (3.37), the following theoretical estimate for the double quantum photocurrent* obtains:

$$i^{(2)}_{theor}\ (160mW) \sim .5\times10^{-12}amp.$$

This may be compared with the experimental value from Fig. 7 at the same power, also referred to cw laser radiation:

$$i^{(2)}_{expt}\ (160mW) \sim 1\times10^{-12}amp.$$

It is encouraging that both results are of the same order of magnitude. However, an absolute comparison between the experimental and theoretical currents may not be made because of uncertainies in both.

It should be mentioned that this order of magnitude agreement does not preclude contributions to the double quantum photocurrent from other mechanisms (e.g. nondirect transitions). On the other hand, because this current is several orders of magnitude larger than the predicted two quantum <u>surface</u> photocurrent (see Eq. 3.8), this latter

---

* This is referred to cw radiation.

mechanism seems to have little importance in the observations reported here.

C. Experimental Results for As-Received Sodium Surface*

1. Presentation of data

Using the same experimental method as described previously (section A), photocurrent measurements were made from the sodium surface in KM2462, in its as-received (unrecoated) condition. Since this experiment was performed prior to recoating KM2462 (see Chapter II, section C5), the radiation power incident on the sodium surface was identical to that incident on the photomultiplier face,** in contradistinction to the experiments described in the last section (see also Chapter II, section C6).

The results of a typical run for the as-received sodium surface are shown in Fig. 9, where the photoelectric current has been plotted against the peak radiation power incident on the sodium surface. The resulting experimental data may be fitted quite well by the curve A+B, obtained by adding line A of slope 1 to line B of slope 2. Line A shows a linear dependence of photoelectric current on light power and represents the single quantum photoelectric

---

* A preliminary account of this section has been given in Phys. Rev. Letters 13, 611 (1964).

** Neglecting reflection losses at the glass face.

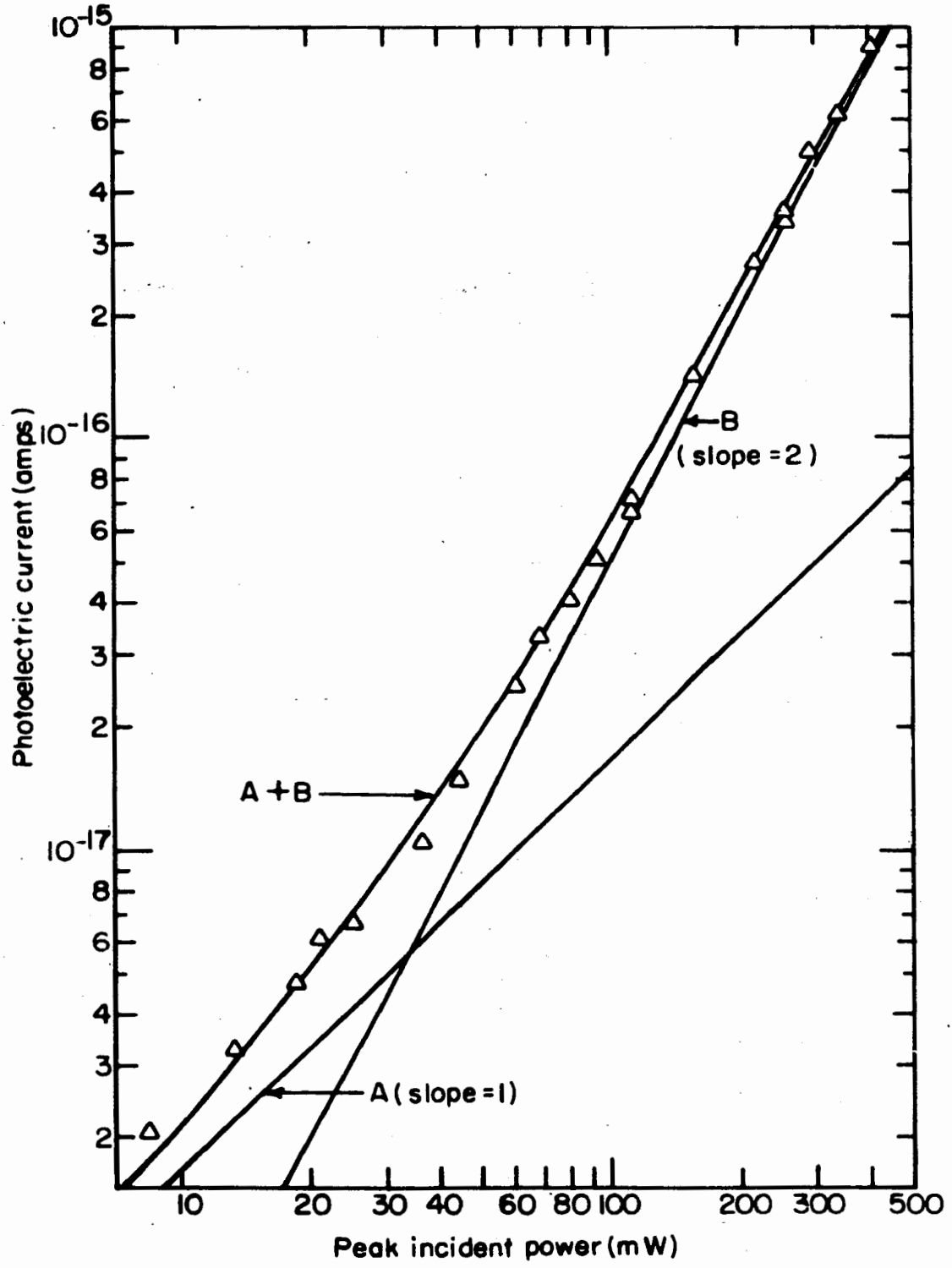

Figure 9. Fundamental frequency component of photoelectric current vs peak radiation power incident of the as-received sodium surface for a typical run. At high powers, the current is seen to approach the line of slope 2, corresponding to double quantum photoemission. As the power is reduced, the admixture of single quantum photoelectrons from the Fermi tail increases, causing the current to approach the limit of slope 1.

contribution from the Fermi tail, as will be justified in section E, while line B shows a quadratic dependence of photoelectric current on light power representing the double quantum photocurrent.

It is seen that the experimental points near the maximum values of incident power fall very close to line B, indicating that the total current in this region arises almost exclusively from two quantum transitions. The admixture of single quantum current at maximum incident power is seen to be less than 7%. At a peak radiation power of 400mW, corresponding to 1.7×10^{18} photons/sec, the fundamental component of the two quantum photoelectric current is $\sim 10^{-15}$amp. The knee of the curve, where the contribution of double and single quantum currents are equal, occurs at 6×10^{-18}amp. This current corresponds to approximately 40 electrons/sec. Below this point, and down to the lowest current value measured (2×10^{-18}amp, or about 12 electrons/sec), the curve showed a power dependence which was predominantly that of single quantum emission.

The overall gain γ of the system for the particular experimental parameters used in this measurement was about 1.3×10^{-14}mho, as shown in Table III.

The maximum current obtained from the as-received sodium surface was several orders of magnitude below that obtained from the freshly coated sodium surface. This may be accounted for by the difference in film thickness in the two cases: The volume photoelectric effect is

proportional to film thickness for films below a certain critical thickness, d_{crit}.[14,16] This large difference in the magnitudes of the current therefore substantiates both the proposition that the observed effect is a volume effect (since it would be very difficult to explain the large increase in current in terms of a surface effect) and the proposition which was set forth in Chapter II, that a very thin layer of sodium was present on the as-received surface. Furthermore, the large increase in current observed with the laser beam focused at the very edge of the photocathode, rather than toward the middle, is understood in terms of the increased depth of sodium at the cathode edge.

2. Single quantum photoemission from the Fermi tail

For very thin films (defined as films whose thickness is below d_{crit}),[14] the volume photoelectric current (both single and double quantum) is expected to be proportional to the thickness of the film, d. In this case, the ratio of the two currents should be independent of the film thickness. Experimentally, however, the ratio is not observed to be constant: In contrast to the data for the as-received surface (Fig. 9), the data for the recoated surface (Fig. 7) shows no unity slope (single quantum) contribution. In fact, since photocurrent measurements from the recoated surface were taken with lower values of incident radiation

power (the minimum power used was 1mW) than from the unrecoated surface (the minimum power used was 8mW), the relative contribution of unity slope for the recoated surface would be expected to be greater than for the unrecoated surface.*

A possible explanation for this observation is that the single quantum photoelectric emission arising from electrons in the Fermi tail**is a surface rather than a volume effect. In this case, the magnitude of the single quantum photocurrent would not necessarily increase upon recoating. The nature of single quantum photoemission from metals in the immediate vicinity of the work function threshold and/or the interband threshold is not completely understood, as discussed in Chapter II, section C3.

An alternative explanation for the effect relies on the presence of some other material, of work function 2.0eV, on the as-received sodium surface. Upon recoating the surface, this hypothetical impurity might have been covered over, thus becoming unable to contribute a single quantum photocurrent in experiments with the recoated cathode. However, no decision between these alternatives may be made on the basis of available experimental data.

* As discussed in Chapter III, d_{crit} is dependent upon the excitation energy of the electron: it is larger for lower energy electrons.[14] Electrons absorbing two photons via the double quantum effect are expected to have higher energies than electrons absorbing only one photon (Fermi tail electons). Therefore, if the film thickness were above the lower value of d_{crit}, the unity slope contribution would be further enhanced.

** Footnote on following page.

In any case, the work function may be estimated by the method set forth in Chapter II (section C3), from the value for the experimentally measured single quantum yield: From line A, and the known radiation power content at the fundamental frequency, the yield $Y(T,\lambda)$ of the unrecoated surface is

$$Y(300°K,\ 8450A) = 1.7\times10^{-15}\ \text{amp/watt}.$$

The value obtained for the work function by this method is in good agreement with the value obtained from a Fowler plot. As discussed in Chapter II, this method is expected to be valid, independent of the mechanism of photoemission.

D. Fourier Coefficients of the Modulated Photocurrent

The experiments described in the first part of this chapter were carried out at the fundamental repetition frequency of the laser modulation, 2.2kHz. Additional experiments were conducted in which the photocurrent was phase sensitive detected at multiples of the fundamental frequency up to 19.8 kHz (corresponding to the 9th multiple), rather than at the fundamental frequency itself. The

---

** Obviously, this is a valid interpretation only if the unity slope contribution to the photocurrent arises from single quantum photoemission from the Fermi tail. As mentioned previously, justification for this is given in section E.

results of these measurements are understood in a simple way, as discussed below.

1. Measurements with freshly coated sodium surface

Measurements of the Fourier components of the double quantum current from KM2462 and of the single quantum current from the 6911 photomultiplier were made by phase sensitive detecting at various multiples of the fundamental frequency. The same experimental conditions were used for the single and double quantum measurements, so that the results could be directly compared. In order to achieve the same dc photocurrent and therefore the same spacing between electron pulses in both cases, it was necessary to attenuate the light intensity impinging on the 6911 with filters. Rolloffs on the preamplifier were broad (LO: 300 Hz/HI: 300kHz) so that no correction factor for the Fourier components was necessary for the preamplifier. As discussed in Chapter II (section D2), the gain of the phase sensitive detector was essentially constant over the frequency range in which measurements were made.

In these experiments, the time constant of the load-resistor (10kΩ)/photomultiplier-cable combination, τ_{RC}, was about 1μsec. During the "on" time of the laser pulse, the double quantum current in these experiments had its maximum value of 10^{-12}amp (6.2×10^6 electrons/sec). The

average time between pulses from the photocathode was therefore, $\bar{t}_d \simeq 0.2\mu sec$. Therefore, $\tau_{RC} \sim 5\bar{t}_d$ and the resistor/cable combination is seen to act as an integrator. This causes the current pulses to take on the shape of the waveform p(t) for the double quantum current, and $\ell(t)$ for the single quantum current (see Fig. 8). In this case, where $\tau_{RC} > \bar{t}_d$, ordinary signal theory [121] along with its Fourier transform properties may be used.* It is this fact which makes the experimental results easy to interpret.

A plot of the Fourier coefficients of the one and two quantum currents vs the phase sensitive detection frequency is shown in Fig. 10. The difference in the Fourier spectrum

---

* A rigorous treatment for the case where $\tau_{RC} < \bar{t}_d$ would entail using the PSD for the stochastic process (e.g. the PSD calculated in Chapter II section D4 for the rectangularly pulsed Poisson process). However, since the "signal" is considered as the non-white part of the PSD and in view of the large RC filter on the phase sensitive detector, it would appear that ordinary Fourier components could even be used in this case. This seems to be experimentally borne out by the correct quadratic dependence observed for the first Fourier component of p(t) at all values of current, down to $\sim 10^{-17}$ amp. That is, the first Fourier component is indeed proportional to the number of emitted photoelectrons per unit time, even at very low current levels.

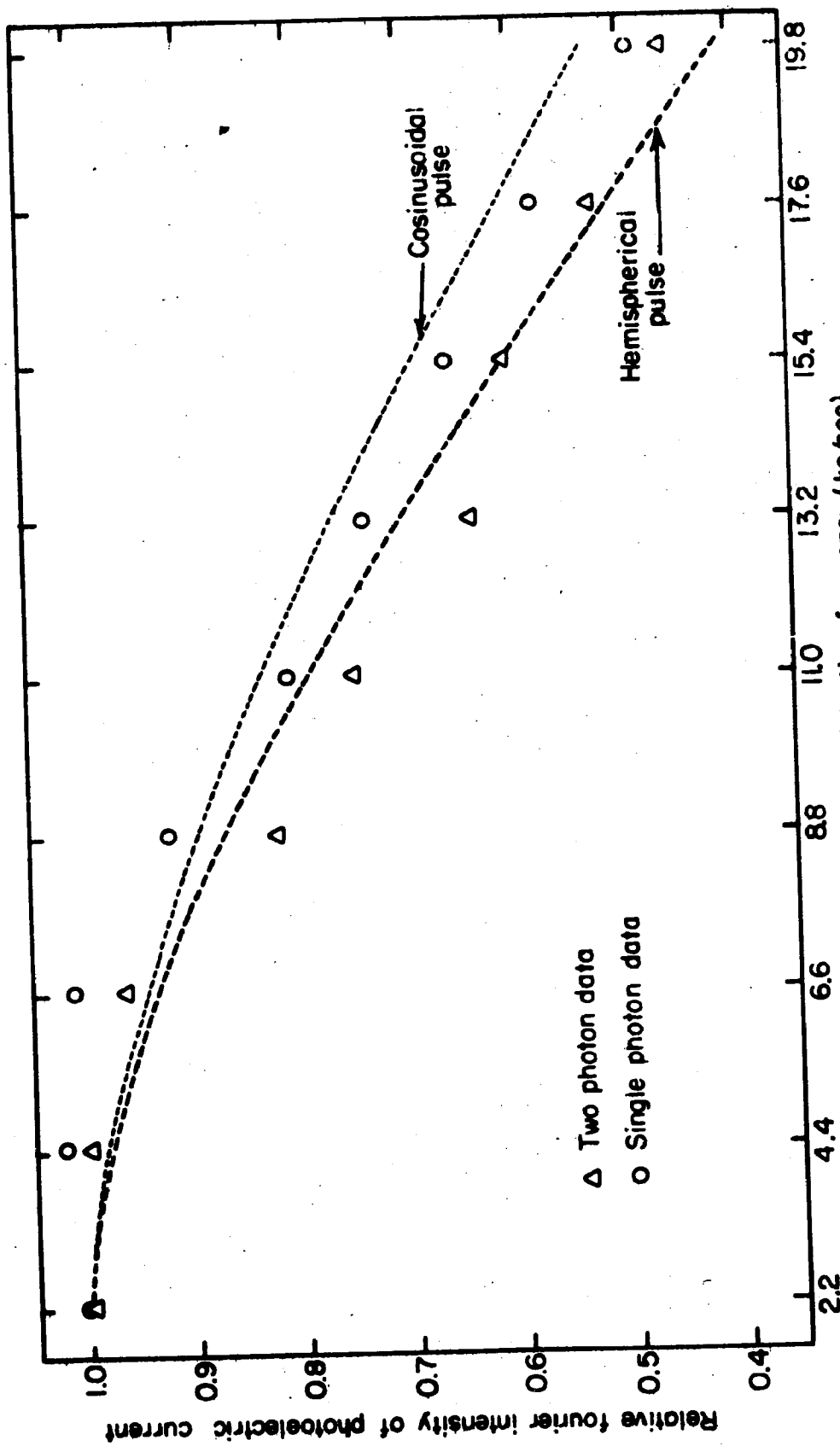

Figure 10. Fourier coefficients of the single and double quantum photocurrents for freshly deposited sodium surface at maximum incident radiation power (160 mW). Both cases have been normalized to unity at the fundamental repetition frequency of 2.2 kHz.

for the two cases is seen to reflect the difference in the single quantum current pulse shape $\ell(t)$ and the double quantum current pulse shape p(t), both shown in Fig. 8. A quantitative interpretation of the difference in the spectra is too difficult, however, for the following reasons: (a) the particular Fourier components for any model depend strongly on the fine details of the pulse shape and pulse width. This is demonstrated by the calculated cosinusoidal and hemispherical pulse spectra* shown in Fig. 10; and (b) only a small portion of the Fourier spectrum, from 2.2 kHz to 19.8 kHz, is available for comparison with theory. Thus, the qualitative interpretation given above will have to suffice.

2. Measurements with as-received sodium surface

A measurement of the Fourier components was also carried out before recoating the sodium surface. In this experiment, a load resistor of 100kΩ was used both for the single and double quantum data, so that τ_{RC} = 18μsec. For the maximum average current of 10^{-14}amp during the "on" time of the laser pulse (see Fig. 9), the mean time between electron emissions from the cathode is $\bar{t}_d$ = 17μsec so that $\tau_{RC} \simeq \bar{t}_d$. In this case, however, τ_{RC} = 18μsec is an

* Both spectra have been calculated for a full pulse width of 36μsec.

appreciable fraction of the width of the laser pulse, $\tau_1 = 36\mu sec$. Thus, in the time domain, the processed pulse width is expected to be approximately $\tau_1 + 2\,\tau_{RC} = 72\mu sec$, from the convolution theorem. This large pulse width ($\sim 70\mu sec$) has been observed with the 6911 photomultiplier.

In the frequency domain, the high ratio of τ_{RC}/τ_1 represents a cutoff of the high frequency response of the photocurrent by the load-resistor/photomultiplier-cable combination.

A plot of the power spectral density (PSD) of this current is shown in Fig. 11. In this case, it is the PSD, or the square of the Fourier spectrum, which is plotted. As expected, the width of the spectrum is considerably less than the width of the equivalent spectrum for the data discussed in the last section. This data is presented as an example of very strong filtering. Here, the entire laser pulse envelope is smoothed, rather than just the individual current spikes within it, as in the last section.

E. Other Effects

The experimental data presented in Fig. 7 and 9 has been attributed to two specific but distinct effects: (a) double quantum volume photoemission for the region of slope two, and (b) single quantum photoemission from electrons in

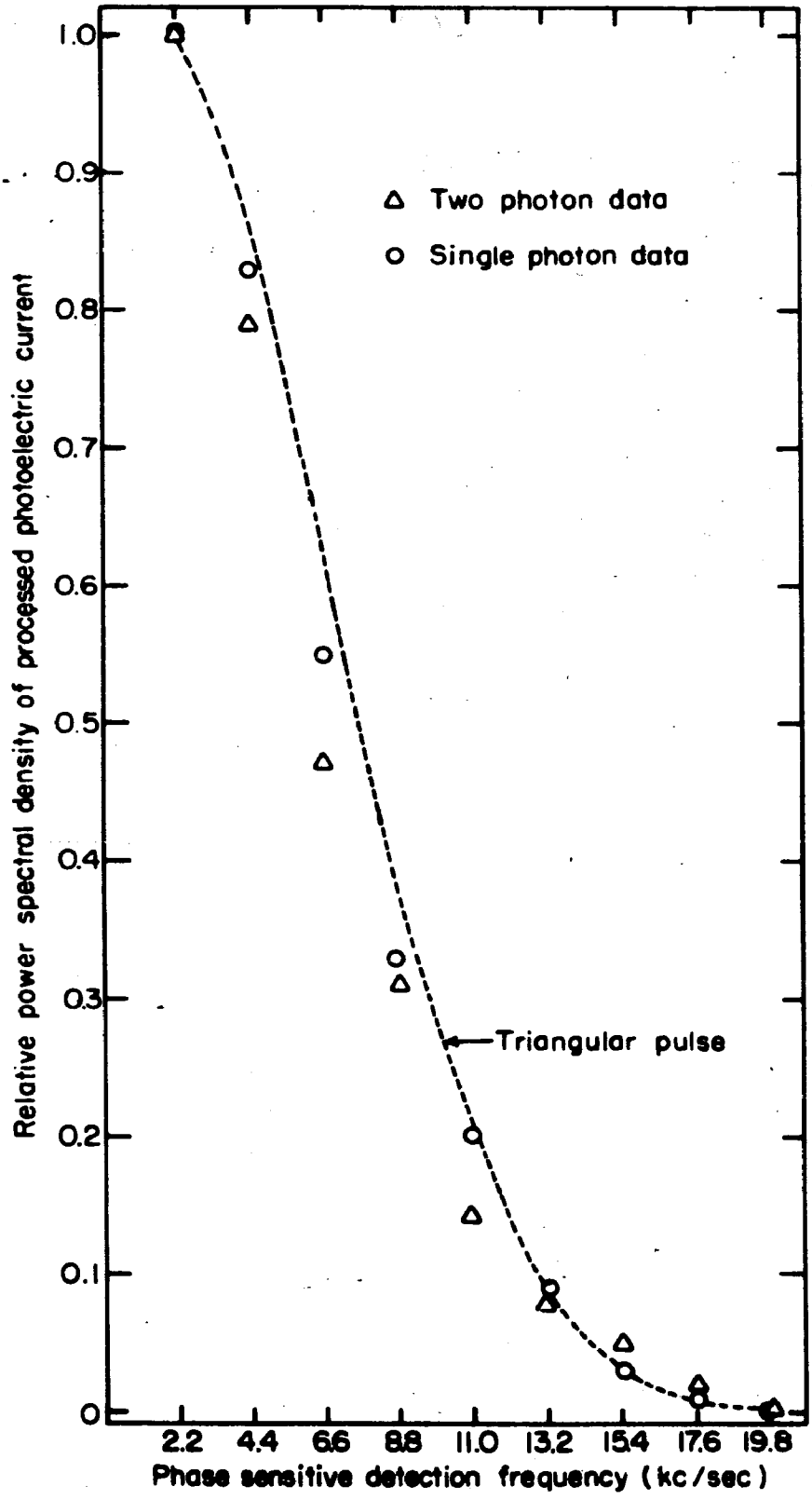

Figure 11. Power spectral density of the single and double quantum photocurrents for as-received sodium surface at maximum incident radiation power (400mW). Both cases have been normalized to unity at the fundamental repetition frequency of 2.2 kHz.

the Fermi tail for the region of unity slope. In the discussion to follow, it will be shown that other possible effects yielding electron emission do not contribute to the observed current. The following effects are discussed: 1. thermionic emission, 2. harmonic generation in the laser, and 3. harmonic generation at the metallic surface.

1. Thermionic emission

The following experiment was performed to enable the magnitude of the thermionic emission current to be estimated: The 400mW laser beam used in the previously described experiments was focused onto a chromel-alumel thermocouple which registered an (average) temperature increase of 2°C. Using a model for pulsed-laser-induced metallic heating,[9] which is based on the one-dimensional classical diffusion equation, the temperature rise at the peak of the laser pulse was estimated to be below 10°C. This corresponds to a maximum thermionic emission current below 10^{-26} amp (from the Richardson equation), which is well below the lowest current observed. The four decades of quadratic dependence of photocurrent on the incident light intensity is further evidence that the emission was not thermionic.

2. Harmonic generation in laser

Another possible cause of electron emission was the second harmonic generation of blue light (4225 A) in the

laser itself. This emission would cause a photocurrent of unity slope, since the decrements in incident radiation power were provided by calibrated filters, rather than by changing the laser power itself. Therefore, this effect could only masquerade as the single quantum emission from the Fermi tail, and not as the double quantum emission (which is of slope 2).

To ascertain that this effect was of no importance, the single quantum yield from the sodium phototube $Y(T,\lambda)$ was measured both with and without a blue attenuating filter in the laser beam. No difference in the behavior of the current could be detected, indicating that blue light from the laser was not producing an observable current. By this means, the peak second harmonic power generated in the laser was estimated to be $<10^{-11}$ watt for a power output of 0.4 watt at 8450A.

3. Harmonic generation at sodium surface

The emission of second harmonic radiation at an illuminated metallic boundary has been recently considered by several authors.[122,123,124] In particular, Brown, Parks, and Sleeper[123] have measured the second harmonic radiation from an evaporated silver surface, illuminated by a ruby laser producing pulses of 1MW peak power. They have estimated the harmonic generation efficiency at about 10^{-15}.

This will provide an upper limit to the efficiency for the case under consideration (which corresponds to a mixiumum intensity of $\sim 10^4 W/cm^2$ vs $\sim 10^6 W/cm^2$ for the ruby laser used by Brown, et al.).

Considering an incident radiation power of $\simeq$ .4 watt, the blue light generated at the sodium surface should therefore have a power well below 5×10^{-16} watt. If all of this harmonic radiation were absorbed to create photoelectrons from the sodium, this effect would provide an electron current below $5 \times 10^{-16} W \times 10^{-4} A/W \simeq 5 \times 10^{-20}$ amp, which is below detectability.

In any case, the current from this effect would be expected to depend quadratically on the incident power, so that this effect could not contribute at lower current values where the unity slope contribution becomes important. Furthermore, by examining the photosurface through a blue transmitting filter in the darkened laboratory, no blue light could be detected visually. Even a very small number of photons would be expected to be visible under these conditions.

Finally, it should be mentioned that the unity slope contribution at very low currents was independent of the beam focusing, as would be expected for single quantum photoemission.

V. CORRELATION FUNCTIONS AND TWO QUANTUM dc PHOTOMIXING

In this chapter, experiments are described in which double quantum photoemission was observed from a sodium surface illuminated simultaneously by two superimposed beams. In distiction to the ordinary single quantum photocurrent, a dc "photomixing" term is observed. This term reflects electron emission arising from the simultaneous absorption of one photon from each of the two beams. The experimental setup and observations are described in section A. In section B, the n^{th} order correlation functions, as defined by Glauber, will be used to provide a theoretical justification for the observations reported in section A. The second and fourth order correlation functions obtained for two particular experiments using a thermal source are considered in section C. Finally, a brief description of two quantum excess noise and photocounting statistics is given in the last section (section D).

A. The dc Photomixing Experiment

1. Experimental method and procedure

The apparatus used for the experimental measurement of the two quantum dc photomixing is shown in the block diagram of Fig. 12. The radiation source was a pulsed GaAs semiconductor injection laser (both LD256 and LD259 were

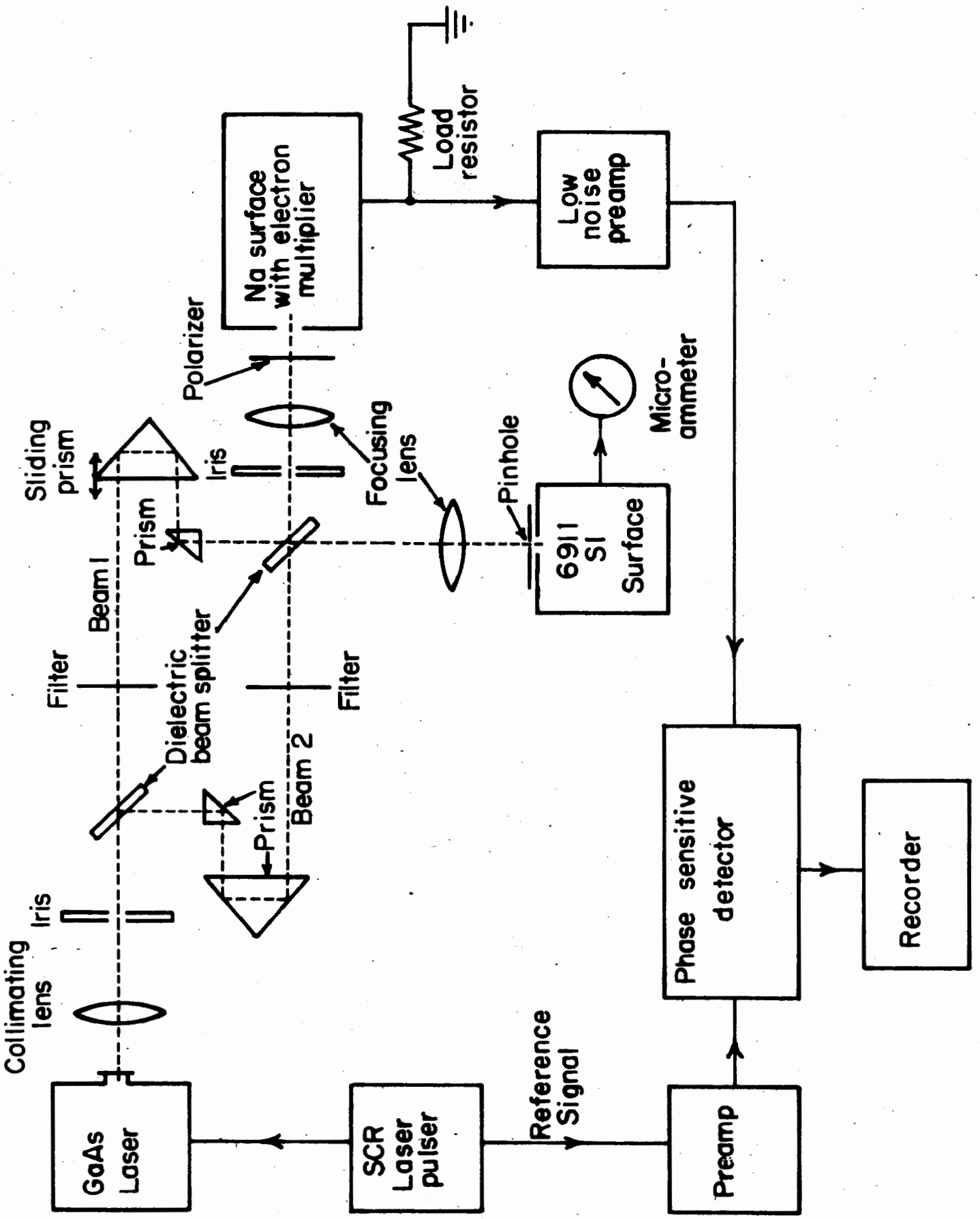

Figure 12. Block diagram of double quantum photomixing setup.

used) operated at 77°K and emitting a peak radiation power of 400mW at 8450A. The laser radiation was collimated by means of a lens ($\simeq$ 10cm focal length) and passed through a configuration of (dielectric) beam splitters* and (anti-reflection coated) prisms which resembles the Mach-Zehnder interferometer. The recombined beams were focused onto the vapor-deposited sodium surface in photomultiplier KM2462 by means of a focusing lens ($\simeq$ 6cm focal length) mounted on a Lansing Research Corp. translation stage. The two beams (denoted as Beam 1 and Beam 2) could be adjusted to go through different path lengths before being recombined at the final beam splitter. The intensities of the beams could also be adjusted independently by means of filters placed in either one of the beams. The radiation impinging on the photomultiplier was sometime polarized with a polarizer** placed in front of the face of photomultiplier KM2462 (see Fig. 12). With the exception of the 6911 photomultiplier also shown in Fig. 12, which will be discussed below, the remainder of the system was exactly the same as that used in the ordinary double quantum experiments described in Chapter IV.

---

* The beam splitters (2/3 transmitting, 1/3 reflecting) were only flat to about one wavelength; therefore fringes are effectively washed out.

** Polaroid Corporation, type HN-7 sheet polaroid.

A 6911 photomultiplier with a small pinhole (25μ diameter) acting as an aperture stop on the face of the photomultiplier was used in one leg of the "interferometer" output to provide a method of superimposing the two beams. Since the laser junction size is greater than the diffraction limit of the optics in the system, the laser junction is imaged by the focusing lens. Thus the purpose of the 6911 (which was also mounted on a translation stage) was to achieve coincidence of two imaged laser junctions, which are rectangles 10μx200μ in size (see Chapter II, section A2). The first beam splitter, and the small prism in Beam 2 were placed in adjustable gimbals (Lansing Research Corp., model GS-203) so that very precise adjustments of the relative positions of the two beams could be made. Beam alignment was effected by adjusting the various gimbals and translation stages for maximum photocurrent output from the 6911, as registered by the microammeter.

In order to be one-half superimposed at the focal plane of a (25cm focal length) lens, the two beams must be parallel to within about 5×10^{-5} radians, which corresponds to 10sec of arc. Although the gimbals supporting the optical components are adjustable to 6 sec of arc, the limiting factor for spot superposition was the photomultiplier field stop. Because the pinhole was too large for the

focused laser junction in one dimension, and too small in the other, the superposition procedure was, to a large degree, arbitrary. Furthermore, the distance between the pinhole at the front face of the photomultiplier and the cathode of the photomultiplier was about 3-4mm, permitting further arbitrariness in the superposition procedure. The 25μ pinhole diameter seemed to be about the optimum size; both larger and smaller diameters made superposition more difficult. Undoubtedly, a "pinhole" the size and shape of the laser junction would have made alignment easier. Because of the inhomogeneity of the sodium surface, nevertheless, this method of beam alignment was found to be more suitable than the alternative method of peaking the double quantum photocurrent by adjusting the gimbals.

The purpose of this experiment was to examine the dependence of the two quantum photocurrent for two superimposed beams on the relative intensities of the two beams, and on the path length difference between the two beams. Initially, the experiment was to be used as a self-integrating Hanbury Brown-Twiss type coincidence counter (as described in sectionC) in order to enable photon correlations to be observed with a very small resloving time, and to permit a measurement of the coherence time of the radiation. However, such second order correlations cannot

be observed with a source having coherence of order higher than 1,[26] as does the laser.[66] Therefore, such an experiment must be performed with either a thermal source, or with the laser operating below threshold. However, the radiation power below threshold was so low that it was not possible to observe double quantum emission. Furthermore, the difficulty in obtaining good superposition of the two laser beams made the experiment too difficult to perform.

Therefore, the double quantum photocurrent was investigated primarily as a function of the intensities of the constituent light beams, with the laser operating well above threshold. Since the laser radiation is assumed to have second order coherence,[66] the path length difference between the beams should have no effect on these experimental results (for a laser operating well above threshold). This independence on the path length difference was indeed observed, and measurements were therefore made with arbitrary values for this parameter.

In performing an experiment, the following procedure was followed: (a) The beams were first aligned to give maximum current from the alignment photomultiplier (6911); (b) Beam 1 was then blocked. The double quantum current from Beam 2 alone was first maximized by imaging the laser junction on the sodium surface, and then recorded. By

using a filter with a known decrement, it was then ascertained that this was pure two quantum emission. Thus, this current was proportional to I_2^2, where I_2 is the intensity of Beam 2; (c) Beam 2 was then blocked and the double quantum current from Beam 1 alone was recorded. This current was proportional to I_1^2. The constant of proportionality is the same in both cases; (d) Both beams were then unblocked, and the total double quantum photocurrent $i_T^{(2)}$ was recorded.* Experiments were performed with different values of I_1/I_2, obtained by attenuating one of the beams relative to the other by means of filters.

2. Experimental results

A plot of the total two quantum photoelectric current for both beams superimposed $i_T^{(2)}$ vs the intensity ratio of the two beams I_1/I_2 is shown in Fig. 13. In this plot, the intensity I_2 was normalized to unity. The experimental points are observed to lie on the parabola $(1 + \frac{I_1}{I_2})^2$ which indicates that the total two quantum dc photocurrent is proportional** to $(I_1+I_2)^2 = (I_1^2+2I_1I_2+I_2^2)$ since I_2 has been normalized to unity. Because the coefficient of the cross

---

* Pure double quantum emission was once again verified here.
** No reduction factor (to take account of the presence of many modes) need be applied to a dc photomixing term.[125]

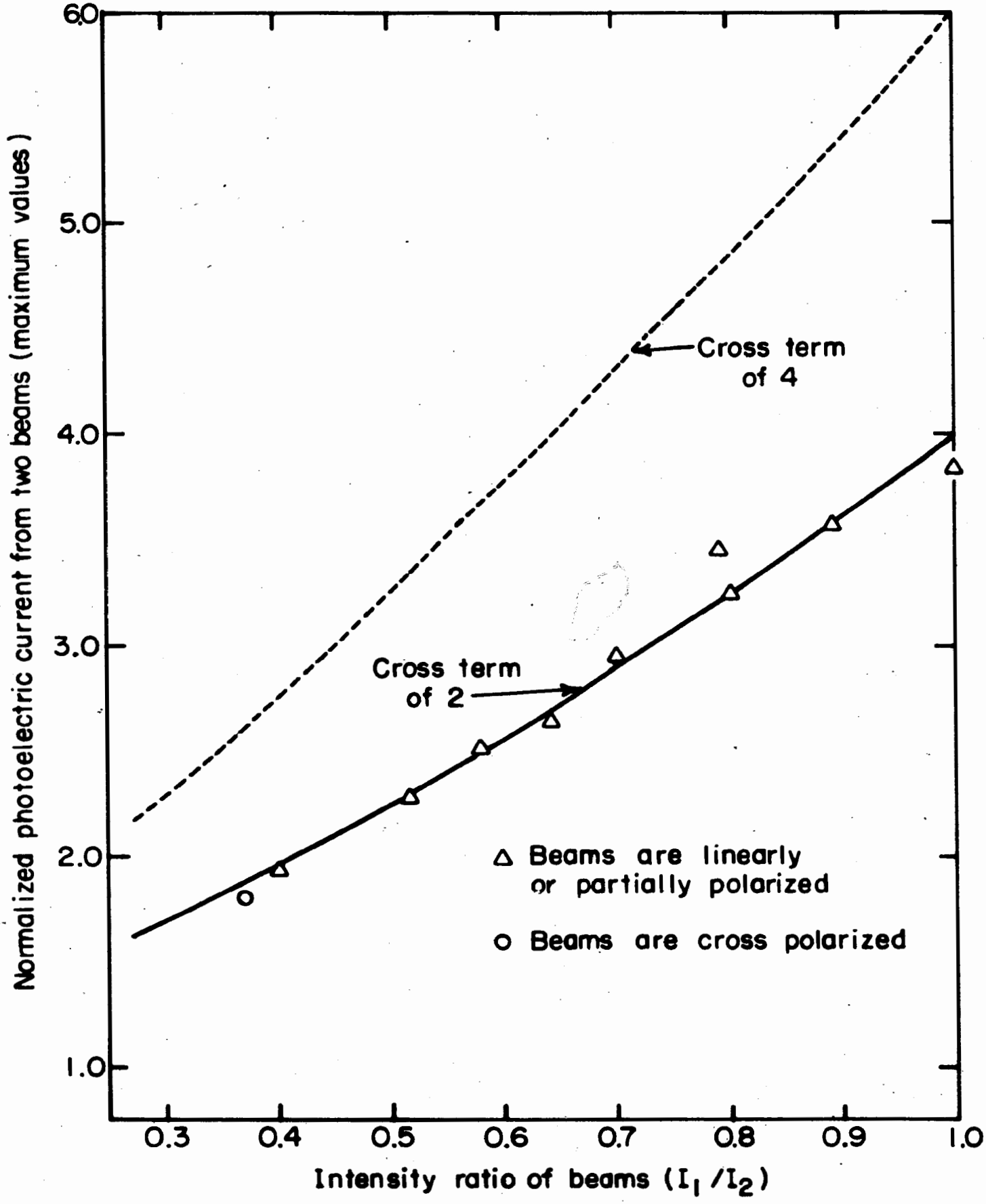

Figure 13. dc double quantum photocurrent from two beams vs intensity ratio of beams.

term I_1I_2 is 2, this curve has been labeled "cross term of 2". The dotted line in Fig. 13 corresponds to a current which is proportional to $I_1^2+4I_1I_2+I_2^2$ (also with I_2 normalized to unity) and is labeled "cross term of 4". It will be discussed later.

Only the highest observed values of $i_T^{(2)}$ are plotted in Fig. 13. Many more points than are plotted were found to lie below the "cross term of 2" curve. This result has been attributed to the difficulty in obtaining superposition of the two radiation beams (and hence superposition of the focused spots) on the sodium surface, as discussed earlier. The points plotted were obtained at path length differences δ of the two beams ranging from 0 to 100cm ($0<\delta<1m$). As expected, δ had no effect on the results. With one anomalous exception, there were no points observed above the "cross term of 2" curve.

It is seen from the circular point on Fig. 13, that two quantum dc photomixing may be obtained with orthogonally polarized light beams. This is not true for first order interference effects or photomixing[126,127] (see also Ref. 128, 129).

B. Second Order Correlation Functions: Laser Source

For an ideal single quantum photodetector the average counting rate at a space-time point $x_o = r_o,t_o$ is

proportional to a first order correlation function* which has been defined as follows by Glauber:[26]

$$G^{(1)}(x_o x_o) = \mathrm{tr}\left\{\rho E^-(x_o)E^+(x_o)\right\} \qquad (5\text{-}1)$$

The symbols E^- and E^+ represent the negative and positive frequency portions of the electric field operator E, and represent a photon creation and a photon annihilation, respectively. The state of polarization of the radiation has been included in x_o. The Hermitian density operator ρ is defined as the averaged outer product of field state vectors

$$\rho = \{|\times|\}_{av} \qquad (5\text{-}2)$$

so that

$$\mathrm{tr}\left\{\rho\theta\right\} = \{\langle|\theta|\rangle\}_{av} \qquad (5\text{-}3)$$

where tr is an abbreviation for the trace. The trace of the density operator is unity ($\mathrm{tr}\rho = 1$).

Similarly, the general second order correlation function may be written as

$$G^{(2)}(x_1x_2x_3x_4) = \mathrm{tr}\left\{\rho E^-(x_1)E^-(x_2)E^+(x_3)E^+(x_4)\right\} . \qquad (5\text{-}4a)$$

The average counting rate (at x_o) for the ideal <u>two photon</u>

---

* The correlation function used by Glauber is defined more generally as a function of two space-time points x_1 and x_2. This is a special case of the more general function, with $x_1 = x_2$.

detector is then proportional to the following special case of the second order correlation function:*

$$G^{(2)}(x_o x_o x_o x_o) = \mathrm{tr}\left\{ \rho E^-(x_o) E^-(x_o) E^+(x_o) E^+(x_o) \right\} . \qquad (5\text{-}46)$$

While the formalism of quantum mechanical coherence theory is not required for the development presented in this section, the second order correlation functions are nonetheless useful for this purpose. As Titulaer and Glauber[28] point out, with regard to a discussion of averages of nonlinear functions of the intensity, "the higher order coherence properties of the field furnish a natural basis for describing the results of such experiments." Furthermore, the applicability of the second order correlation function to a description of the double quantum process forms a link between this process and the photon correlation experiments of Hanbury Brown and Twiss,[29-32] since these also may be described in terms of the second order correlation functions.**[25-28]

Correlated photon annihilations must be discussed in terms of the incident radiation field. Considering an

---

* For an actual detector, the absorption of the photons cannot be localized too closely, and the photoemission rate must be written as an integral over the microscopic range of all the variables x_n, including the "lifetime" of the virtual (or real) intermediate state. This is analogous to the case for the real single quantum detector (see reference 26). This complication is neglected here.

** Glauber's (and our) second order correlation functions are referred to as fourth order correlation functions by Mandel and Wolf.[25]

experiment with n separate detectors, of which the Hanbury Brown-Twiss experiment is a special example, the space-time points for photon annihilations correspond to the space-time points of the photodetectors.

For the two quantum experiment, however, this is (in general) true only when one light beam is present. If two individual (but superimposed) beams are present, which are time delayed with respect to each other, the two photons giving rise to the photoelectron may come from different space-time points in the beam, although the photon annihilations occur at the same space-time point in the detector. Therefore, the x's above must be space-time points relative to the radiation source.

The total two quantum counting rate, for the case where two superimposed beams illuminate the detector, is therefore taken to be the sum of second order correlation functions corresponding to the following contributions: (a) the absorption of two photons from the same space-time point (both from the same beam) -- there are two of these terms (one for each beam); and (b) the absorption of two photons from different space-time points (each from a different beam) -- there are also two of these terms (one for each permutation of photon absorption). Denoting the space-time points of the beams by x_o and x_1, the average counting rate for the two photon detector illuminated by

two beams is then proportional to the following sum, denoted as

$$\gamma^{(2)} \equiv G^{(2)}(x_o x_o x_o x_o)+G^{(2)}(x_1 x_1 x_1 x_1)+G^{(2)}(x_o x_1 x_1 x_o)+G^{(2)}(x_1 x_o x_o x_1). \tag{5-5}$$

Terms of the form $G^{(2)}(x_o x_1 x_1 x_1)$ do not correspond to a photon annihilation, and therefore do not contribute to the counting rate. They correspond to interference terms.[28]

For a field possessing first order coherence,* Titulaer and Glauber[28] have shown that the higher order correlation functions must factorize into forms similar to those required for full coherence, differing from them only by a sequence of constants, g_n. In particular, for a field possessing second order coherence as well,** the second order correlation functions above may be written[28]

$$|G^{(2)}(x_i x_j x_j x_i)| = G^{(1)}(x_i x_i) \cdot G^{(1)}(x_j x_j) .$$

But, since the correlation function $G^{(1)}(x_j x_j)$ is proportional to the average single quantum counting rate at the space-time point x_j, the second order correlation function becomes

---

* This condition is assumed to be satisfied for the laser.[28]

** This condition is assumed to be satisfied for the single mode laser operating sufficiently above threshold. This is discussed by Armstrong and Smith,[66] and by Freed and Haus.[130]

$$G^{(2)}(x_i x_j x_j x_i) = c' \langle I_i \rangle \langle I_j \rangle \qquad (5\text{-}7)$$

where c' is a constant.

Using these relations, $\gamma^{(2)}$ may be written

$$\gamma^{(2)} = [G^{(1)}(x_o x_o)]^2 + 2[G^{(1)}(x_o x_o)][G^{(1)}(x_1 x_1)] + [G^{(1)}(x_1 x_1)]^2 \qquad (5\text{-}8)$$

and since the double quantum current $i_T^{(2)}$ is proportional to $\gamma^{(2)}$, it is given by

$$i_T^{(2)} = c[\langle I_1 \rangle^2 + 2\langle I_1 \rangle \langle I_2 \rangle + \langle I_2 \rangle^2] = c\langle I_1 + I_2 \rangle^2. \qquad (5\text{-}9)$$

Here, I_j represents the intensity of beam j, and c is another constant.* This relation shows that the total two quantum photocurrent is proportional to the square of the total intensity of the two beams.** This is the experimentally observed result, as shown in the last section. Furthermore, since the space-time index x carries a polarization coordinate μ, the separation of $\gamma^{(2)}$ into products of the form $G^{(1)}(x_j x_j)$ insures that the same result is obtained for orthogonally polarized radiation sources. This has also been observed experimentally (see Fig. 13).

---

* It is assumed that the laser is operating in a single mode so that the constant c does not contain the mode enhancement factor $\{2N-1/N\}$ which was discussed in Chapter III, section D5.

** A similar result has been obtained by Mandel and Wolf,[131] which is valid under certain conditions.

This result for the total double quantum photocurrent $i_T^{(2)}$ differs from that which is obtained classically, however, as will now be shown. Consider an electric field of the following form:

$$\vec{E}(\vec{r},t) = \vec{E}_1 \cos(2\pi\nu t - \vec{k}\cdot\vec{r} + \varphi_1{}^o) \quad . \tag{5-10}$$

In analogy with the treatment of the angular selectivity in single quantum photomixing,[126,25] let the above plane wave be incident on a flat photosurface, which is taken to coincide with the plane $z = 0$. If the wave vector $\vec{k}$ is in the x-z plane, and makes an angle θ_1 with the photosurface normal, the $\vec{E}$-field on the photosurface may be written

$$\vec{E}_1(x,t) = \vec{E}_1 \cos(2\pi\nu t - kx\sin\theta_1 + \varphi_1{}^o) \quad . \tag{5-11}$$

A second plane wave of the same frequency ν and wave number $\vec{k}$, incident at a different angle θ_2 (in the same x-z plane), with a phase angle $\varphi_2{}^o$ may be written as

$$\vec{E}_2(x,t) = \vec{E}_2 \cos(2\pi\nu t - kx\sin\theta_2 + \varphi_2{}^o) \quad . \tag{5-12}$$

The angles $\varphi_1{}^o$ and $\varphi_2{}^o$ are taken to be the phases of the two waves at the midpoint of the photocathode.

To observe (two quantum) dc photomixing, the above two beams of the same frequency and wave number are considered to mix. The total two quantum current is then expected to

be proportional to the integral $\int_A \langle E_T^4(x,t)\rangle_t \, dA$ where $\langle\ \rangle_t$ indicates a time average for optical frequencies, A is the illuminated area of the cathode, and E_T represents the total electric field present. For $E_T = E_1(x,t)+E_2(x,t)$, in the special case where both waves are polarized in the plane of incidence, the above integral becomes

$$i_T^{(2)} = E_1^4+E_2^4+4E_1^2E_2^2\left[1 + \frac{1}{2}\cos 2(\varphi_1^{\circ}-\varphi_2^{\circ})\cdot\frac{1}{A}\int_A \cos\left\{2kx(\sin\theta_2-\sin\theta_1)\right\} dA\right]$$

$$+ 4E_1E_2^3\cos(\varphi_2^{\circ}-\varphi_1^{\circ})\cdot\frac{1}{A}\int_A \cos\left\{kx(\sin\theta_1-\sin\theta_2)\right\} dA$$

$$+ 4E_1^3E_2\cos(\varphi_1^{\circ}-\varphi_2^{\circ})\cdot\frac{1}{A}\int_A \cos\left\{kx(\sin\theta_2-\sin\theta_1)\right\} dA \qquad (5\text{-}13)$$

Various perturbing effects such as the non-flat beam splitters in the Mach-Zehnder interferometer, the unprecise superposition in the focal plane,* schlieren, vibrations, etc. will result

* Boivin and Wolf[132] have shown that the field structure in the focal plane is a complicated and rapidly varying function (see also reference 133). Hence, if the two beams are poorly superimposed, there will be an averaging effect.

in an average over the variable $\varphi_1^o - \varphi_2^o$ in the above equation. Furthermore, spatial incoherence results in a reduction in terms above which contain the integral.[126]

Therefore, under the conditions of the experiment, the classical result for the dc double quantum photocurrent reduces to

$$i_T^{(2)} = c(E_1^4 + E_2^4 + 4E_1^2E_2^2) = c(I_1^2 + 4I_1I_2 + I_2^2). \tag{5-14}$$

Thus, it is seen that this classical treatment of the superposition of two equal frequency beams gives rise to a cross term coefficient of 4. The current $i_T^{(2)}$ as calculated above is shown in Fig. 13 for comparison with experiment and the (correct) result which was discussed previously.

That the cross term coefficient must indeed be equal to 2 may be seen from the following physical argument: Consider a gedanken experiment in which one beam is amplitude divided into two parts of equal intensity and then recombined to impinge on the photodetector. The recombined beam should be physically equivalent to the original beam. Since the double quantum current for a single beam is proportional to the square of the intensity for that beam, this current must also be proportional to $(I_1+I_2)^2$ where I_1 and I_2 are the intensities of the constituent beams. Thus the coefficient for the cross term is again 2.

The preceding argument is simply a statement of the fact that a beam of light consists of photons. Its properties cannot be described solely in terms of wave theory. Mathematically, this argument takes the following form: Use of the vector potential A as the photoelectron creating operator is not appropriate; it is the positive frequency part A^+ which must be used on the (radiation field) wave function. This point has been discussed by Glauber.[26]

However, since the correlation functions considered previously are formulated in terms of quantized field theory, they give the correct result. It is to be noted that the full field theoretical approach is not necessary for a calculation of the matrix elements, since in that case, attention is not focused on the photon: If one beam is present, the transition amplitude is simply proportional to the intensity of that beam. Similarly, when there are two beams of different frequencies present, no confusion arises in the semiclassical treatment.

A similar problem is seen to arise in the simple treatment of ordinary single quantum photomixing[126,25,129] if the two incident beams have precisely the same frequency, and enter perfectly parallel to each other and perpendicular to the photosurface. Considering a unity efficiency single quantum detector, energy would appear not to be conserved. Again, if there is a small frequency difference between the beams, no problem arises.

C. Higher Order Correlation Functions: Chaotic Source

1. Description of a double quantum self-integrating Hanbury Brown-Twiss type experiment

In the last section, a discussion of the double quantum counting rate was given for the case of the laser field, where $g_1 = g_2 = 1$. For a thermal source, this condition is not satisfied. Since the second order correlation function (for a source with first order coherence) obeys the following relation[28]

$$G^{(2)}(x_i x_j x_j x_i) = g_2[G^{(1)}(x_i x_i)][G^{(1)}(x_j x_j)] , \tag{5-15}$$

the average counting rate, which is proportional to $\gamma^{(2)}$, must be multiplied by g_2. Thus, for a time delay between the beams which is short compared to the coherence time, the double quantum photocurrent is given by

$$i_T^{(2)} = g_2 c\langle I_1+I_2\rangle^2 > c[I_1^2+2I_1I_2+I_2^2] . \tag{5-16}$$

Here, c is the same constant used in Eq. (5-9). This current is seen to be g_2 times as large as that obtained when the excitation source is a single mode laser (compare Eq. (5.9)).* This increase in current arises from the bunching of photons (photon correlations) in the radiation from the thermal

---

* An analogous enhancement in other two quantum effects is also expected.

source: The probability for the simultaneous arrival of two photons is greater than if no bunching were present (as for the laser source).

When the time delay between the beams is greater than the coherence time of the radiation, however, there is no correlation between a photon from one beam and a photon from the other beam. The counting rate for such a process, which is given by terms of the form $G^{(2)}(x_o x_1 x_1 x_o)$, then factors into the product

$$G^{(2)}(x_o x_1 x_1 x_o) = [G^{(1)}(x_o x_o)][G^{(1)}(x_1 x_1)] , \qquad (5\text{-}17)$$

indicating that no excess coincidences occur. At a given x, correlations between photons from the same beam still remain, of course. Therefore, for large path length differences between the beams, $\gamma^{(2)}$ is given by

$$\gamma^{(2)} = g_2[G^{(1)}(x_o x_o)]^2 + g_2[G^{(1)}(x_1 x_1)]^2 + 2[G^{(1)}(x_o x_o)][G^{(1)}(x_1 x_1)] . \qquad (5\text{-}18)$$

For the special case of chaotic fields (including thermal radiation), $g_2 = 2$, and the two quantum photocounting rate $i_T^{(2)}$ is

$$i_T^{(2)} = 2c[I_1^2 + I_1 I_2 + I_2^2] . \qquad (5\text{-}19)$$

Again, this current is higher than that for the single mode laser (see Eq. (5-9)). Here, however, it is seen that the cross term no longer has a coefficient of 2 (relative to the coefficients of the terms I_1^2 and I_2^2). Physically, this corresponds to the enhancement of the single beam counting rates [$G^{(2)}(x_o x_o x_o x_o)$ and $G^{(2)}(x_1 x_1 x_1 x_1)$], arising from the tendency of these photons to arrive in correlated pairs. Since the beam delay is greater than the coherence time of the radiation, however, there is no correlation between the arrival time of a photon from one beam and the arrival time of a photon from the other. (Just as there is none with laser radiation.) Thus, the double quantum current arising from the absorption of 1 photon from each beam is the same for this case and for the laser: It is equal to $c(2I_1I_2)$.

The expressions for the double quantum photocurrent arising from a thermal source are summarized:

$$i_T^{(2)} = 2c[I_1^2+2I_1I_2+I_2^2] \qquad \tau_\delta < \tau_c \qquad (5\text{-}20)$$

and

$$i_T^{(2)} = 2c[I_1^2+I_1I_2+I_2^2]. \qquad \tau_\delta > \tau_c \qquad (5\text{-}21)$$

Here τ_δ represents the delay time between the beams, and τ_c is the coherence time of the radiation. The (relative) accidental coincidence rate is obtained from the cross term

in the equation for $\tau_\delta > \tau_c$; it is unity. The (relative) observed coincidence rate for delay times short compared with the coherence time is obtained from the cross term in the equation for $\tau_\delta < \tau_c$, and is equal to 2. A measure of the difference between the observed and accidental coincidence rates is therefore $\frac{2-1}{1} = 1 = g_2-1$. This factor, g_2-1, was also obtained by Titulaer and Glauber[28] for the Hanbury Brown-Twiss experiment with small detecter separation compared to the coherence length, and small delay time compared to the coherence time. For the limiting case of very small resolving time of the coincidence counter, Hanbury Brown and Twiss[134] also found this result.

The double quantum detector, illuminated by two beams which are superimposed (but have a time delay between them) is therefore seen to behave like a self-integrating Hanbury Brown-Twiss apparatus. For the two photon experiment, it is the relative magnitude of the cross term which reflects the correlations.* The extremely short resolving time of the double quantum detector ($\sim 10^{-15}$-10^{-14} sec which is the "lifetime" of an intermediate state in the two photon

---

* For this experiment, it would appear that the superposition of the beams insures spatial coherence at each point; therefore the partial coherence factor $\overline{\Delta}$ and the correlation factor $\overline{\Gamma^2(d)}$ (see reference 31 , section 2) should not result in a reduction of the excess coincidence counting rate.

absorption) results in this relatively large excess coincidence counting rate. Of course, only time delay type photon correlation experiments may be performed with this apparatus.

Nevertheless, an experimental test of these predictions could not be made for the following reasons: (a) The power output of the laser operating below threshold is quite low. Since the double quantum current depends on the square of the laser power, it is difficult to observe at these low levels; and (b) The double quantum current also depends inversely on the illuminated area. Therefore, the laser beam must be focused to a very small (almost diffraction limited) size in order to obtain observable currents. The small spot size makes complete superposition of the spots very difficult, as observed earlier. This results in a large loss of accuracy in comparing results for different values of δ.

2. Method of measurement for fourth order correlation function

With few exceptions,[135] most photon correlation experiments have been concerned with the measurement of a second order correlation function. As a particular use of the double quantum effect, the following experiment is proposed. It could furnish information about the fourth order correlation function, but would probably be quite difficult to do.

Consider a Hanbury Brown-Twiss type experiment[136] employing two <u>double quantum</u> detectors rather than two single quantum detectors.* The appropriate fourth order correlation function describing the coincidence experiment would be of the following form:

$$G^{(4)}(x_o x_o x_1 x_1 x_1 x_1 x_o x_o) = \mathrm{tr}\left\{\rho E^-(x_o)E^-(x_o)E^-(x_1)E^-(x_1) E^+(x_1)E^+(x_1)E^+(x_o)E^+(x_o)\right\}. \tag{5-22}$$

There are 8 field operators corresponding to the absorption of 4 photons. For a source with first order coherence, this separates into the product[28]

$$G^{(4)}(x_o x_o x_1 x_1 x_1 x_1 x_o x_o) = g_4 G^{(1)}(x_o x_o)G^{(1)}(x_o x_o)G^{(1)}(x_1 x_1) G^{(1)}(x_1 x_1) . \tag{5-23}$$

In this case, the following relation is also satisfied

$$G^{(2)}(x_j x_j x_j x_j) = g_2 G^{(1)}(x_j x_j)G^{(1)}(x_j x_j) \tag{5-24}$$

so that

$$G^{(4)}(x_o x_o x_1 x_1 x_1 x_1 x_o x_o) = \frac{g_4}{(g_2)^2}\,[G^{(2)}(x_o x_o x_o x_o)]\,[G^{(2)}(x_1 x_1 x_1 x_1)] . \tag{5-25}$$

---

* (see next page)

Now $G^{(2)}(x_o x_o x_o x_o)$ is proportional to the double quantum counting rate at detector A and $G^{(2)}(x_1 x_1 x_1 x_1)$ is proportional to the double quantum counting rate at detector B, so that the fourth order correlation function has been expressed in terms of two double quantum counting rates.

For thermal sources, Glauber has shown[27] that $g_n = n!$. Therefore, $g_2 = 2$ and $g_4 = 24$. For a photon coincidence counting experiment such as that described above, with small detector separation compared to the coherence length of the field, and with a short time delay compared to the coherence time, the number $(\frac{g_4}{(g_2)^2} - 1)$ furnishes a measure of the difference between the observed and the accidental coincidence rates. This is in analogy with the case for the ordinary Hanbury Brown-Twiss experiment where this number is g_2-1. The number $(\frac{g_4}{(g_2)^2} - 1)$ is positive for fields with positive definite P-functions[28]** (of which chaotic thermal sources are a special example), indicating that the excess coincidence counting rates are positive, as will now be demonstrated for the special example of the thermal source.

---

* Apertures should be used before the focusing lenses to insure spatial coherence over the focused spot.[31,66]

** These fields are characterized by the fact that their density operator possesses a positive definite weight function $\rho(\{\alpha_i\})$ in the representation which is diagonal in the eigenstates of the annihilation operators. Fields of this nature have well defined classical analogs.

Inserting the values $g_4 = 4! = 24$ and $g_2 = 2! = 2$ for thermal sources, the excess counting rate becomes

$$\frac{g_4}{(g_2)^2} - 1 = 5 \ . \qquad (5\text{-}26)$$

Therefore, the coincidence rate for small separations exceeds the accidental coincidence rate by a factor of 5, while for the ordinary Hanbury Brown-Twiss experiment, for small separations, they are equal.* In this case, the peaking of the coincidence rates should therefore be quite pronounced.

For radiation fields with positive definite P-functions, first and second order coherence implies n^{th} order coherence. Assuming the laser field to satisfy these properties, it is clear that $(\frac{g_4}{(g_2)^2} - 1) = 0$ showing that no excess coincidences would be observed if the incident radiation were obtained from a laser operating above threshold.

Performing such an experiment could provide information both about the validity of the gaussian weight function in describing a general chaotic field,[27]** as well as permit

---

* These statements are valid only when $\tau_n << \tau_c$ where τ_n is the resolving time of the coincidence counter, and τ_c is the coherence time of the source. This is <u>not</u> the usual experimental situation.[31,66]

** The chaotic source is presumed to differ from the thermal source only in the spectral distributions of their outputs.[137]

the observation of correlation functions for higher than second order.* Although it is difficult to obtain double quantum emission from non-laser sources because of their low intensity, this experiment might be feasible.

D. Excess Noise and Photocounting Statistics

The bunching of photons from a thermal source, as described in section C above, results in a deviation of the photoelectron counting distribution from Poisson, and leads to the observation of excess noise. The three effects: coincidence counting, photocounting statistics, and excess noise are intimately related, and the connections between these various manifestations of photon bunching have been discussed in detail from both an experimental and a theoretical point of view in the literature.[130,66,25] In particular, the theoretical relationship between the excess noise and the photocounting statistics is discussed by Freed and Haus,[130] while the relationship between excess noise and coincidence counting is discussed by Armstrong and Smith.[66] A brief discussion of these quantities, in relation to double quantum photoemission, is given below.

Excess noise measurements using a double quantum detector are of interest because they would provide in-

---

* Information about the third order correlation function may be obtained by a similar experiment in which only <u>one</u> of the single quantum detectors in the Hanbury Brown-Twiss experiment is replaced by a double quantum detector. For this case, the excess coincidence counting rate for a thermal source would be $(g_3/g_2) - 1 = 2$.

formation about the fourth order correlation functions of the field. Using the experimental setup shown in the block diagram of Fig. 14, which was patterned after the setup used by Armstrong and Smith,[138] an attempt was made to measure excess laser noise using a double quantum detector. The experiment was performed by measuring the root-mean-square noise at the output of the phase sensitive detector, as a function of the laser injection level. This attempt was unsuccessful because the two quantum current became too small when the laser was operated close to threshold. Armstrong and Smith observed quiet operation of their laser at about 25% above threshold,* and it would therefore be expected that unless the laser was operating reasonably close to threshold, no excess noise would be seen. In the case of one quantum photoemission, many modes operating simultaneously precludes the observation of excess noise,[66] but for a nonlinear effect such as the two quantum effect, this would probably not be true.[119]

In analogy with the single quantum case,[65] the two quantum photocounting statistics may probably be obtained in terms of the density operator for the field. The single quantum problem has been treated theoretically in great

---

* Their source may not be directly compared with ours, however, since they used a specially constructed, single mode laser operating continuously at 10°K.

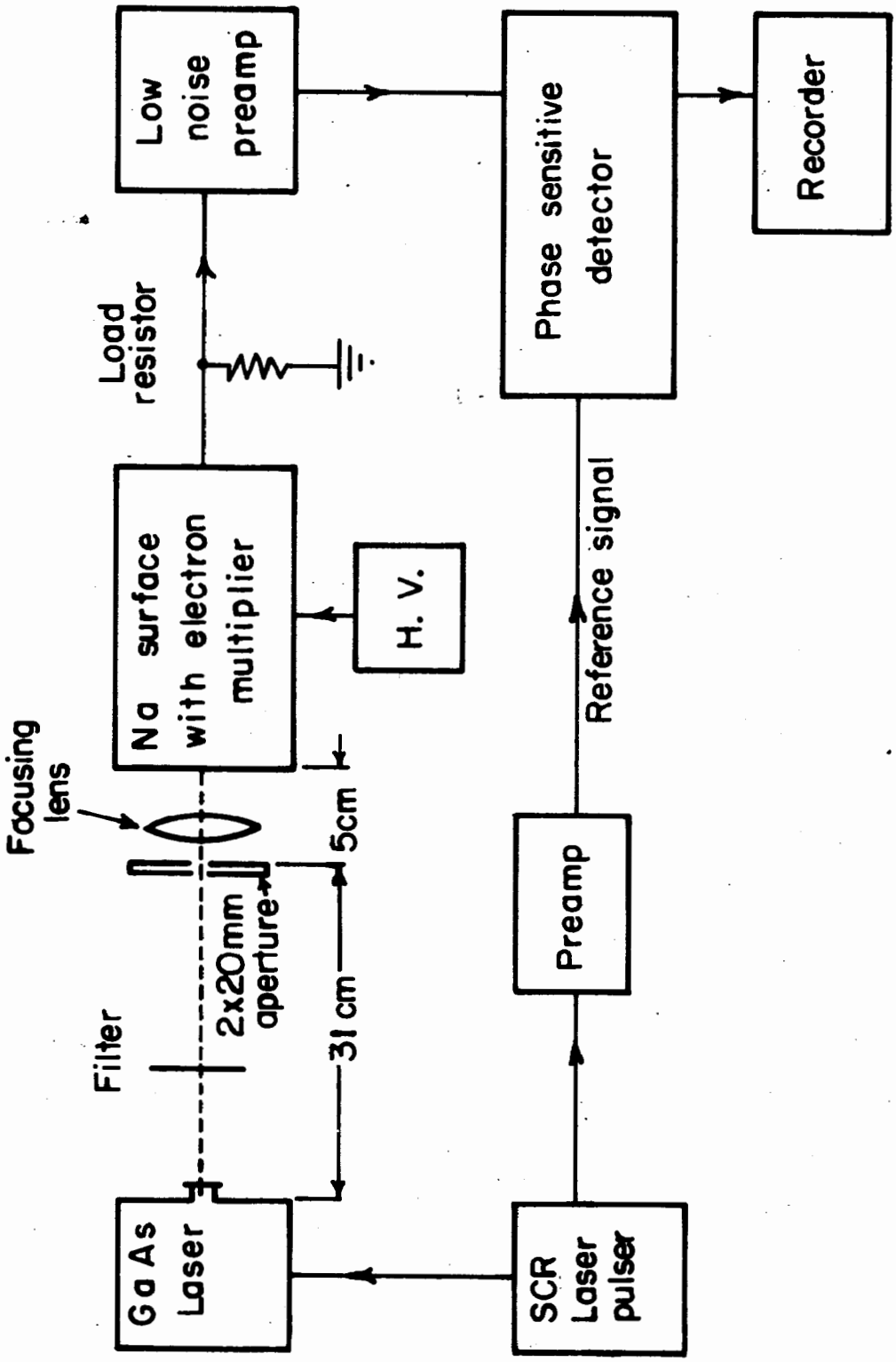

Figure 14. Block diagram of excess noise measurement apparatus.

detail by Kelley and Kleiner[65] and also by Mandel.[25] The photocounting distribution experiment is very useful because sufficiently accurate measurements of the statistical distribution of photons detected by a single photomultiplier, such as those carried out by Freed and Haus,[139*] implicitly provide values for the full set of moments for an radiation field.[28]

The assumptions used in a simply derivation of the single quantum photocounting distribution (such as the assumption of independent photon emissions in successive time intervals) might be applicable to the case of two photon photoemission if the short term intensity average[31] of the source is replaced by a short term average over the square of the intensity. Thus, for a coherent state with a perfectly stable intensity (quiet oscillation), the two quantum photocounting distribution would also be Poisson. For a thermal source, on the other hand, the intensity fluctuations would be accentuated by the nonlinear character of the double quantum photoelectric effect, so that the statistics would be expected to depart significantly from Poisson statistics, much as for the single quantum photoelectron distribution for the Gaussian-squared amplitude case treated by Kelley and Kleiner.[65]

---

* Freed and Haus[139] have recently observed the predicted Bose-Einstein probability distribution of photoelectrons by illuminating the detector with radiation from a laser operating below threshold.

REFERENCES

1. For a partial review of work involving two quantum transitions where both of the photons come from the incident radiation, see:

   N. Bloembergen, Nonlinear Optics, (W. A. Benjamin, Inc., New York, 1965), especially section 5.7.

   S. Yatsiv, W. G. Wagner, G. S. Picus, and F. J. McClung, Phys. Rev. Letters 15, 614 (1965). (Saturation of a Resonant Optical Double-Quantum Transition).

   R. W. Terhune, P. D. Maker, and C. M. Savage, Phys. Rev. Letters 14, 681 (1965). (Measurements of Nonlinear Light Scattering).

   Fielding Brown, Robert E. Parks, and Arthur M. Sleeper, Phys. Rev. Letters 14, 1029 (1965). (Nonlinear Optical Reflection from a Metallic Boundary).

   Sudhanshu S. Jha, Phys. Rev. Letters 15, 412 (1965). (Nonlinear Optical Reflection from a Metal Surface).

2. For examples of other higher-order processes not involving the absorption of two quanta, see:

   N. Bloembergen, Nonlinear Optics, (W. A. Benjamin, Inc., New York, 1965), chapter 5.

   D. F. Dubois, Phys. Rev. Letters 14, 818 (1965). (Nonlinear Scattering of Radiation from Plasmas).

   L. S. Bartell, H. Bradford Thompson, and R. R. Roskos, Phys. Rev. Letters 14, 851 (1965). (Observation of Stimulated Compton Scattering of Electrons by Laser Beam).

   J. A. Giordmaine and Robert C. Miller, Phys. Rev. Letters 14, 973 (1965). (Tunable Coherent Parametric Oscillation in $LiNiO_3$ at Optical Frequencies).

3. R. Braunstein and N. Ockman, Phys. Rev. 134, A499 (1964). (Optical Double-Photon Absorption in CdS).

4. M. Lipeles, R. Novick, and N. Tolk, Phys. Rev. Letters 15, 690 (1965). (Direct Detection of Two-Photon Emission from the Metastable State of Singly Ionized Helium).

5. J. J. Hopfield, J. M. Worlock, and Kwangjai Park, Phys. Rev. Letters 11, 414 (1963). (Two-Quantum Absorption Spectrum of KI).

A. W. Smith and N. Braslau, IBM J. Research Develop. 6, 361 (1962). (Optical Mixing of Coherent and Incoherent Light).

6. S. Z. Weisz, A. B. Zahlan, J. Gilreath, and R. C. Jarnagin, J. Chem. Phys. 41, 3491 (1964). (Two Photon Absorption in Crystalline Anthracene and Naphthalene Excited with a Xenon Flash).

D. H. McMahon and A. R. Franklin, J. Appl. Phys. 36, 2807 (1965). (Detection of Nonlinear Optical Sum Spectra in ADP Using Incoherent Light).

7. Martin Pope, Hartmut Kallmann, and Joseph Giachino, J. Chem. Phys. 42, 2540 (1965). (Double-Quantum External Photoelectric Effect in Organic Crystals).

8. R. L. Smith, Phys. Rev. 128, 2225 (1962). (Two-Photon Photoelectric Effect).

9. H. C. Bowers, M. S. thesis, Cornell University, February 1964 (unpublished). (Theoretical and Experimental Considerations of the Double-Quantum Photoelectric Effect).

10. I. Adawi, Phys. Rev. 134, A788 (1964). (Theory of the Surface Photoelectric Effect for One and Two Photons).

11. P. Bloch, J. Appl. Phys. 35, 2052 (1964). (Preliminary Investigation of the Two-Photon Photoelectric Effect).

12. K. Mitchell, Proc. Roy. Soc. (London) A146, 442 (1934); A153, 513 (1936). (The Theory of the Surface Photoelectric Effect in Metals - I; The Theory of the Surface Photoelectric Effect in Metal - II).

13. H. Y. Fan, Phys. Rev. 68, 43 (1945). (Theory of Photoelectric Emission from Metals).

14. H. Thomas, Z. Physik 147, 395 (1957). (Zum Äusseren lichtelektrischen Effekt der Alkalimetalle - I. Seine Abhängigkeit von der Schichtdicke bei Kalium Reichweite der Photoelektronen im Metall).

15. H. Mayer and H. Thomas, Z. Physik 147, 419 (1957). (Zum äusseren lichtelektrischen Effect der Alkalimetalle - II. Die spektrale Verteilung der Quantenausbeute bei Kalium).

16. H. Mayer, R. Nossek and H. Thomas, J. Phys. Radium 17, 204 (1956). (Le libre parcours moyen des électrons de conductibilité et des électrons photoélectriques mesuré au moyen de la methode des couches minces).

17. A. Meessen, J. Phys. Radium 22, 308 (1961). (Théorie de L'effect Photoélectrique des Métaux).

18. C. N. Berglund and W. E. Spicer, Phys. Rev. 136, A1030 (1964); Phys. Rev. 136, A1044 (1964). (Photoemission Studies of Copper and Silver: Theory; Photoemission Studies of Copper and Silver: Experiment).

19. W. E. Spicer, Phys. Rev. Letters 11, 243 (1963). (Optical Transitions in which Crystal Momentum is not Conserved).

20. R. H. Dicke, Rev. Sci. Instr. 17, 268 (1946). (The Measurement of Thermal Radiation at Microwave Frequencies).

21. C. A. Stutt, "Low-Frequency Spectrum of Lock-in Amplifiers", (Massachusetts Institute of Technology RLE Technical Report No. 105), March, 1949.

22. H. Sonnenberg, H. Heffner, and W. Spicer, Appl. Phys. Letters 5, 95 (1964). (Two-Photon Photoelectric Effect in Cs_3Sb).

23. R. J. Maurer, Phys. Rev. 57, 653 (1940). (The Photoelectric and Optical Properties of Sodium and Barium).

24. W. E. Spicer and F. Wooten, Proc. IEEE, 51, 1119 (1963). (Photoemission and Photomultipliers).

25. L. Mandel and E. Wolf, Rev. Mod. Phys. 37, 231 (1965). (Coherence Properties of Optical Fields).

26. R. J. Glauber, Phys. Rev. 130, 2529 (1963). (The Quantum Theory of Optical Coherence).

27. R. J. Glauber, Phys. Rev. 131, 2766 (1963). (Coherent and Incoherent States of the Radiation Field).

28. U. M. Titulaer and R. J. Glauber, Phys. Rev. 140, B676 (1965). (Correlation Functions for Coherent Fields).

29. R. Hanbury Brown and R. Q. Twiss, Nature 177, 27 (1956). (Correlation Between Photons in Two Coherent Beams of Light).

30. R. Hanbury Brown and R. Q. Twiss, Proc. Roy. Soc. (London) A242, 300 (1957). (Interferometry of Intensity Fluctuations in Light - I. Basic Theory: The Correlation Between Photons in Coherent Beams of Radiation).

31. R. Hanbury Brown and R. Q. Twiss, Proc. Roy. Soc. (London) A243, 291 (1957). (Interferometry of the Intensity Fluctuations in Light - II. An Experimental test of the Theory for Partially Coherent Light).

32. R. Q. Twiss and A. G. Little, Australian J. Phys. 12, 77 (1959). (The Detection of Time-Correlated Photons by a Coincidence Counter).

33. T. M. Quist, International Science and Technology, #26 (1964), p. 80. (Semiconductor Lasers).

34. H. K. Henisch, Progress in Physics (1964), p. 398. (Electroluminescence).

35. A. Yariv, "Dielectric-Waveguide Confinement and Laser Threshold in PN Junction Lasers", seminar at Cornell University, March, 1964.

36. P. P. Sorokin, J. D. Axe, and J. R. Lankard, J. Appl. Phys. 34, 2553 (1963). (Spectral Characteristics of GaAs Lasers Operating in "Fabry-Perot" Modes).

37. C. H. Gooch, Phys. Letters 16, 5 (1965). (Transient Thermal Effects in Gallium Arsenide Injection Lasers).

38. F. N. Hooge and H. Kalter, Phys. Letters 12, 191 (1964). (Injection Lasers far above Threshold).

39. Y. Nannichi, Japan J. Appl. Phys. 3, 360 (1964). (On the Polarization of Light from the GaAs Diode Laser).

40. For the standard SCR multivibrator circuit and its operation, see F. W. Gutzwiller, Silicon Controlled Rectifier Manual, (General Electric Company, Auburn, New York, 1964), 3rd. ed., p. 111.

41. R. H. Fowler, Phys. Rev. 38, 45 (1931). (The Analysis of Photoelectric Sensitivity Curves for Clean Metals at Various Temperatures).

42. R. J. Maurer in Handbook of Physics, edited by E. U. Condon and H. Odishaw (McGraw-Hill, New York, 1958), p. 8-67.

43. This measurement was made by J. M. Schroeer.

44. W. Summer, Photosensitors, (Chapman and Hall, London, 1957), p. 59.

45. A. H. Sommer and W. E. Spicer, Photoelectronic Materials and Devices, edited by S. Larach (D.Van Nostrand, Princeton, N. J., 1965), chapter 4, pp. 175, 192.

46. H. C. Bowers, Ph. D. Thesis, Cornell University (unpublished).

47. J. G. Koosman, private communication.

48. H. E. Bennett, M. Silver, and E. J. Ashley, J. Opt. Soc. Am. 53, 1089 (1963). (Infrared Reflectance of Aluminum Evaporated in Ultra-High Vacuum).

49. M. Born and E. Wolf, Principles of Optics, (Macmillan, New York, 1959), 1st. edition, chapter 13.

50. O. S. Heavens, Optical Properties of Thin Solid Films, (Academic Press, New York, 1955), p. 161, 176.

51. H. Mayer, Physik Dünner Schichten, (Wissenschaftliche Verlagsgesellschaft M.B.H., Stuttgart, 1950) Vol. I, p. 228.

52. ibid., p. 304.

53. ibid., p. 296.

54. R. S. Sennett and G. D. Scott, J. Opt. Soc. Am. 40, 203 (1950).

55. Some theoretical work for translucent photocathodes, using a model similar to that of Berglund and Spicer[18] for the bulk material, might be pertinent. See J. L. Gumnick, Bull. Am. Phys. Soc. 10, 433 (1965), AF7.

56. Y. W. Lee, Statistical Theory of Communication, (John Wiley and Sons, New York, 1960), pp. 312-319.

57. Reference Data for Radio Engineers, edited by H. P. Westman, (International Telephone and Telegraph, New York, 1956), edition 4, pp. 408-410.

58. W. B. Davenport, Jr. and W. L. Root, An Introduction to the Theory of Random Signals and Noise, (McGraw-Hill, New York, 1958), p. 144, problem 6.

59. Dumont Multiplier Phototubes, (Fairchild Camera and Instrument, Clifton, N. J., 1965), 4th. edition.

60. Low-Noise Preamplifier Instruction Manual, (Princeton Applied Research Corp., Princeton, N. J., 1964), "Typical Noise Figure Contours", p. 4.

61. ibid., pp. 6-8.

62. W. B. Davenport, Jr. and W. L. Root, An Introduction to the Theory of Random Signals and Noise, (McGraw-Hill, New York, 1958), p. 209.

63. ibid., p. 209, equation 10-17.

64. An elementary treatment of the application of the Poisson distribution to photoelectric emission is given by E. Parzen, Modern Probability Theory and Its Applications, (John Wiley and Sons, New York, 1960), p. 251.

65. P. L. Kelly and W. H. Kleiner, Phys. Rev. 136, A316 (1964). (Theory of Electromagnetic Field Measurement and Photoelectron Counting).

66. J. A. Armstrong and A. W. Smith, Phys. Rev. 140, A155 (1965). (Intensity Fluctuations in GaAs Laser Emission); Phys. Rev. Letters 14, 68 (1965). (Intensity Fluctuations in a GaAs Laser); Phys. Rev. 16, 38 (1965) (Intensity Fluctuations and Correlations in a GaAs Laser).

67. The autocorrelation function and the PSD for this problem are thoroughly discussed in W. B. Davenport, Jr. and W. L. Root, An Introduction to the Theory of Random Signals and Noise, (McGraw-Hill, New York, 1958), p. 121.

68. See, for example W. B. Davenport, Jr. and W. L. Root, An Introduction to the Theory of Random Signals and Noise, (McGraw-Hill, New York, 1958), section 6-3, p. 91.

69. A similar model for the random digital train pulsing of a Poisson process has been discussed by S. Karp, Proc. IEEE 52, 1264 (1964).

70. Table of Important Transforms (Hewlett-Packard Co., Palo Alto, Calif., 1954), transforms #6 and #6S. Note that there is an error in transform #6S: $F(\omega)$ should be multiplied by $2\pi/\tau$.

71. W. B. Davenport, Jr. and W. L. Root, An Introduction to the Theory of Random Signals and Noise, (McGraw-Hill, New York, 1958), p. 90, equation 6.14.

72. N. Abramson, Statistical Theory of Communication, (Course #EE251 at Stanford University, Palo Alto, Calif., 1962), problem set #1, problem #5.

73. A. Einstein, Ann. Physik 17, 132 (1905); Translation: Am. J. Phys. 33, 367 (1965).

74. L. I. Schiff, Quantum Mechanics, (McGraw-Hill, New York, 1955), 2nd. edition, p. 135, 246.

75. ibid., p. 248.

76. For a review of these papers, see the references in: D. H. McMahon, R. A. Soref, and A. R. Franklin, Phys. Rev. Letters 14, 1060 (1965). (Quantitative Measurements of Double-Photon Absorption in the Polycyclic Benzene Ring Compounds).

77. L. I. Schiff, Quantum Mechanics, (McGraw-Hill, New York, 1955), 2nd. edition, p. 254.

78. D. H. McMahon, R. A. Soref, and A. R. Franklin, Phys. Rev. Letters 14, 1060 (1965). (Quantitative Measurements of Double-Photon Absorption in the Polycyclic Benzene Ring Compounds).

79. W. L. Peticolas and K. E. Rieckhoff, Phys. Letters 15, 230 (1965). (Polarization of Anthracene Fluorescence by One and Two Photon Excitation).

80. Rosalia Guccione and J. Van Kranendonk, Phys. Rev. Letters 14, 583 (1965). (Theory of Higher Multipole Contributions to Two-Photon Absorption Processes).

81. G. Fornaca, M. Iannuzzi, and E. Polacco, Nuovo Cimento 36, 1230 (1965). (Two-Photon Absorption in Atomic or Molecular Systems).

82. E. Corinaldesi, Phys. Rev. Letters 15, 335 (1965). (Theoretical Estimate of Double Quantum Photodetachment of Iodine Ions).

83. J. L. Hall, E. J. Robinson, and L. M. Branscomb, Phys. Rev. Letters 14, 1013 (1965). (Laser Double-Quantum Photodetachment of I^-).

84. K. Mitchell, Proc. Cambridge Phil. Soc. 31, 416 (1935). (The Temperature Dependence of the Photoelectric Effect).

85. A. J. Dekker, Solid State Physics, (Prentice-Hall, Englewood Cliffs, N. J., 1957), chapter 9, p. 225.

86. R. E. B. Makinson, Proc. Roy. Soc. (London) A162, 367 (1937). (Metallic Reflexion and the Surface Photoelectric Effect).

87. M. J. Buckingham, Phys. Rev. 80, 704 (1950). (The Surface Photoelectric Effect).

88. H. B. Huntington and L. Apker, Phys. Rev. 89, 352 (1953); H. B. Huntington, Phys. Rev. 89, 357 (1953). (Transition Probability for Photoelectric Emission from Semiconductors; Extension of Makinson's Theory of Photoelectric Emission to a Periodic Potential).

89. C. Kittel, Introduction to Solid State Physics, (John Wiley and Sons, New York, 1956), Second edition, p. 267.

90. I. Tamm and S. Schubin, Z. Physik 68, 97 (1931). (Zur Theorie des Photoeffektes an Metallen).

91. This is the same specification as for a billiard ball.

92. L. I. Schiff and L. H. Thomas, Phys. Rev. 47, 860 (1935). (Quantum Theory of Metallic Reflection).

93. S. Methfessel, Z. Physik 147, 442 (1957). (Zum äusseren lichtelektrischen Effekt der Alkalimetalle - III. Die Energieverteilung bei Kalium und Caesium).

94. P. N. Butcher, Proc. Phys. Soc.(London) 64, 765 (1951). (The Absorption of Light by Alkali Metals).

95. F. Seitz, Phys. Rev. 47, 404 (1935). The Theoretical Constitution of Metallic Lithium.

96. H. Ehrenreich and H. R. Philipp, Phys. Rev. 128, 1622 (1962). (Optical Properties of Ag and Cu).

97. R. A. Smith, Wave Mechanics of Crystalline Solids, (Chapman and Hall, London, 1961), section 13.5, p. 445.

98. J. Dickey, Phys. Rev. 81, 612 (1951). (New Aspects of the Photoelectric Emission from Na and K).

99. J. J. Quinn, Phys. Rev. 126, 1453 (1962). (Range of Excited Electrons in Metals).

100. A. Vašíček, Optics of Thin Films, (North-Holland Publishing Co., Amsterdam, 1960).

101. R. C. Faust, Phil. Mag. 41, 1238 (1950). (An Interferometric Study of some Optical Properties of Evaportated Silver Films).

102. A. Elbel, Z. Phys. 147, 465 (1957). (Optische Untersuchen an Kaliumschichten atomarer Dicke).

103. J. C. Maxwell Garnett, Phil. Trans. 203, 385 (1904); 205, 237 (1906).

104. O. S. Heavens, Optical Properties of Thin Solid Films, (Academic Press, New York, 1955), p. 201.

105. It is possible that new data has recently been reported, however. See J. J. Hopfield, J. Opt. Soc. Am. 55, 1574 (1965), TA2.

106. C. Kittel, Introduction to Solid State Physics, (John Wiley and Sons, New York, 1956), second edition, p. 234.

107. A. Vašíček, Optics and Spectroscopy 11, 128 (1961). (Theory of Light Reflection from a Thin Absorbing Film Deposited on a Metal).

108. L. I. Schiff, Quantum Mechanics, (McGraw Hill, New York, 1955), second edition, p. 201-205.

109. W. Heitler, The Quantum Theory of Radiation, (Oxford University Press, New York, 1954), 3rd. ed., p. 142.

110. R. A. Smith, Wave Mechanics of Crystalline Solids, (Chapman and Hall, London, 1961), section 13.3 p. 403.

111. C. Kittel, Introduction to Solid State Physics, (John Wiley and Sons, New York, 1956), second edition, p. 286.

112. L. I. Schiff, Quantum Mechanics, (McGraw Hill, New York, 1955), second edition, p. 254.

113. C. Kittel, Introduction to Solid State Physics, (John Wiley and Sons, New York, 1956), second edition, p. 285.

114. R. A. Smith, Wave Mechanics of Crystalline Solids, (Chapman and Hall, London, 1961), p. 409, 464.

115. C. Kittel, Introduction to Solid State Physics, (John Wiley and Sons, New York, 1956), second edition, p. 289.

116. ibid., p. 288.

117. ibid., p. 317.

118. R. A. Smith, Wave Mechanics of Crystalline Solids, (Chapman and Hall, London, 1961), p. 410.

119. N. Bloembergen, Nonlinear Optics, (Benjamin, New York, 1965), p. 131.

120. A. Ashkin, G. D. Boyd, and J. M. Dziedzic, Phys. Rev. Letters 11, 14 (1963). (Observation of Continuous Optical Harmonic Generation With Gas Masers).

121. W. B. Davenport, Jr. and W. L. Root, An Introduction to the Theory of Random Signals and Noise, (McGraw-Hill, New York, 1958), chapter 9, p. 171.

122. B. Lax, J. G. Mavroides, and D. F. Edwards, Phys. Rev. Letters 8, 166 (1962). (Nonlinear Interband and Plasma Effects in Solids).

123. F. Brown, R. E. Parks, and A. M. Sleeper, Phys. Rev. Letters 14, 1029 (1965). (Nonlinear Optical Reflections from a Metallic Boundary).

124. S. Jha, Phys. Rev. Letters 15, 412 (1965). (Nonlinear Optical Reflection from a Metal Surface);

S. Jha, Phys. Rev. 140, A2020 (1965). (Theory of Optical Harmonic Generation at a Metal Surface).

125. N. Bloembergen, Nonlinear Optics, (Benjamin, New York, 1965), p. 134.

126. A. E. Siegman, Photomixing with Coherent Light, (Stanford University, 1963), unpublished.

127. A. Javan, E. A. Ballik, and W. L. Bond, J. Opt. Soc. Am. 52, 96 (1962). (Frequency Characteristics of a Continuous-Wave He-Ne Optical Maser).

128. A. T. Forrester, R. A. Gudmunsen, and P. O. Johnson, Phys. Rev. 99, 1691 (1955). (Photoelectric Mixing of Incoherent Light).

129. P. S. Pershan and N. Bloembergen, Appl. Phys. Letters 2, 117 (1963). (Frequency Response of the Photo-Mixing Process);

M. Bernard, Appl. Phys. Letters 2, 9 (1963). (Optical Absorption as a Photomixing Process).

130. C. Freed and H. A. Haus, Phys. Rev. (to be published). (Photocurrent Spectrum and Photoelectron Counts Produced by a Gas Laser).

131. L. Mandel and E. Wolf, Rev. Mod. Phys. 37, 231 (1965), equation 4.43b.

132. A. Boivin and E. Wolf, Phys. Rev. 138, B1561 (1965). (Electromagnetic Field in the Neighborhood of the Focus of a Coherent Beam).

133. A. I. Carswell, Phys. Rev. Letters 15, 647 (1965). (Measurements of the Longitudinal Component of the Electromagnetic Field at the Focus of a Coherent Beam).

134. R. Hanbury Brown and R. Q. Twiss, Proc. Roy. Soc. (London) A243, 291 (1957), appendix B-3.

135. M. Bertolotti, B. Daino, and F. Gori, Phys. Rev. Letters 15, 279 (1965). (Measurement of the Fourth-Order Moment for Non-Gaussian Electromagnetic Fields);

F. T. Arecchi and A. Berné, Phys. Rev. Letters 16, 32 (1966). (High-Order Fluctuations in a Single-Mode Laser Field).

136. R. Q. Twiss and A. G. Little, Australian J. Phys. 12, 77 (1959), see figure 1.

137. R. J. Glauber, Phys. Rev. 131, 2766 (1963), see page 2787.

138. J. A. Armstrong and A. W. Smith, Phys. Rev. 140, A155 (1965), see figure 4.

139. C. Freed and H. A. Haus, Phys. Rev. Letters 15, 943 (1965). (Photoelectron Statistics Produced by a Laser Operating Below the Threshold of Oscillation).